Global methane action pays for itself at least six times over

Thomas Stoerk[1,2*], James Rising[3], Drew Shindell[4], Simon Dietz[2]

[1]Economics and Research Department, National Bank of Belgium, Brussels, 1000, Belgium.

[2]Grantham Research Institute on Climate Change and the Environment,

London School of Economics and Political Science, London, WC2A 2AE, UK.

[3]School of Marine Science and Policy, University of Delaware, Newark, DE 19716, USA.

[4]Nicholas School of the Environment, Duke University, Durham, NC 27708, USA.

[*]Corresponding author. Email: t.a.stoerk@lse.ac.uk

We provide a comprehensive assessment of the economic benefits and costs of global methane emissions abatement, anchored on the Global Methane Pledge. We use an Integrated Assessment Model to estimate avoided climate damages at the global and country levels, including quantification of tipping points and risk. We further estimate air quality co-benefits and methane abatement costs. We find global methane action would be highly beneficial, yielding a benefit-cost ratio of at least six. It would provide larger benefits in lower-income countries, and it would reduce tipping-point intensity and risk. We provide estimates of the social cost of methane to compare with previous literature and show that they imply key economies such as the US, EU and China should be self-interested to abate methane emissions substantially.

Methane is a potent, short-lived climate pollutant (SLCP) that has contributed around one third of the total warming from well-mixed greenhouse gases (GHGs) since the 19th century (*1*). Having

plateaued in the early 2000s, atmospheric concentrations of methane are once again increasing at a rapid rate due to anthropogenic emissions from fossil fuel production and distribution, agriculture, and waste, as well as anthropogenic/natural emissions from wetlands (*2–6*).

Because it is a major driver of current warming and its atmospheric concentration responds rapidly to emissions reductions, methane abatement has been identified as "very likely to be the most powerful lever in reducing near-term warming" (*7*). Moreover, substantial technical potential has been identified to reduce methane emissions, much of which is argued to be negative-cost or low-cost (*7–11*).

Previous work has argued that climate policy is too focused on long-term climate stability (*11, 12*), for example on mid-century, net-zero CO_2 emissions as the key target to be adopted by both state and non-state actors. Even the more near-term Nationally Determined Contributions to the 2015 UN Paris Agreement have been found to contain variable, but generally low, coverage of methane-focused mitigation measures (*13*). In the background to policy-making, it has also been argued that the accounting practice of converting methane into CO_2 equivalents using its 100-year Global Warming Potential (GWP) contributes to overlooking the importance of methane, because such a conversion understates the impact of methane in the short term (*12*). The contrary view is that methane abatement, alongside mitigation of other SLCPs, risks delaying efforts to abate CO_2, and can be "deferred without much harm" if the ultimate goal is controlling long-term warming (*14*).

Policy-makers appear to be listening to arguments in favor of methane action. The *Global Methane Pledge*, launched at COP26 in 2021, commits participating countries to take voluntary, domestic actions in service of at least a 30 percent reduction in global methane emissions below the 2020 level by 2030 (*15*). At the time of writing, 159 countries have signed on (including the EU and US, but not China, India or Russia), and some have reflected the global ambition of the Pledge in domestic targets and plans (*13*).

Understanding the role of methane abatement in climate policy can be aided by quantifying the benefits of methane abatement and comparing them with the costs. Previous studies have quantified the benefits of global methane abatement scenarios in terms of physical climate variables such as carbon budgets (*16, 17*), global mean temperatures (*9, 11, 18–23*), and sea levels (*24*). The 2021 Global Methane Assessment extended the literature by quantifying selected economic and health benefits of global methane abatement, including heat and ozone-related mortality, ozone-related

morbidity, lost labour productivity due to extreme heat, and crop yield losses via both climate and ozone effects (*7*). (*23*) have provided a simple calculation of the overall economic benefits of methane abatement by feeding global mean temperature pathways into an aggregate climate damage function.

In addition to these studies on the benefits of global methane action scenarios, there is a literature on the social cost of methane (SC-CH_4), i.e., the discounted present value of the future stream of damages from an incremental (marginal) emission of the gas (*25–35*). The literature on the SC-CH_4 is much smaller than its counterpart on the social cost of carbon dioxide (SC-CO_2), but it is valuable because social/marginal costs provide a natural and consistent way of comparing GHGs with different atmospheric lifetimes (*36*). As (*19*) pointed out, "direct comparisons of the climate influence of SLCPs and CO_2 require making a judgment about the relative importance of short and long time scales". Economics would compare the SC-CH_4 with the SC-CO_2, as doing so does not depend on an arbitrary choice of time horizon unlike GWP (e.g., GWP20 versus GWP100), although the discount rate becomes a key choice (*37*). The SC-CH_4 is also an important policy quantity given its routine application in cost-benefit analyses (CBAs) of specific methane abatement policies (e.g., rules on methane flaring in oil and gas). However, the standard practice in national policy analysis of multiplying GHG emissions reductions by the social cost of a GHG cannot in general be used to quantify large global emissions reductions brought about by agreements such as the Global Methane Pledge. That is because the marginal approximation relied upon can be highly inaccurate for large, non-marginal changes in emissions (*38, 39*). Therefore, an assessment of the total economic benefits of global methane action should be based on running emissions scenarios through an Integrated Assessment Model (IAM).

In this paper, we seek to advance the literature by providing a comprehensive assessment of the economic benefits of global methane abatement, anchored on the Global Methane Pledge, and comparing them with the costs. This includes a distributional analysis across countries, and an analysis of how global methane abatement affects tipping points and macro-economic risk. We proceed in three steps. First, we create a set of emissions scenarios, which simulate methane action at the global level against a background of emissions of CO_2 and other GHGs/radiative forcing agents. These scenarios are anchored on successful achievement in 2030 of the Global Methane Pledge, followed by continued methane abatement post-2030.

The second step is to take the scenarios and run them through the META (Model for Economic Tipping point Analysis) IAM (*40,41*) to estimate total economic benefits. META has several useful features for present purposes: (i) it incorporates a recent Simple Climate Model from the climate science literature (*42*), thus producing global mean temperature projections consistent with observations and Earth System Models; (ii) it provides relatively comprehensive benefit/damage estimates, including both market and non-market damages, via temperature and sea-level mechanisms; (iii) it estimates damages at the country level for 179 countries, thus enabling the distributional effects of emissions abatement to be analyzed; (iv) it can quantify the role of climate tipping points (including methane-based tipping points) and climate tail risk in the overall benefits of methane action (though it is important to bear in mind that the coverage of tipping point damage mechanisms is incomplete, a reflection of the underlying literature).

The third step brings in methane abatement costs and air quality co-benefits. For the former, we aggregate sectoral estimates of methane abatement costs from (*43*) and (*10*), which were used in the Global Methane Assessment (*7*), as well as using the methane marginal abatement cost (MAC) curve estimated by (*8*). For the latter, we use data on premature deaths due to respiratory and cardiovascular diseases, and on the Value of a Statistical Life (VSL), also from the Global Methane Assessment (*7*).

In addition to quantifying the total benefits and costs of global methane action, we also include an analysis of the SC-CH_4. This facilitates a comparison with previous literature, which as mentioned has tended to be about marginal rather than total damages. In addition, with META we can provide the first set of country-level estimates of the SC-CH_4, to the best of our knowledge. In light of current geopolitics, this enables us to evaluate incentives of countries to act in their own self-interest rather than just in pursuit of a global agreement like the Global Methane Pledge.

Results

Methane emissions and effect on temperatures

Fig. 1 plots methane emissions and resulting global mean temperatures under our methane action scenarios, of which there are three: central, low emissions and high emissions. The central scenario

contains a subset of 1.5°C scenarios that approximate the Global Methane Pledge's 30% reduction. The low and high emissions scenarios are subsets of 1.5°C scenarios that bracket the central scenario and give, respectively, roughly 50% bigger and smaller cuts than the central scenario. The scenario spread is intended to reflect uncertainty about technical abatement potential across IAMs, and about policy implementation (within the context of methane action above current trends). Our preferred specification chooses a background scenario of SSP2-4.5, which we take to be the Shared Socioeconomic Pathway (SSP) scenario corresponding most closely to a current policies/trends storyline (*44*). This sets both baseline methane emissions and emissions of other GHGs and forcing agents. In Fig. S1 in the SM, we also show a high-emissions background scenario (SSP3-7.0) and a 1.5°C background scenario. The former amounts to a storyline where the Global Methane Pledge is successfully implemented but the rest of the world's climate agenda fails completely. This is a less likely combination in our view, although we should point out that observations imply methane emissions specifically are currently increasing faster than projected on SSP2-4.5 (*45*). The use of a 1.5°C background scenario just assesses whether the Global Methane Pledge requires similar, more or less methane abatement than the full suite of 1.5°C scenarios.

The central methane action scenario reduces methane emissions by 30% in 2030 relative to 2020 (implementation of the Global Methane Pledge), 47% in 2050 and 62% in 2100 (Fig. 1, left panel). The methane action high-low scenario range is a 19-46% cut in 2030, 34-63% in 2050 and 52-72% in 2100, all relative to 2020. The SM shows that while the Global Methane Pledge is well within the range of 1.5°C scenarios, it is actually less ambitious than the mean cut in 2030 across 1.5°C scenarios. Emissions are 4% higher under the Global Methane Pledge than in the mean 1.5°C scenario.

The central methane action scenario reduces global mean surface temperature change by an expected 0.02°C in 2030, 0.13°C in 2050 and 0.18°C in 2100 (Fig. 1, right panel). The temperature reduction under the methane action scenarios flattens out after 2070 because baseline methane emissions reductions under SSP2-4.5 follow a similar trajectory to the methane action scenarios, albeit at an overall higher emissions level. The range of uncertainty in the expected temperature response to the high-low methane scenario variants is 0.09-0.19°C in 2050. Temperature uncertainty conditional on the central methane scenario is also 0.09-0.19°C in 2050. This comes from parametric uncertainty in the FaIR Simple Climate Model, as well as tipping points in META that affect

Figure 1: **Methane emissions (left panel) and effect on global mean temperature (right panel) of methane action scenarios**. Background emissions scenario is SSP2-4.5. The shaded area is the 90% confidence interval of temperature outcomes pertaining to the central methane action scenario, based on parametric uncertainty in META sampled by 1000 Monte Carlo runs. 'Methane action - high' and 'Methane action - low' describe methane action scenarios resulting in high and low emissions, respectively. Specification includes tipping points.

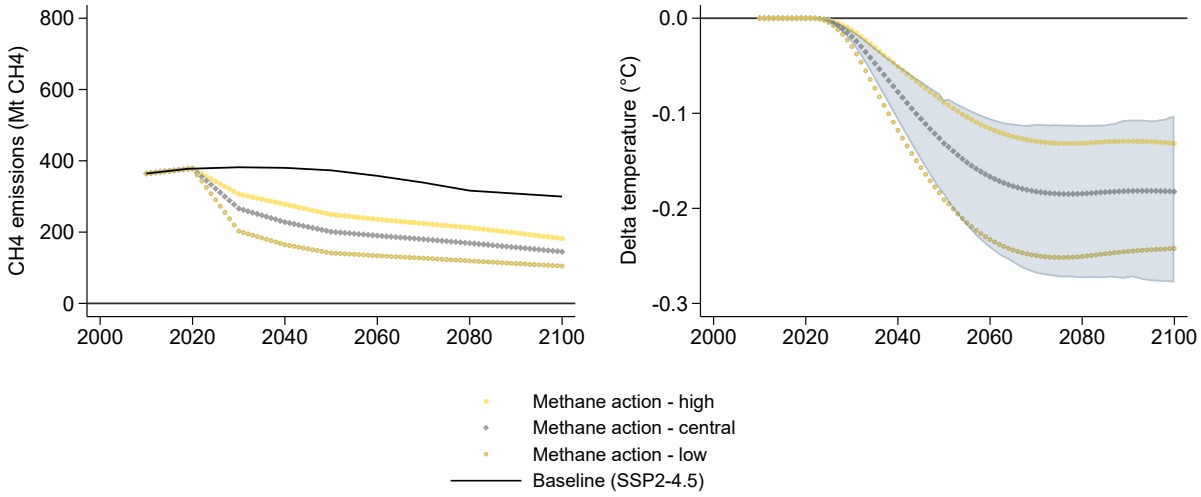

temperature, and is quantified as the 90% confidence interval. The expected 0.13°C of avoided warming in 2050 on the central methane scenario is lower than the ~0.3°C of avoided warming reported in the Global Methane Assessment (*7*) using similar emissions-temperature impulse-response functions to those in FaIR. The difference is presumably due to higher baseline emissions in the Global Methane Assessment, more consistent with no policy than current policies. Fig. S2 in the SM shows that the temperature reduction is 0.2°C in 2050 relative to an SSP3-7.0 baseline. This is still lower than the Global Methane Assessment but both scenario and temperature-response uncertainty extend to ~0.3°C.

Total economic benefits of methane action

Fig. 2 plots the total economic benefits (avoided market damages) of the methane action scenarios over the rest of this century. Under the SSP2-4.5 background scenario, climate change causes mean damages equivalent to a 1.8% loss in global consumption in 2030, rising to 3.5% in 2050 and 6.1%

in 2100 (since savings rates are fixed in META, these percentages also apply to global GDP). These are relative to counterfactual consumption along SSP2-4.5 without climate change. Focusing on 2050, the central methane action scenario reduces damages by 0.4 % points, from 3.5% of global consumption to 3.1%. In absolute money terms, this reduction in damages – the gross benefit of global methane action – equates to a little over $1 trillion per year in 2050 (in 2020 prices). The range of uncertainty across the high-low methane scenario variants is a 0.3-0.6 % point reduction in damages. The range of uncertainty (90% confidence interval) conditional on the central methane scenario is larger than this, running from 0.2 to 0.7 % points. This comes from the joint effect of many parametric uncertainties in META, including climate uncertainties in FaIR, uncertainties in the tipping point modules and in the interactions between tipping points, and uncertainties in the temperature and sea-level damage functions. Further analysis in Fig. S3 in the SM shows that, as expected, total climate damages are higher under the SSP3-7.0 background scenario and that the reduction in damages due to methane action is around a quarter higher than under SSP2-4.5 (a reduction in damages of 0.5 % points in 2050).

The above estimates of total economic benefits can only be properly understood when compared to the total costs of methane action. It is also important to take into account non-market climate damages and the direct health co-benefits of methane action via improved air quality. META contains a non-market damages module, but, as a social-cost IAM focused on damages (*46*), META does not include abatement costs or air quality co-benefits. Therefore, we bring in data on abatement costs and air quality co-benefits from previous major studies (*7, 8*) (see Methods). Table 1 reports the results of the CBA. Three out of five estimates of abatement costs are negative throughout, thus the central methane action scenario would pay for itself irrespective of climate benefits. The mechanism behind negative abatement costs is the opportunity for private profits, including revenue from methane capture/use in the energy sector, reduced disposal costs and increased revenue from waste recycling instead of landfilling, and yield increases from abatement measures in rice farming. In these three cost scenarios, IIASA low/high and EPA low, the net present value (NPV) of the central methane scenario ranges from $0.6-5.2trn without climate benefits, $7.0-11.5trn including climate benefits (market and non-market), and $13.0-17.5trn additionally including air quality co-benefits (2.5% discount rate).

Although “bottom-up” estimates of GHG abatement costs can yield substantial negative-cost

Figure 2: **Reduction in total climate damages due to methane action**. Left panel shows total climate damages expressed as a percentage loss in consumption relative to a no-climate change counterfactual. Right panel shows the gross monetary value of avoided damages, i.e., benefits of methane action. The shaded area is the 90% confidence interval, based on parametric uncertainty in META sampled by 1000 Monte Carlo runs. Specification includes market damages and tipping points.

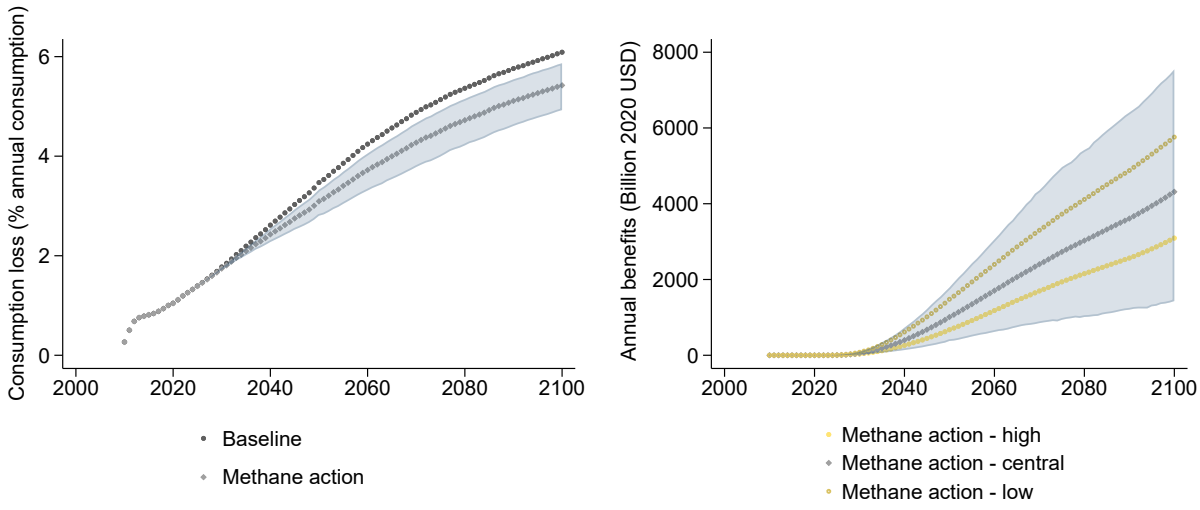

potential (*47*), such measures face behavioral, financial, informational and structural barriers, which prevent them from being realized. These can be conceptualized as hidden costs of adoption. Especially the low-cost scenarios implicitly assume that implementation of the Global Methane Pledge reduces the barriers to adoption of negative-cost measures. Alternatively, a conservative approach would be to place particular emphasis on the two scenarios with positive abatement costs, EPA high and Harmsen et al. (*8*). The latter scenario explicitly assumes there are no negative-cost measures. However, here again the benefits of methane action far exceed the costs, giving an NPV of $4.4-4.5trn ($10.4-10.5trn including air quality co-benefits), or equivalently a benefit-cost ratio of 3.3-3.4 (6.5-6.7 including air quality co-benefits). As a further alternative, we can back-calculate what constant stream of undiscounted abatement costs would be necessary to drive the NPV of the central methane scenario to zero. This 'switching value' is $301.6bn/year ($589.0bn/year including air quality co-benefits), much higher than any of the cost scenarios except for Harmsen et al. (*8*) towards 2050 if air-quality co-benefits are ignored. The cost-benefit comparison is also

Table 1: **Comparison of benefits and costs of central methane scenario**. All values are in USD 2020 billions. Discount rate is 2.5%. Values for 2030, 2040, and 2050 are snapshots of benefits and abatement costs in single years. Net present values (NPVs) represent the discounted sums for years 2020 through 2050.

		2030	2040	2050	NPV
Climate benefits (market)		52.2	401.0	1008.5	5310.0
Climate benefits (non-market)		9.1	70.3	200.4	1001.8
Air quality co-benefits		298.8	393.3	444.6	6015.7
Abatement costs	EPA low	-34.0	-39.7	-45.3	-638.3
	EPA high	108.2	113.8	119.5	1885.2
	IIASA low	-226.6	-342.5	-458.4	-5176.3
	IIASA high	-186.4	-123.1	-59.7	-2387.7
	Harmsen et al. (2019)	18.3	130.9	437.6	1847.8
Discounted net climate benefits (market and non-market)	EPA low	74.4	311.8	597.9	6950.1
	EPA high	-36.6	218.2	519.4	4426.6
	IIASA low	224.9	496.6	794.8	11488.1
	IIASA high	193.5	362.7	604.8	8699.4
	Harmsen et al. (2019)	33.6	207.7	367.7	4464.0
Discounted net climate benefits (market and non-market) and air quality co-benefits	EPA low	307.8	551.8	809.9	12965.7
	EPA high	196.7	458.2	731.4	10442.2
	IIASA low	458.3	736.6	1006.8	17503.7
	IIASA high	426.9	602.7	816.8	14715.1
	Harmsen et al. (2019)	267.0	447.7	579.7	10479.6

conservative in the sense that we only consider costs and benefits in the period 2020-2050. Methane has an atmospheric residence time of around nine years, so this approach omits benefits of abatement towards 2050 that occur after the end of the horizon. Persistence of climate damages has a similar effect.

Distributional effects of methane action

It is well known that climate damages are heterogeneous across the world for reasons of differential exposure and sensitivity/adaptive capacity. META incorporates both of these sources of heterogeneity. Insofar as these are correlated with national income, so will be the benefits of methane action. Fig. 3 explores the relationship between national income and benefits of methane action directly by taking country-level avoided market damages from methane action and aggregating them according to the World Bank's four country groupings: low-income, lower-middle income, upper-middle income and high-income. These damages are differences in consumption levels, before utility/welfare valuation. Larger benefits from methane action are concentrated in low-, lower-middle and to a lesser extent upper-middle income countries, while high-income countries, which tend to be located at higher latitudes, benefit the least. With the exception of low-income versus lower-middle income countries, group differences across countries are statistically significant at the 10% level or lower for any pairwise comparison of World Bank income groups. Fig. S4 in the SM repeats this analysis under the SSP3-7.0 background scenario, showing that the equity benefits of methane mitigation are robust to switching to an emissions scenario with substantially higher emissions. Fig. S5 in the SM also repeats this analysis on a scenario with rapid methane action plus action on CO_2, in order to explore whether the effects of methane abatement on inequality are different from CO_2 abatement. We find the effects are very similar, which indicates that action on methane and CO_2 are equally pro-poor. Lastly, Fig. S6 in the SM repeats the analysis for avoided market and non-market damages together. It shows that once again benefits are negatively correlated with income, but the differences are now smaller and statistically insignificant, because non-market benefits increase with income.

Effect of methane action on climate risk

Fig. 4 reports the effect of methane action on climate risk. Methane action reduces climate risks, shifting the probability density function of damages in 2050 to the left (downward). Mean damages (market) fall from 3.5 to 3.1% as mentioned above, and the standard deviation of damages decreases from 1.5 to 1.4. As measures of tail risk, we compute Value at Risk (VaR) and Conditional VaR (CVaR) at the 95% and 99% confidence levels. These are defined as damages at the 95th/99th

Figure 3: **Change in climate damages in 2050 by central methane action scenario, disaggregated by World Bank country income group**. Violin plots combine a kernel density plot and a box plot. Box plot contains estimates for the median (white dot), interquartile range (black box) and +/- 1.5 times the interquartile range (range of thin dark gray line). Note negative values signify avoided climate change damages. Specification includes market damages and tipping points.

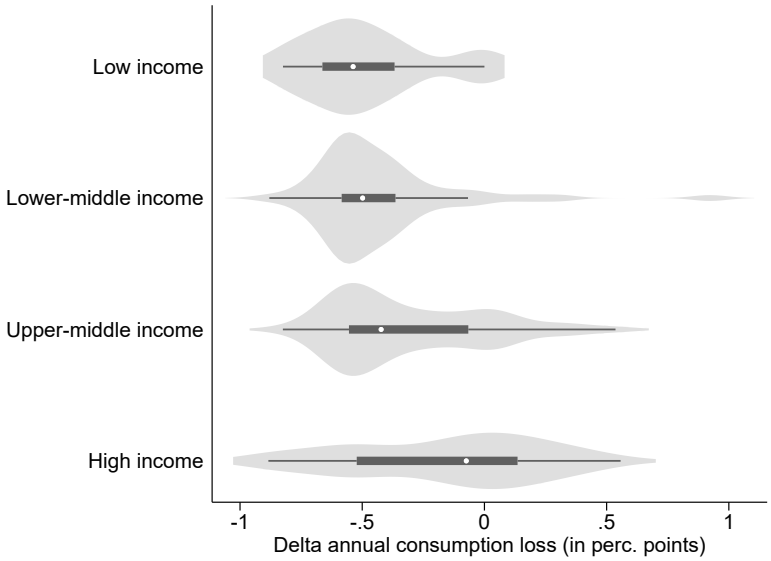

percentiles (VaR), and average damages above the 95th/99th percentiles (CVar). Methane action reduces VaR at the 95% confidence level from 6.4 to 5.9%, and at the 99% confidence level from 7.8% to 7.3%. CVaR at the 95% confidence level is reduced from 7.4% to 6.7%, and at the 99% confidence level from 8.9% to 8.0%. Thus, methane action reduces climate risk in general, including tail risk. Without tipping points, the effects of methane action are very similar but if anything they are slightly larger in relative terms, indicating that methane action is slightly more effective in reducing damages from other channels. Additional analysis in Fig. S7 in the SM shows that methane action similarly reduces climate risk under a SSP3-7.0 background scenario, albeit on higher baseline climate damages.

This raises the question, what is the effect of methane action on tipping points themselves? As explained in more detail in (*40*) and in the SM, economic models of tipping points synthesized by META belong to two distinct classes. One class is process-based models, where each equation directly represents an underlying geophysical process. The permafrost carbon feedback (PCF),

Figure 4: **Probability density functions for climate damages in 2050 with methane action (red) and without (grey). Left panel includes tipping points, right panel omits tipping points.** Specification includes market damages. The height of each bar corresponds to the frequency of observations in the corresponding bin. Table reports associated distribution statistics (% of consumption lost in 2050 due to climate change).

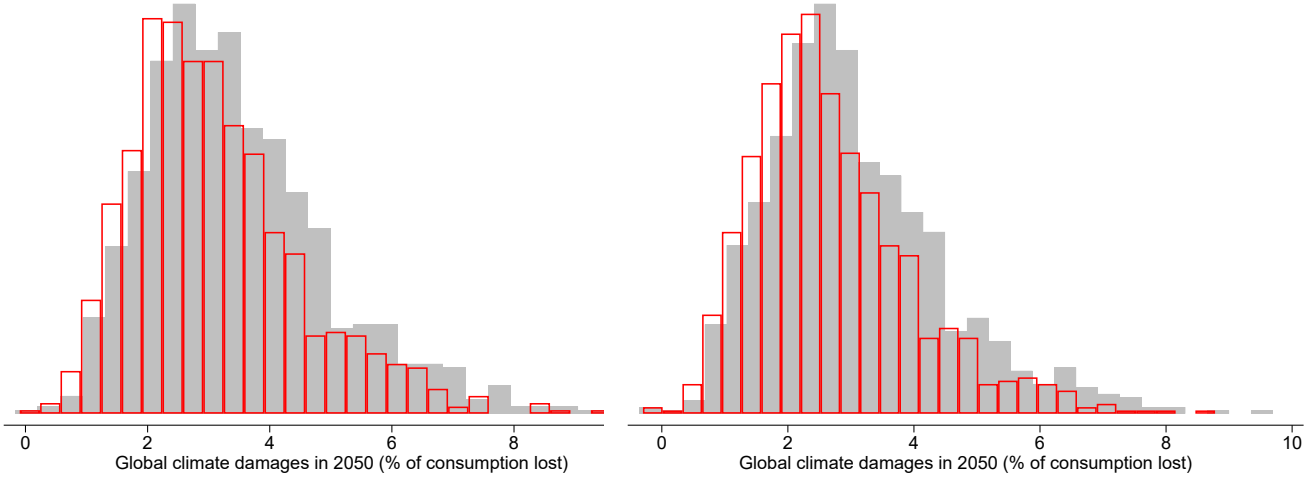

	Mean	Std. dev.	VaR 95%	VaR 99%	CVaR 95%	CVaR 99%
Tipping points						
Baseline	3.5	1.5	6.4	7.8	7.4	8.9
Methane action	3.1	1.4	5.9	7.3	6.7	8.0
No tipping points						
Baseline	3.1	1.4	5.9	7.3	6.8	8.1
Methane action	2.7	1.3	5.3	6.5	6.2	7.4

melting of the Antarctic and Greenland Ice Sheets (AIS and GIS, respectively), and variability of the Indian Summer Monsoon (ISM) are modeled in this way. The other class uses survival analysis, whereby the underlying geophysical processes are represented more abstractly by a hazard event with an associated hazard rate. Slowdown of the Atlantic Meridional Overturning Circulation (AMOC) and Amazon rainforest dieback (AMAZ) are modeled in this second way. Both classes of model are probabilistic in META.

As a common measure of the extent to which different climate tipping elements have 'tipped',

Figure 5: **Percentage change in tipping point intensity due to methane action, for six tipping points**. Background emissions scenario is SSP2-4.5. Tipping point indicators are described in the methods section.

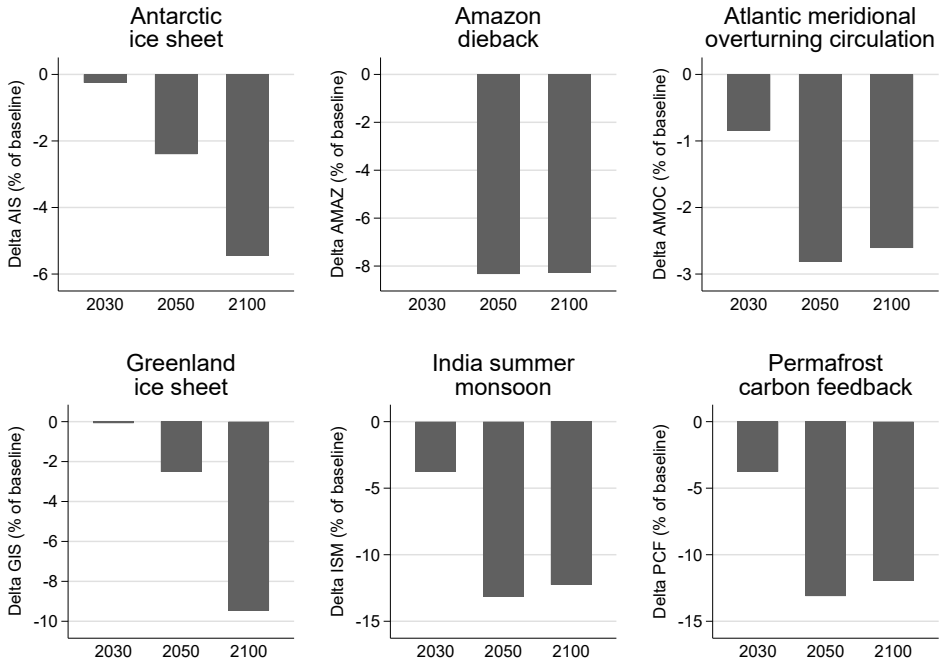

here we report an indicator of tipping point intensity on a scale from zero to one (see SM). Zero corresponds to tipping elements whose state has been completely unaltered by climate change, and one corresponds to elements that have fully transitioned to an alternative state (as such it is similar to the tipping state variable in (*48*)). An indicator value of 0.5 means half-transformed in the case of process-based models (e.g., the Ice Sheets are half-melted), or a hazard event that is 50% likely in the case of the survival-analysis models. Although it is damages from tipping points that ultimately matter, one advantage of this physical indicator is that it focuses attention on tipping processes, whose impacts are particularly poorly covered by existing economic studies. AMOC slowdown and Amazon dieback are leading examples (*40*). As can be seen in Fig. 5, methane action takes time to affect tipping point intensity. By 2050, however, the effect of methane action on tipping points becomes more clear. AIS and GIS tipping intensity decreases by 2.5%, the likelihood of AMOC slowdown decreases by 3%, the likelihood of Amazon dieback decreases by 8%, and ISM and PCF tipping intensity falls by 13%. After 2050, the effect of methane action on tipping point intensity

generally mimics the effect of methane action on global mean temperature by plateauing. The exceptions are AIS and GIS tipping intensity, which are subject to considerable inertia. Therefore, methane action has its largest effect on these by the end of the century, reducing tipping intensity by ~5.5% (AIS) and 9.5% (GIS). Fig. S8 in the SM again repeats the analyses in this section under the SSP3-7.0 background scenario, finding larger reductions in tipping point intensity than under SSP2-4.5.

Social cost of methane, and non-cooperative action

The top panel of Fig. 6 shows probability density functions for the SC-CH_4 in 2020. These estimates reflect the marginal damage (market and non-market) from one metric tonne of CH_4 emitted in 2020. The distribution has a strong positive skew with a mean of \$7,381/tCH_4, a median of \$6,837 and a 90% confidence interval of \$3,824-11,548. We also plot the corresponding PDF excluding all tipping points, which has a mean of \$6,307. Thus, the tipping points we include increase the mean SC-CH_4 by 17%. If the more speculative ocean methane hydrates tipping point is included, the SC-CH_4 in 2020 is \$23,319, which is 270% higher than the SC-CH_4 without tipping points. This is a far bigger impact of the ocean methane hydrates tipping point than on the SC-CO_2 (*40*). In the SM, we report the results of Global Sensitivity Analysis of the SC-CH_4 with respect to climate, damage and tipping-point parameters.

Table S1 in the SM reports values for the SC-CH_4 in future years. These increase due to rising incomes and temperatures. For an emission in 2030, the mean SC-CH_4 in our preferred specification is \$9,988/tCH_4, rising to \$13,824 for an emission in 2050 and \$27,044 for an emission in 2100. This corresponds to a compound annual real growth rate of 1.6% between 2020 and 2100. The SM also reports values for the SC-CO_2. The mean SC-CO_2 in 2020, including tipping points, is \$309/tCO_2, rising to \$485 in 2050 and \$688 in 2100, a compound annual real growth rate of 1%. The ratio of the SC-CH_4 to the SC-CO_2 is 24 in 2020, rising to 39 in 2100. This ratio can be compared to the GWP of methane, which is 27-30 when measured over 100 years and 81-83 when measured over 20 years (*49*). Thus, using GWP100 would slightly overstate the value of methane abatement in the short run and slightly understate it in the long run, with the crossover period being about mid-century (SC-CH_4/SC-CO_2=28.5 in 2050). Using GWP20 would greatly overstate the value of

Figure 6: **Probability density function for the global SC-CH_4 in 2020 (top panel) and map of expected values of national SC-CH_4s (bottom panel)**. Social costs are reported in 2020 US dollars for a 2020 emissions pulse in the SSP2-4.5 emissions scenario. Welfare changes are normalized to global mean consumption per capita for global SC-CH_4 and national mean consumption per capita for national SC-CH_4s. Specification includes non-market damages, EMUC=1.05, and PRTP=0.5%. Tipping points are included in map. Previous estimates of the global SC-CH_4 are superimposed on the probability density function.

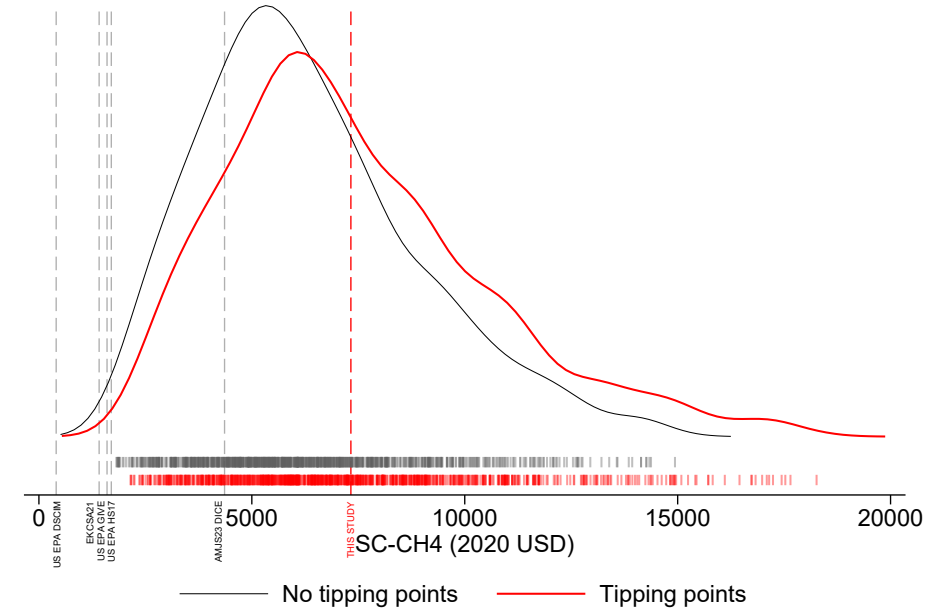

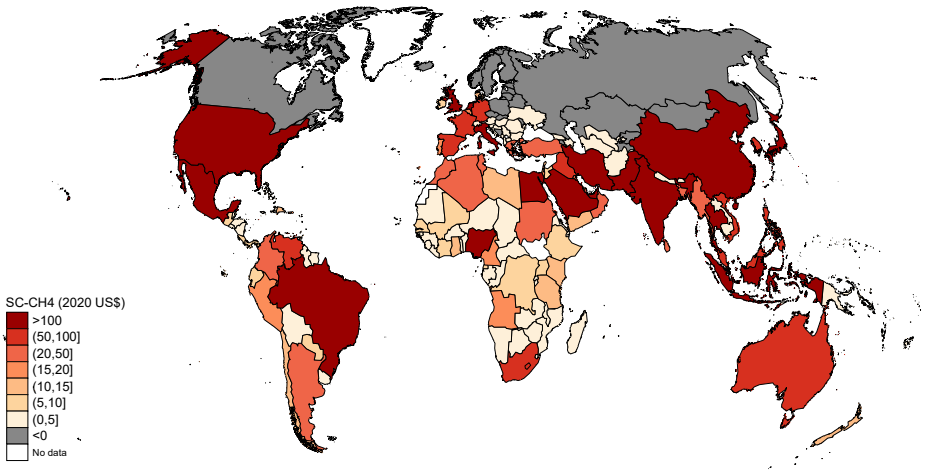

methane abatement. The discount rate is a factor here. Building on the expert survey results of (*50*) and recent changes in practice (*51*), we set a pure rate of time preference of $\rho = 0.5\%$ and an elasticity of marginal utility of consumption $\eta = 1.05$. With global economic growth on SSP2-4.5 of $g \sim 2\%$, this yields a discount rate of $r = \rho + \eta g \sim 2.5\%$ (as g varies over time, country and Monte Carlo draw, this is approximate). Results from Table S2 in the SM show that if we instead set $\rho = 1\%$ and $\eta = 1.5$, the ratio is 39 in 2020, higher than GWP100 but still much lower than GWP20. GWP100 appears to be a reasonable approximation of the relative social value of methane action, with two caveats: (i) it is a better approximation at low discount rates; (ii) these results are obtained from META and are hence limited to an analysis of avoided climate damages, rather than air quality co-benefits.

The bottom panel of Fig. 6 reports the SC-CH_4 at the national level. To the best of our knowledge, we are the first to provide country-level estimates of the SC-CH_4. Previous studies such as (*52*) have provided country-level estimates of the SC-CO_2. Formally, the social cost of a GHG is the change in social welfare from emitting one tonne of the GHG, divided by the marginal utility of consumption to convert it into money units. The choice of consumption level for the denominator is important. The higher this is, the smaller is the marginal utility of consumption under the standard assumption of diminishing marginal utility, the smaller is the denominator in turn, and the higher is the SC-GHG in money terms. Using global mean consumption per capita normalizes national welfare changes to the same level and effectively disaggregates the global SC-GHG that each country would refer to under full international cooperation into national shares. If instead each country's welfare change is normalized using its own national consumption per capita, this yields an estimate of climate damages to that country valued at its own income level. This corresponds to the SC-GHG that each country would use under non-cooperation. Since we already analyzed the implications of cooperative global methane abatement for global inequality above, we take the latter approach. Studying non-cooperative incentives is also highly relevant in current geopolitical conditions.

Negative SC-CH_4s are reported for 20 primarily high-latitude countries, consistent with previous results generated from non-linear temperature damage functions (*53*), even allowing for additional damage channels in META. These countries would not have a private incentive to reduce methane emissions at the margin today, assuming of course that META's damage estimates are not biased

towards being too small. 159 countries have a positive SC-CH_4 and 17 of these have a national SC-CH_4 above \$100/tCH_4, The three highest national values are for China (\$536/tCH_4), India (\$548/tCH_4) and the United States (\$1112/tCH_4). The size of the US SC-CH_4 is notable as it implies significant methane abatement would be optimal even if the US returned to the first Trump administration practice of valuing only domestic damages from domestic methane abatement, as seems highly likely. The European Union (EU27)'s SC-CH_4 – computed as the sum of its member states' national SC-CH_4s – is \$631/tCH_4, above China's and India's.

Discussion

The basic message of this paper is that the benefits of global methane action look so much larger than the costs that the economic case for action is clear. Implementation of the Global Methane Pledge might come at a negative cost, according to leading estimates from (*43*) and (*10*). Even if one is skeptical of negative abatement-cost estimates, our modeling suggests much higher benefits from avoided climate damages and improved air quality. An important part of the global benefit of methane abatement is that avoided climate damages are higher in low- and middle-income countries, making the climate benefits of methane abatement pro-poor. Another important factor is that methane abatement reduces climate risk to the economy, something the risk-averse social planner values. Implementation of the Global Methane Pledge supposes a high degree of cooperation between countries, but in a world of fracturing geopolitics it is worth asking how much methane abatement countries should undertake in their own self-interest. We analyzed this by estimating each country's domestic marginal damages and found that methane abatement at marginal costs of several hundred US\$/tCH_4 is economical for several major players such as China, the EU, India and the US (where the domestic SC-CH_4 is as high as US\$1,112/tCH_4). Lastly, while the best basis for comparing methane and CO_2 abatement should be relative social costs, we have found that the convention of using GWP100 is a reasonable approximation.

How do our estimates of climate benefits from methane abatement compare with previous literature? Estimates of climate benefits are famously sensitive to the discount rate (albeit less so for methane than CO_2, due to its shorter atmospheric residence time), so any comparison needs to control for the discount rate as far as possible. It also needs to adjust for inflation, so we inflate

values reported in previous studies where necessary using the US GDP deflator. In terms of total benefits of global methane action scenarios, the only point of comparison is (*23*). Using an aggregate damage function from a meta-analysis (*54*), they estimate total benefits of somewhere in the range of approximately US$3.5-10 trillion for discount rates of 2% and 3%. Our estimates overlap this range significantly but are at the high end of it.

In terms of marginal damages, our global estimate of the 2020 SC-CH_4 (e.g., mean of US$7,381/t$CH_4$) can be compared with a wider range of studies. (*32*) calculate the SC-CH_4 by coupling a set of four Simple Climate Models to damages from the DICE and FUND IAMs. For a discount rate of 2.5% and on a high-emissions scenario (RCP8.5), they report a multi-model mean estimate of $1,414/t$CH_4$ and a 90% confidence interval of $678–2,454. But some model combinations yield values close to $4,000, notably using DICE damages instead of FUND. The United States Environmental Protection Agency (*55*) reports values of $470/t$CH_4$ with damages from the DSCIM IAM, $1,600 with damages from the GIVE IAM and $1,700 with damages from (*54*), for a near-term discount rate of 2.5%. Using an updated version of DICE (including FaIR v2.0.0), (*35*) estimate $4,360/t$CH_4$, within a range of $959–8,829. Their central estimate is generated along the optimal emissions path using a comparable discount rate to ours, and a damage function calibrated on (*54*) like the US EPA meta-analysis variant (but choosing a different model variant in (*54*) with higher damages for given temperature). Their SC-CH_4 exhibits strong sensitivity to the emissions path, however, and when it is calculated on a business-as-usual path it is at the high end of their reported range, about 20% above our central estimate.

Overall, our estimated SC-CH_4 is higher than most of the existing literature, including estimates provided in the latest US EPA guidance. In particular, it extends the uncertainty range well above $10,000. Having controlled for the discount rate and with META using an almost identical climate model to (*55*) and (*35*) (FaIR), remaining differences in the SC-CH_4 most likely arise from different socio-economic/emissions scenarios, different spatial disaggregation and different modeling of damages (such as inclusion of tipping points in META). One point to note is that our mean estimate looks consistent with (*35*) when one considers that we calculate the SC-CH_4 on an emissions path that is between their optimum and BAU. But the analysis in (*35*) is deterministic – we add quantification of uncertainty, which naturally spreads the distribution of the SC-CH_4 to higher values. Another point to note is that META combines spatial disaggregation to the country level with

welfare valuation using diminishing marginal utility. Thus, SC-GHG estimates from META include so-called "distributional/equity weighting", unlike (*55*), or (*23*) for total benefits. The literature on the SC-CO_2 shows that estimates can increase strongly after distributional weighting (*56, 57*), because greater value is placed on damages in low-income countries, which are relatively higher. This is not to be confused with the opposite role of diminishing marginal utility in normalizing welfare changes discussed above when computing national SC-CH_4s.

There are several limitations to the current study. Like any IAM, META is affected by multiple uncertainties ranging from what emissions/socio-economic scenario to choose, through how the climate system responds to emissions, to, in particular, the damages climate change causes and the welfare value of those damages. We have sought to quantify those uncertainties both through scenario analysis and probabilistic modeling, but the resulting climate benefits could be mis-estimated and uncertainty is likely under-estimated, on balance. On the other side of the ledger, the abatement costs provided for (*7*) that we use could also be mis-estimated. Our analysis only quantifies the impacts of methane emissions via climate damages and air pollution on health. But methane emissions have other economic impacts, for example, via ground-level ozone reducing agricultural productivity. Moreover, as is standard in economic benefit-cost analysis, we abstract from political costs. Still, the economic case for methane action is clear.

Brief summary of methods

Our methods are described in detail in the Supplementary Materials. In summary, we proceed in three steps.

First, we create a set of emissions scenarios, which simulate methane action at the global level. These are anchored on successful achievement in 2030 of the 30% emissions reduction target in the Global Methane Pledge, followed by continued methane abatement post-2030. They are built using raw scenario data from the IAMC 1.5°C Scenario Explorer (*58*). These methane action scenarios are then superposed on a set of background emissions scenarios, which (i) set baseline methane emissions for comparison and (ii) set emissions of CO_2 and the other GHGs and radiative forcing agents, which are held constant while methane emissions are varied. We consider a range of background emissions/forcing scenarios: a low-emissions scenario that limits the increase in global

mean temperature to 1.5°C above pre-industrial with low/no overshoot, a "middle-of-the-road" emissions/socio-economic scenario (SSP2-4.5), and a higher emissions scenario characterized by "regional rivalry" in economic/political relations (SSP3-7.0). This approach assumes that methane action can be independent of action on other GHGs to a first-order approximation, which is supported by evidence that targeted methane abatement measures, which would be sufficient to achieve the Global Methane Pledge, do not also reduce CO_2 (e.g., improved leak detection and repair in oil and gas infrastructure; landfill gas capture) (*7*). Note that the opposite is unlikely to be true: CO_2 abatement would also reduce methane (e.g., switching to renewables reduces fossil fuel use, which in turn reduces methane emissions from upstream fossil fuel production and distribution).

The second step is to take the scenarios and run them through the META IAM to project climate and economic effects. For this paper, we implemented several improvements and updates to the META model, including: converting the model to the open-source Mimi.jl platform; integrating the FaIRv2.0.0 climate model (*42*); re-estimating our downscaling functions from global to national temperature on the CMIP6 dataset instead of CMIP5; replacing the original West Antarctic Ice Sheet tipping point module with a new Antarctic Ice Sheet tipping point module (*41*), which replicates the impulse responses of major Ice Sheet Models (*59*); revising hazard rates for the Atlantic Meridional Overturning Circulation and Ocean Methane Hydrates tipping point modules; revising estimates of the country-level temperature damage function parameters, still using (*53*); and improving the representation of non-market damages using more up-to-date literature (*54*). These changes, as well as the full set of equations comprising the META model, are described in the SM.

The third step brings in additional, scenario-consistent data on methane abatement costs and air quality co-benefits. For the former, we use sectoral estimates of methane abatement costs from (*43*) and (*10*), which were used in the Global Methane Assessment (*7*), to construct streams of undiscounted abatement costs from 2020 to 2050 that are compatible with the quantity of abatement required to shift methane emissions from current trends to the central methane action scenario. We also use the methane MAC curve estimated by (*8*) to construct a further stream of undiscounted abatement costs over the same period. For the latter, we again use data from the Global Methane Assessment (*7*), from which we obtain estimates of premature deaths from respiratory and cardiovascular diseases due to tropospheric ozone generated by methane emissions. We convert these to marginal economic damages using the VSL and assumptions about the income elasticity

of a VSL. We then multiply this quantity by the emissions reductions from our methane action scenarios, giving us a stream of undiscounted air-quality co-benefits.

References and Notes

1. IPCC, *Climate Change 2021: The Physical Science Basis. Contribution of Working Group I to the Sixth Assessment Report of the Intergovernmental Panel on Climate Change*, V. Masson-Delmotte, *et al.*, eds. (Cambridge University Press, Cambridge, UK and New York, NY, USA, 2021).

2. D. Shindell, *et al.*, The methane imperative, *Frontiers in Science* **2** (2024).

3. J. Canadell, *et al.*, *Climate Change 2021: The Physical Science Basis. Contribution of Working Group I to the Sixth Assessment Report of the Intergovernmental Panel on Climate Change*, V. Masson-Delmotte, *et al.*, eds. (Cambridge University Press, Cambridge, UK and New York, NY, USA, 2021), book section 5.

4. M. Saunois, *et al.*, Global methane budget 2000–2020, *Earth System Science Data* **In press** (2025).

5. L. Feng, P. Palmer, S. Zhu, R. Parker, Y. Liu, Tropical methane emissions explain large fraction of recent changes in global atmospheric methane growth rate, *Nature Communications* **13**, 1378 (2022).

6. Z. Qu, *et al.*, Inverse modeling of 2010–2022 satellite observations shows that inundation of the wet tropics drove the 2020–2022 methane surge, *Proceedings of the National Academy of Sciences* **121**, e2402730121 (2024).

7. UN Environment, Climate and Clean Air Coalition, *Global Methane Assessment: Benefits and Costs of Mitigating Methane Emissions* (UN Environment, Nairobi, 2021).

8. M. Harmsen, *et al.*, Long-term marginal abatement cost curves of non-co 2 greenhouse gases, *Environmental Science and Policy* **99**, 136 (2019).

9. M. Harmsen, *et al.*, The role of methane in future climate strategies: mitigation potentials and climate impacts, *Climatic Change* **163**, 1409 (2020).

10. L. Höglund-Isaksson, A. Gómez-Sanabria, Z. Klimont, P. Rafaj, W. Schöpp, Technical potentials and costs for reducing global anthropogenic methane emissions in the 2050 timeframe–results from the gains model, *Environmental Research Communications* **2**, 025004 (2020).

11. I. B. Ocko, *et al.*, Acting rapidly to deploy readily available methane mitigation measures by sector can immediately slow global warming, *Environmental Research Letters* **16**, 054042 (2021).

12. I. B. Ocko, *et al.*, Unmask temporal trade-offs in climate policy debates, *Science* **356**, 492 (2017).

13. C. S. Malley, *et al.*, A roadmap to achieve the Global Methane Pledge, *Environmental Research: Climate* **2**, 011003 (2023).

14. R. T. Pierrehumbert, Short-lived climate pollution, *Annual Review of Earth and Planetary Sciences* **42**, 341 (2014).

15. European Commission, United States of America, Global Methane Pledge (2021).

16. J. Rogelj, M. Meinshausen, M. Schaeffer, R. Knutti, K. Riahi, Impact of short-lived non-CO2 mitigation on carbon budgets for stabilizing global warming, *Environmental Research Letters* **10**, 075001 (2015).

17. W. J. Collins, *et al.*, Increased importance of methane reduction for a 1.5 degree target, *Environmental Research Letters* **13**, 054003 (2018).

18. D. Shindell, *et al.*, Simultaneously mitigating near-term climate change and improving human health and food security, *Science* **335**, 183 (2012).

19. J. K. Shoemaker, D. P. Schrag, M. Molina, V. Ramanathan, What role for short-lived climate pollutants in mitigation policy?, *Science* **342**, 1323 (2013).

20. A. Stohl, *et al.*, Evaluating the climate and air quality impacts of short-lived pollutants, *Atmospheric Chemistry and Physics* **15**, 10529 (2015).

21. M. T. Lund, *et al.*, A continued role of short-lived climate forcers under the shared socioeconomic pathways, *Earth System Dynamics* **11**, 977 (2020).

22. S. J. Smith, *et al.*, Impact of methane and black carbon mitigation on forcing and temperature: a multi-model scenario analysis, *Climatic Change* **163**, 1427 (2020).

23. B. Cael, P. Goodwin, Global methane pledge versus carbon dioxide emission reduction, *Environmental Research Letters* **18**, 104015 (2023).

24. A. Hu, Y. Xu, C. Tebaldi, W. M. Washington, V. Ramanathan, Mitigation of short-lived climate pollutants slows sea-level rise, *Nature Climate Change* **3**, 730 (2013).

25. S. Fankhauser, The social costs of greenhouse gas emissions: an expected value approach, *Energy Journal* **15**, 157 (1994).

26. M. Hoel, I. Isaksen, *Control and Game-Theoretic Models of the Environment*, C. Carraro, J. A. Filar, eds. (Birkhäuser Boston, Boston, MA, 1995), pp. 89–105.

27. R. S. Tol, The marginal costs of greenhouse gas emissions, *The energy journal* **20**, 61 (1999).

28. C. Hope, The marginal impact of co2 from page2002: An integrated assessment model incorporating the ipcc's five reasons for concern, *Integrated Assessment* **6** (2006).

29. A. L. Marten, S. C. Newbold, Estimating the social cost of non-co2 ghg emissions: Methane and nitrous oxide, *Energy Policy* **51**, 957 (2012).

30. D. Shindell, J. Fuglestvedt, W. Collins, The social cost of methane: theory and applications, *Faraday Discussions* **200**, 429 (2017).

31. M. C. Sarofim, S. T. Waldhoff, S. C. Anenberg, Valuing the ozone-related health benefits of methane emission controls, *Environmental and Resource Economics* **66**, 45 (2017).

32. F. C. Errickson, K. Keller, W. D. Collins, V. Srikrishnan, D. Anthoff, Equity is more important for the social cost of methane than climate uncertainty, *Nature* **592**, 564 (2021).

33. J. Sampedro, S. Waldhoff, M. Sarofim, R. Van Dingenen, Marginal damage of methane emissions: ozone impacts on agriculture, *Environmental and Resource Economics* **84**, 1095 (2023).

34. U.S. Environmental Protection Agency, Report on the Social Cost of Greenhouse Gases: Estimates Incorporating Recent Scientific Advances. November 2023, *Tech. rep.* (2023).

35. C. Azar, J. G. Martín, D. J. Johansson, T. Sterner, The social cost of methane, *Climatic Change* **176**, 71 (2023).

36. R. Schmalensee, Comparing greenhouse gases for policy purposes, *The Energy Journal* **14** (1993).

37. D. S. Mallapragada, B. K. Mignone, A theoretical basis for the equivalence between physical and economic climate metrics and implications for the choice of global warming potential time horizon, *Climatic Change* **158**, 107 (2020).

38. N. Stern, *The Economics of Climate Change: the Stern Review* (Cambridge University Press, 2007).

39. S. Dietz, C. Hepburn, Benefit–cost analysis of non-marginal climate and energy projects, *Energy Economics* **40**, 61 (2013).

40. S. Dietz, J. Rising, T. Stoerk, G. Wagner, Economic impacts of tipping points in the climate system, *Proceedings of the National Academy of Sciences* **118**, e2103081118 (2021).

41. S. Dietz, F. Koninx, Economic impacts of melting of the Antarctic Ice Sheet, *Nature Communications* **13**, 5819 (2022).

42. N. J. Leach, *et al.*, Fairv2.0.0: a generalized impulse response model for climate uncertainty and future scenario exploration, *Geoscientific Model Development* **14**, 3007 (2021).

43. U.S. Environmental Protection Agency, Global Non-CO2 Greenhouse Gas Emission Projections & Marginal Abatement Cost Analysis: Methodology Documentation. EPA-430-R-19-012., *Tech. rep.* (2019).

44. United Nations Environment Programme, *Executive summary. Emissions Gap Report 2023: Broken Record – Temperatures hit new highs, yet world fails to cut emissions (again).* (2023).

45. X. Lan, K. Thoning, E. Dlugokencky, Trends in globally-averaged CH4, N2O, and SF6 determined from NOAA Global Monitoring Laboratory measurements. version 2024-02 (2022).

46. S. Dietz, *Handbook of the Economics of Climate Change* (Elsevier, 2024), vol. 1, pp. 1–51.

47. M. J. Kotchen, J. A. Rising, G. Wagner, The costs of "costless" climate mitigation, *Science* **382**, 1001 (2023).

48. Y. Cai, T. S. Lontzek, The Social Cost of Carbon with Economic and Climate Risks, *Journal of Political Economy* **127**, 2684 (2019). Publisher: The University of Chicago Press.

49. P. Forster, *et al.*, *Climate Change 2021: The Physical Science Basis. Contribution of Working Group I to the Sixth Assessment Report of the Intergovernmental Panel on Climate Change*, V. Masson-Delmotte, *et al.*, eds. (Cambridge University Press, Cambridge, UK and New York, NY, USA, 2021), book section 7.

50. M. Drupp, M. Freeman, B. Groom, F. Nesje, Discounting disentangled, *American Economic Journal: Economic Policy* **10**, 109 (2018).

51. United States Office of Management and Budget, Circular No. A-4 (November 9, 2023), *Tech. rep.* (2023).

52. K. Ricke, L. Drouet, K. Caldeira, M. Tavoni, Country-level social cost of carbon, *Nature Climate Change* **8**, 895 (2018).

53. M. Burke, S. M. Hsiang, E. Miguel, Global non-linear effect of temperature on economic production, *Nature* **527**, 235 (2015).

54. P. H. Howard, T. Sterner, Few and not so far between: a meta-analysis of climate damage estimates, *Environmental and Resource Economics* **68**, 197 (2017).

55. U.S. Environmental Protection Agency, Report on the Social Cost of Greenhouse Gases: Estimates Incorporating Recent Scientific Advances, *Tech. rep.* (2022).

56. F. Dennig, M. B. Budolfson, M. Fleurbaey, A. Siebert, R. H. Socolow, Inequality, climate impacts on the future poor, and carbon prices, *Proceedings of the National Academy of Sciences* **112**, 15827 (2015).

57. D. Anthoff, J. Emmerling, Inequality and the social cost of carbon, *Journal of the Association of Environmental and Resource Economists* **6**, 243 (2019).

58. D. Huppmann, *et al.*, IAMC 1.5C Scenario Explorer and Data hosted by IIASA, Integrated Assessment Modeling Consortium & International Institute for Applied Systems Analysis (2018).

59. A. Levermann, *et al.*, Projecting Antarctica's contribution to future sea level rise from basal ice shelf melt using linear response functions of 16 ice sheet models (LARMIP-2), *Earth System Dynamics* **11**, 35 (2020).

60. K. Riahi, *et al.*, The Shared Socioeconomic Pathways and their energy, land use, and greenhouse gas emissions implications: An overview, *Global Environmental Change* **42**, 153 (2017).

61. Z. R. J. Nicholls, *et al.*, Reduced complexity model intercomparison project phase 1: introduction and evaluation of global-mean temperature response, *Geoscientific Model Development* **13**, 5175 (2020).

62. M. Meinshausen, *et al.*, The Shared Socio-economic Pathway (SSP) greenhouse gas concentrations and their extensions to 2500, *Geoscientific Model Development* **13**, 3571 (2020).

63. C.-H. Cheng, S. A. Redfern, Impact of interannual and multidecadal trends on methane-climate feedbacks and sensitivity, *Nature communications* **13**, 3592 (2022).

64. S. Gulev, *et al.*, *Climate Change 2021: The Physical Science Basis. Contribution of Working Group I to the Sixth Assessment Report of the Intergovernmental Panel on Climate Change*, V. Masson-Delmotte, *et al.*, eds. (Cambridge University Press, Cambridge, UK and New York, NY, USA, 2021), book section 2, pp. 287–422.

65. S. Szopa, *et al.*, *Climate Change 2021: The Physical Science Basis. Contribution of Working Group I to the Sixth Assessment Report of the Intergovernmental Panel on Climate Change*, V. Masson-Delmotte, *et al.*, eds. (Cambridge University Press, Cambridge, UK and New York, NY, USA, 2021), book section 6, pp. 817–921.

66. D. B. Diaz, Estimating global damages from sea level rise with the coastal impact and adaptation model (ciam), *Climatic Change* **137**, 143 (2016).

67. A. S. Manne, R. G. Richels, *Energy and environment* (Springer, 2005), pp. 175–189.

68. P. Klenow, I. Nath, V. Ramey, How Much Will Global Warming Cool Global Growth?, *Tech. rep.*, Working paper (2023).

69. E. Kriegler, J. W. Hall, H. Held, R. Dawson, H. J. Schellnhuber, Imprecise probability assessment of tipping points in the climate system, *Proceedings of the National Academy of Sciences* **106**, 5041 (2009).

70. R. G. Newell, B. C. Prest, S. E. Sexton, The gdp-temperature relationship: implications for climate change damages, *Journal of Environmental Economics and Management* **108**, 102445 (2021).

71. G. Casey, S. Fried, E. Goode, Projecting the impact of rising temperatures: The role of macroeconomic dynamics, *IMF Economic Review* pp. 1–31 (2023).

72. A. Saltelli, *et al.*, *Global sensitivity analysis: the primer* (John Wiley & Sons, 2008).

73. B. Anderson, E. Borgonovo, M. Galeotti, R. Roson, Uncertainty in climate change modeling: can global sensitivity analysis be of help?, *Risk Analysis* **34**, 271 (2014).

74. E. Plischke, An effective algorithm for computing global sensitivity indices (easi), *Reliability Engineering & System Safety* **95**, 354 (2010).

75. P. Wei, Z. Lu, X. Yuan, Monte carlo simulation for moment-independent sensitivity analysis, *Reliability Engineering & System Safety* **110**, 60 (2013).

76. A. Saltelli, I. M. Sobol, About the use of rank transformation in sensitivity analysis of model output, *Reliability Engineering & System Safety* **50**, 225 (1995).

77. L. Kessler, Estimating the economic impact of the permafrost carbon feedback, *Climate Change Economics* **8**, 1750008 (2017).

78. C. Hope, K. Schaefer, Economic impacts of carbon dioxide and methane released from thawing permafrost, *Nature Climate Change* **6**, 56 (2016).

79. D. Yumashev, *et al.*, Climate policy implications of nonlinear decline of arctic land permafrost and other cryosphere elements, *Nature Communications* **10**, 1900 (2019).

80. G. Whiteman, C. Hope, P. Wadhams, Climate science: vast costs of arctic change, *Nature* **499**, 401 (2013).

81. N. Shakhova, V. Alekseev, I. Semiletov, Predicted methane emission on the east siberian shelf, *Doklady Earth Sciences* **430**, 190 (2010).

82. M. Ceronsky, D. Anthoff, C. Hepburn, R. S. Tol, Checking the price tag on catastrophe: the social cost of carbon under non-linear climate response, *Tech. rep.*, ESRI working paper (2011).

83. Y. Cai, T. M. Lenton, T. S. Lontzek, Risk of multiple interacting tipping points should encourage rapid co2 emission reduction, *Nature Climate Change* **6**, 520 (2016).

84. D. Archer, B. Buffett, V. Brovkin, Ocean methane hydrates as a slow tipping point in the global carbon cycle, *Proceedings of the National Academy of Sciences* **106**, 20596 (2009).

85. D. Archer, A model of the methane cycle, permafrost, and hydrology of the Siberian continental margin, *Biogeosciences* **12**, 2953 (2015).

86. W. Nordhaus, Economics of the disintegration of the greenland ice sheet, *Proceedings of the National Academy of Sciences* **116**, 12261 (2019).

87. R. B. Alley, *et al.*, History of the greenland ice sheet: paleoclimatic insights, *Quaternary Science Reviews* **29**, 1728 (2010).

88. A. Robinson, R. Calov, A. Ganopolski, Multistability and critical thresholds of the greenland ice sheet, *Nature Climate Change* **2**, 429 (2012).

89. J. Garbe, T. Albrecht, A. Levermann, J. F. Donges, R. Winkelmann, The hysteresis of the antarctic ice sheet, *Nature* **585**, 538 (2020).

90. K. Frieler, *et al.*, Consistent evidence of increasing antarctic accumulation with warming, *Nature Climate Change* **5**, 348 (2015).

91. D. Anthoff, F. Estrada, R. S. Tol, Shutting down the thermohaline circulation, *American Economic Review: Papers and Proceedings* **106**, 602 (2016).

92. O. Bahn, N. R. Edwards, R. Knutti, T. F. Stocker, Energy policies avoiding a tipping point in the climate system, *Energy Policy* **39**, 334 (2011).

93. M. Belaia, M. Funke, N. Glanemann, Global warming and a potential tipping point in the atlantic thermohaline circulation: the role of risk aversion, *Environmental and Resource Economics* **67**, 93 (2017).

94. K. Keller, B. M. Bolker, D. F. Bradford, Uncertain climate thresholds and optimal economic growth, *Journal of Environmental Economics and Management* **48**, 723 (2004).

95. R. J. Lempert, A. H. Sanstad, M. E. Schlesinger, Multiple equilibria in a stochastic implementation of dice with abrupt climate change, *Energy Economics* **28**, 677 (2006).

96. P. M. Link, R. S. Tol, Possible economic impacts of a shutdown of the thermohaline circulation: an application of fund, *Portuguese Economic Journal* **3**, 99 (2004).

97. P. M. Link, R. S. Tol, Estimation of the economic impact of temperature changes induced by a shutdown of the thermohaline circulation: an application of fund, *Climatic Change* **104**, 287 (2011).

98. M. E. Schlesinger, *et al.*, *Avoiding Dangerous Climate Change* (Cambridge University Press, Cambridge, UK, 2006), pp. 37–47.

99. T. M. Lenton, J.-C. Ciscar, Integrating tipping points into climate impact assessments, *Climatic Change* **117**, 585 (2013).

100. T. Stocker, *et al.*, *Climate Change 2013: The Physical Science Basis. Contribution of Working Group I to the Fifth Assessment Report of the Intergovernmental Panel on Climate Change*, T. Stocker, *et al.*, eds. (Cambridge University Press, Cambridge, United Kingdom and New York, NY, USA, 2013), pp. 33–115.

101. O. Hoegh-Guldberg, *et al.*, *Global Warming of 1.5°C. An IPCC Special Report on the impacts of global warming of 1.5°C above pre-industrial levels and related global greenhouse gas*

emission pathways, in the context of strengthening the global response to the threat of climate change, sustainable development, and efforts to eradicate poverty, V. Masson-Delmotte, *et al.*, eds. (in press, 2018).

102. S. N. Gosling, The likelihood and potential impact of future change in the large-scale climate-earth system on ecosystem services, *Environmental Science & Policy* **27**, S15 (2013).

103. M. Belaia, Integrated assessment of climate tipping points, Ph.D. thesis, Universität Hamburg Hamburg (2017).

104. M. Ikefuji, J. R. Magnus, H. Sakamoto, The effect of health benefits on climate change mitigation policies, *Climatic Change* **126**, 229 (2014).

105. J. Schewe, A. Levermann, A statistically predictive model for future monsoon failure in india, *Environmental Research Letters* **7**, 044023 (2012).

106. R. H. Moss, *et al.*, The next generation of scenarios for climate change research and assessment, *Nature* **463**, 747 (2010).

107. C. Li, *et al.*, India is overtaking china as the world's largest emitter of anthropogenic sulfur dioxide, *Scientific Reports* **7**, 14304 (2017).

108. R. J. Millar, Z. R. Nicholls, P. Friedlingstein, M. R. Allen, A modified impulse-response representation of the global near-surface air temperature and atmospheric concentration response to carbon dioxide emissions, *Atmospheric Chemistry and Physics* **17**, 7213 (2017).

109. G. Myhre, *et al.*, *Climate Change 2013: The Physical Science Basis. Contribution of Working Group I to the Fifth Assessment Report of the Intergovernmental Panel on Climate Change*, T. Stocker, *et al.*, eds. (IPCC, 2013), pp. 8SM–1–8SM–44.

110. J. A. Church, N. J. White, Sea-level rise from the late 19th to the early 21st century, *Surveys in Geophysics* **32**, 585 (2011).

111. D. Diaz, K. Keller, A potential disintegration of the west antarctic ice sheet: implications for economic analyses of climate policy, *American Economic Review: Papers and Proceedings* **106**, 607 (2016).

112. B. C. O'Neill, *et al.*, A new scenario framework for climate change research: the concept of Shared Socioeconomic Pathways, *Climatic Change* **122**, 387 (2014).

113. S. Dietz, N. Stern, Endogenous growth, convexity of damages and climate risk: how nordhaus' framework supports deep cuts in carbon emissions, *Economic Journal* **125**, 574 (2015).

114. M. Golosov, J. Hassler, P. Krusell, A. Tsyvinski, Optimal taxes on fossil fuel in general equilibrium, *Econometrica* **82**, 41 (2014).

115. E. E. McDuffie, *et al.*, The social cost of ozone-related mortality impacts from methane emissions, *Earth's Future* **11**, e2023EF003853 (2023).

116. W. D. Nordhaus, J. Boyer, *Warming the World: Economic Models of Global Warming* (MIT Press (MA), 2000).

117. K. Rennert, *et al.*, Comprehensive evidence implies a higher social cost of CO2, *Nature* **610**, 687 (2022).

118. World Bank, World development indicators (2020).

119. T. Stoerk, J. Rising, D. Shindell, S. Dietz, Replication package for "Global methane action pays for itself at least six times over" (2025).

Acknowledgments

We thank Tamma Carleton for detailed discussant's comments, Zeb Nicholls for sharing emissions data, as well as audiences at the Asian Development Bank, Barcelona School of Economics, Environmental Defense Fund, European Commission, IE Business School, LSE, NOVA Business School, Oxford, Resources for the Future, ASSA, AERE, AERNA, the Atlantic Workshop on Energy and Environmental Economics, CEPR Paris Symposium and EAERE for their helpful feedback. This work does not necessarily represent the views of the National Bank of Belgium or the Eurosystem.

Funding: D.S. acknowledges the financial support of the Global Methane Hub. S.D. acknowledges the financial support of the Grantham Foundation for the Protection of the Environment.

Author contributions: S.D., J.R., and T.S. conceived the study. D.S. and T.S. constructed the scenarios with input from J.R. and S.D.. S.D., J.R., and T.S. adapted the model, with J.R. leading on software development and implementation. S.D., J.R., and T.S. produced the results and analyzed the data. S.D., J.R., D.S., and T.S. wrote the manuscript.

Competing interests: There are no competing interests to declare.

Data and materials availability: All data underlying the Model for Economic Tipping point Analysis (META) used in this study is fully documented in the SM and draws on public sources. The version of META used in this study is freely available on Github under the following tag: `https://github.com/openmodels/META/releases/tag/META-2025`. All climate data and code necessary to reproduce the analytical steps and results in this work is available from the following permanent public repository: `https://zenodo.org/records/15363212` (*119*).

Supplementary Materials: Materials and methods

Supplementary text

META model description

Figs. S1 to S10

Tables S1 to S4

References (60-119).

Science
AAAS

Supplementary Materials for

Global methane action pays for itself at least six times over

Thomas Stoerk, James Rising, Drew Shindell, Simon Dietz

Corresponding author: Thomas Stoerk, t.a.stoerk@lse.ac.uk

The PDF file includes:

1 Materials and methods

1.1 Methane scenarios

We construct CH_4 action scenarios that are anchored on achievement of the Global Methane Pledge's 30% emissions reduction below the 2020 level in 2030, followed by continued CH_4 abatement post-2030. Reducing CH_4 emissions by 30% between 2020 and 2030 is in line with CH_4 emissions reductions in many 1.5°C scenarios with low/no overshoot. Therefore, we build our CH_4 action scenarios using raw scenario data from the IAMC 1.5°C Scenario Explorer [58]. Although the achievement of the Global Methane Pledge itself could be simulated as a simple linear reduction of 30% from 2020, IAM-based scenarios provide an internally consistent projection of what further emissions reductions might follow after 2030. The range of 1.5°C scenarios with low/no overshoot also enables us to quantify uncertainty across IAMs in technical CH_4 abatement potential and in policy implementation (within the context of CH_4 action beyond current trends). Only models producing global emissions of CO_2, CH_4, N_2O and SO_2 are chosen, so that a consistent set of inputs is provided to META (SO_2 is an input to META's Indian Summer Monsoon module).

1.5°C scenarios with low/no overshoot from the IAMC 1.5°C Scenario Explorer are first harmonized to produce identical emissions in 2020. The central CH_4 scenario is then the average of 34 1.5°C scenarios with low/no overshoot that achieve approximately a 30% cut in CH_4 emissions on the 2020 level in 2030. The low/high CH_4 emissions scenarios are created from 19 and 5 of the 1.5°C scenarios with low/no overshoot, respectively, which project CH_4 emissions reductions in 2030 that are higher/lower than the Global Methane Pledge target. CH_4 emissions post-2100 are projected based on SSP1-1.9.

Baseline CH_4 emissions, and background emissions of CO_2 and other GHGs/radiative forcing agents are obtained from the SSP database [60] and the IAMC 1.5°C Scenario Explorer. These are also harmonized to give identical emissions between 2010 and 2020. To extend baseline/background emissions data beyond 2100, we use the extended SSP scenarios of [61, 62].

We abstract from the positive feedback on natural CH_4 emissions from wetlands, which increases as temperatures rise following the discussion in [2]. Other feedbacks, including from melting permafrost and atmospheric chemistry, are included in META as described below. Regarding the wetland feedback, according to [3], this feedback is expected to be 0.03 +/- 0.01 $W/m^2/°C$, compared with the roughly 2.6 W/m^2 forcing required to increase transient warming by 1°C. Accounting for an additional positive feedback from atmospheric CO_2 on wetland CH_4 emissions increases the

range of the overall estimated feedback to 0.01-0.16 W/m^2/°C, still relatively small. [63] provide a more recent empirical estimate of the wetland feedback of 0.08 W/m^2/°C. The strength of the feedback can also be constrained using paleoclimate data. For example, the CH_4 change during the transition between the last glacial maximum and the Holocene was a response to climate change. The feedback can be estimated based on the CH_4 change of ∼390-750 ppb over this time that accompanied a global mean warming of ∼6°C [64], leading to a direct forcing of 0.3 W/m^2, which is increased by ∼36% to 0.4 W/m^2 when accounting for the chemical responses of ozone, stratospheric water vapor and CO_2 to CH_4 emissions [65]. The feedback in this case is thus 0.07 W/m^2/°C, similar to the other estimates.

1.2 META IAM overview and settings for this study

META (Model for Economic Tipping point Analysis) is a modular IAM designed to estimate the social cost of GHGs. It was designed primarily to incorporate various climate tipping points, each as a module. The original set of tipping point modules replicated studies in the climate economics literature, with the aim of providing a structural meta-analysis [40]. META can be run without tipping points, in which case it functions as a standard IAM of the social-cost type (other social-cost IAMs include DSCIM, `https://github.com/ClimateImpactLab/dscim-epa`, and GIVE, `https://github.com/rffscghg/MimiGIVE.jl`). The model is described in full detail in Section 3 and is publicly available at `https://github.com/openmodels/META`. In brief, META's main modules are:

- **Emissions and socio-economic scenarios**: these are exogenous and are normally taken from the Shared Socio-Economic Pathway (SSP) database. Emissions scenarios are extended beyond 2100 as in [40], while we developed a method of extending the corresponding paths for economic growth and population that is described in Section 3. For this study, we developed bespoke CH_4 scenarios, as explained above.

- **GHG cycles and temperature change**: GHG emissions drive atmospheric concentrations and the change in global mean temperature using the FaIR simple climate model, version 2.0.0 [42]. CO_2 and CH_4 are modeled explicitly, while other GHGs and forcing agents are handled via an exogenous radiative forcing term. An important feature of FaIR is that GHG cycles are state-dependent. In the case of CH_4, this is calibrated on the dependency between atmospheric CH_4 removal and the atmospheric CH_4 concentration, tropospheric air temperature

and water vapor mixing ratio.

- **Country-level temperature damages**: changes in global mean temperature are downscaled to the national level using a statistical relationship based on CMIP6 data. AMOC slowdown also modulates the relationship between global and national temperatures. Changes in national mean temperature are then fed into nonlinear, country-specific damage functions calibrated on empirical evidence from [53].

- **Country-level damages from sea-level rise (SLR)**: changes in global mean temperature drive global mean SLR via thermal expansion and melting of small ice caps and glaciers, plus additional SLR from the Antarctic and Greenland Ice Sheet tipping point modules. Global mean SLR is then mapped directly onto damages at the country level using a set of country SLR damage functions calibrated on high-resolution coastal impact modeling [66]. Uncertainty about how well countries will adapt to SLR is incorporated in the stochastic parameters of the SLR damage functions.

- **Flood and drought due to the Indian Summer Monsoon**: in India, GDP is additionally affected by variability of the summer monsoon, which determines the occurrence of drought or flood via a tipping point module.

- **Persistence of damages**: we adopt a flexible specification allowing damages from temperature and SLR (and in India from the summer monsoon) to affect either the short-term level of GDP or long-term growth prospects. A persistence parameter modulates the extent to which GDP in a given year depends on actual, post-damage GDP in the previous year, or potential GDP in the previous year according to the exogenous growth scenario. Complete dependence on the former corresponds to perfect persistence (pure growth damages), while complete dependence on the latter corresponds to zero persistence (pure levels damages).

- **Non-market damages**: to these sources of market damages can be added non-market damages using a set of country-level non-market damage functions from the MERGE IAM [67]

with an updated calibration on [54]. Non-market damages capture climate damages that affect welfare through channels not governed by market activity and depend on both income and temperature. Examples for such channels include mortality, as well as loss of species and biodiversity.

- **Consumption, welfare and the social cost of GHGs**: National GDP per capita is converted into national consumption per capita using country-specific exogenous savings rates, estimated using World Bank data on savings over the period 2005 to 2015. Consumption per capita is converted into utility per capita using an isoelastic utility function and this is aggregated into social welfare using a utilitarian social welfare functional. To estimate the social cost of a GHG, we run the model twice with consistent assumptions, the second time with an additional pulse of emissions in the year 2020. The social cost is the difference in welfare between the two runs per ton of GHG emissions, converted into dollar equivalents.

- **Tipping point modules**: META incorporates eight tipping point modules: (1) the PCF results in additional CO_2 and CH_4 emissions, which flow back into their respective cycles; (2) dissociation of ocean CH_4 hydrates results in additional CH_4 emissions, which flow back into the CH_4 cycle; (3) Arctic sea ice loss (also known as the surface albedo feedback) results in changes in radiative forcing, which directly affect warming; (4) dieback of the Amazon rainforest releases CO_2, which flows back into the CO_2 cycle; disintegration of the (5) AIS and (6) GIS increases SLR; (7) slowdown of the AMOC modulates the relationship between global mean temperature and national mean temperature; (8) variability of the Indian summer monsoon directly affects GDP per capita in India. Thus, tipping points do not directly cause damages (except for (8)). Instead, they affect temperatures or SLR, which in turn cause damages.

For most of the results in this study, we run META with the following specific settings:

- **Discounting**: based on the expert survey results of [50], we set a pure rate of time preference $\rho = 0.5\%$ and an elasticity of marginal utility of consumption $\eta = 1.05$. The former enters the social welfare function, the latter the utility function – welfare changes are calculated directly – but as an approximation one can think of the consumption/money discount rate as $r = \rho + \eta g$, where g is the growth rate of consumption per capita.

- **Persistence of damages**: this is calibrated to 0.25 (75% weight on post-damage GDP in the previous year) based on new results from macro-economics [68]. This implies a relatively high degree of damage persistence.

- **Tipping points**: the surface albedo feedback is switched on in all cases including the no-tipping-point runs, as the surface albedo feedback is conceptually part of the climate's base response to forcing. Runs with tipping points on include all featured tipping points except the dissociation of ocean CH_4 hydrates, which are only used for sensitivity analysis given its low likelihood.

- **Non-market damages**: these are switched on.

We run Monte Carlo simulations with a sample size of 1000 to ease computation. As shown in Section 2, our testing of META found that calculations are robust to use of different random seeds and to increasing the sample size by an order of magnitude.

1.3 Abatement costs and air quality co-benefits from the Global Methane Assessment

We constructed four streams of undiscounted abatement costs from 2020 to 2050 by aggregating the sectoral estimates of [43] and IIASA [10]. We estimate a range of costs for both the EPA and IIASA data by varying the contribution of behavior changes towards total emissions abatement – the more is achieved by behavior change, the less is required of technical abatement measures, particularly those at high marginal cost. For a fifth scenario/cost stream, we used the methane marginal abatement cost (MAC) curve estimated by [8] (specifically their 2050 MAC curve). We fit an exponential function $\text{MAC}(\Delta E) = a\left(e^{b\Delta E} - 1\right)$ to the data reported in [8], where ΔE is the percentage change in methane emissions relative to the baseline. The fitted parameter values are $a = 0.0184$ and $b = 0.2011$ for units of 2010 US dollars per tonne of methane. We then integrate the MAC function over the methane emissions reductions given by our central methane scenario to generate total abatement costs.

We similarly constructed streams of undiscounted air quality co-benefits using data from the Global Methane Assessment [7] on premature deaths due to respiratory and cardiovascular diseases caused by tropospheric ozone formation attributable to methane. These air quality co-benefits are available at the country level for the year 2018. While methane is a well-mixed greenhouse gas, so that emissions from any location have virtually identical impacts on radiative forcing, the

tropospheric ozone response to methane is highly spatially variable. That photochemical response depends upon levels of nitrogen oxides (NO_x) and sunlight, as well as temperatures and levels of other volatile hydrocarbons and carbon monoxide. The health impacts of the ozone changes are in turn highly sensitive to population distributions and underlying health risks for specific populations. This leads to very distinct geographical patterns of methane-driven ozone-attributable health burdens.

Despite the highly inhomogeneous response to a specific methane change, population-weighted ozone changes have been shown to be extremely linear across a range of methane increases and decreases at the national level [7]. Our use of national level impacts therefore captures a large part of the heterogeneity of the response to methane emissions changes (although within-country heterogeneity adds complexity beyond the scope of our analysis). We note that the ozone response does exhibit some sensitivity to background nitrogen oxide conditions, but this is a second-order effect [7].

We aggregate these to the global level using assumptions about the value of a statistical life (VSL) and its income elasticity taken from the Global Methane Assessment [7], and extrapolate over the period 2020 to 2050 assuming a constant economic value of avoided health damages per tonne of methane emitted. This extrapolation is conservative in the sense that it does not account for an increasing VSL over time due to rising incomes in the socioeconomic scenarios we consider in this study.

1.4 Tipping point intensity indicators

As a common measure of the extent to which different climate tipping elements have 'tipped', we compute an indicator of tipping point intensity on a scale from zero to one. Zero corresponds to tipping elements whose state has been completely unaltered by climate change, and one corresponds to elements that have fully transitioned to an alternative state (as such it is similar to the tipping state variable in 48). An indicator value of 0.5 means half-transformed in the case of process-based models (e.g., the Ice Sheets are half-melted), or a hazard event that is 50% likely in the case of the survival-analysis models.

For the cryospheric tipping points (PCF, AIS and GIS), tipping intensity is mapped onto the proportion of ice mass that has melted. For PCF and GIS, the tipping point modules include a

variable that represents this directly:

$$I_{\text{PCF}}(t) = 1 - PF_{\text{extent}}(t), \tag{1}$$

$$I_{\text{GIS}}(t) = 1 - V_{\text{GIS}}(t), \tag{2}$$

where $PF_{\text{extent}}(t)$ is the area of permafrost remaining at time t relative to time zero, and $V_{\text{GIS}}(t)$ is the volume of the GIS expressed as a fraction of the initial volume. Both have a range of zero to one. For AIS, there is no single variable describing the proportion of initial ice volume that has melted. There is a function mapping subsurface ocean temperatures into a flow of basal melting, and a function mapping basal melt into SLR increase. [69] provide a definition of AIS tipping in terms of SLR, which we can instead use to define the extent to which the AIS has tipped. Note that [69] only consider the West AIS, therefore we constrain our analysis to the four regions of West Antarctica accordingly. In their questionnaire, [69] define WAIS tipping as a state where "West Antarctica becomes an archipelago when discharge exceeds accumulation for warmer temperatures", and associate this with "4-6 meters of total sea level rise at potentially high rates". Accordingly, we define WAIS tipping as

$$I_{\text{WAIS}}(t) = 1/5\left[S(\text{Ross}, t) + S(\text{Amundsen}, t) + S(\text{Weddell}, t) + S(\text{Peninsula}, t)\right]. \tag{3}$$

The sum of SLR over the four regions of the WAIS is divided by 1/5 because the final state of the system as defined by [69] is 5m SLR (midpoint of the 4-6m range).

For ISM, tipping intensity is a function of the strength of the Walker circulation, a key determinant of ISM activity:

$$I_{\text{ISM}}(t) = \min\left[10000\left[1 - m_{\text{NINO3.4}}(t)/m_{\text{NINO3.4}}(0)\right], 1\right], \tag{4}$$

where $m_{\text{NINO3.4}}(t)$ is the strength of the Walker circulation, i.e., the Pacific Ocean atmospheric circulation, in May.

For the tipping points modeled using survival analysis (AMAZ and AMOC), tipping intensity can be more straightforwardly interpreted as the probability of occurrence of the hazard event, corresponding to the indicator variables $I_{\text{AMAZ}}(t)$ and $I_{\text{AMOC}}(t)$, respectively. Section 3 provides further detail on how the variables on the right-hand sides of the above equations are determined.

2 Supplementary text

2.1 Results for alternative background scenarios

2.1.1 Methane action scenarios compared to alternative background scenarios

Figure S1 plots methane emissions on the methane action scenarios compared to alternative background scenarios (the main text uses SSP2-4.5, representative of a current trends and policies storyline). The left panel shows that mean methane emissions across 1.5°C scenarios with low or no overshoot from the IAMC 1.5°C Scenario Explorer fall within the range of our methane action scenarios, but the central methane action scenario actually has slightly higher emissions than this mean (4% higher in 2030). This just serves to put the Global Methane Pledge in the context of 1.5°C scenarios with low or no overshoot. The right panel compares the methane action scenarios with an SSP3-7.0 background scenario, which is intended to be representative of no policies. The central methane action scenario reduces emissions by 37% in 2030 relative to SSP3-7.0 (high-low range 28-52%), 60% in 2050 (range 51-72%) and 79% in 2100 (range 74-85%). Naturally these constitute larger cuts than if the background scenario is SSP2-4.5.

Figure S1: **Methane emissions on the methane action scenarios compared to mean emissions across 1.5°C scenarios with low/no overshoot from the IAMC 1.5°C Scenario Explorer (left panel) and SSP3-7.0 (right panel)**. 'Methane action - high' and 'Methane action - low' describe high and low methane emissions outcomes to capture policy uncertainty.

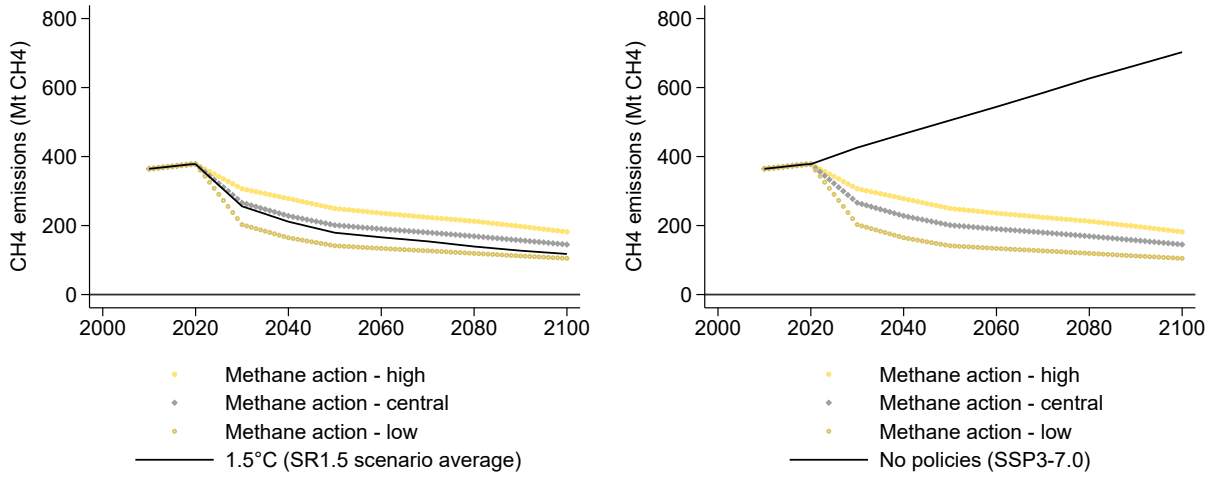

2.1.2 Temperature effect of methane action scenarios against an SSP3-7.0 background scenario

Figure S2 plots the reduction in global mean temperature due to the methane action scenarios, relative to an SSP3-7.0 background scenario. The central methane action scenario reduces warming by 0.03°C in 2030, 0.20°C in 2050 and 0.53°C in 2100. The range of uncertainty due to methane scenario uncertainty is 0.16-0.26°C in 2050. Temperature uncertainty conditional on the central methane scenario is 0.13-0.29°C in 2050, generated as in the main text by quantifying parametric uncertainty in META using Monte Carlo simulation. Unlike the comparison with SSP2-4.5, temperature reductions from methane action do not flatten out towards the end of the century, because under SSP3-7.0 emissions keep increasing.

Figure S2: **Reduction in global mean temperature due to methane action, relative to SSP3-7.0**. The shaded area is the 90% confidence interval of temperature outcomes conditional on the central methane action scenario, based on parametric uncertainty in META sampled by 1000 Monte Carlo runs. Specification includes tipping points.

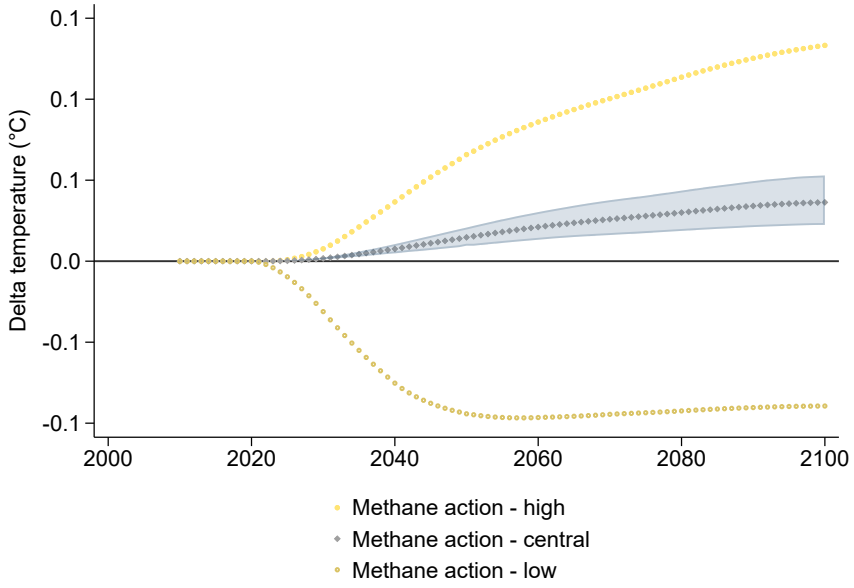

2.1.3 Avoided damages and total economic benefits of methane action relative to an SSP3-7.0 background scenario

Figure S3 plots the total economic benefits of the methane action scenarios over the rest of this century, relative to an SSP3-7.0 baseline. The top panel shows total climate damages expressed as a percentage loss in consumption relative to a no-climate-change counterfactual. The bottom panel

shows the gross monetary value of avoided damages, i.e., the benefits of methane action. Under the SSP3-7.0 background scenario, climate change causes damages equivalent to a 1.8% loss in global consumption in 2030, rising to 3.8% in 2050 and 10.2% in 2100 (since saving rates are fixed in META, these percentages also apply to global GDP). Focusing on 2050, the central methane action scenario reduces damages by 0.5 percentage points, from 3.8% of global consumption to 3.3%. In relative terms, damages are 15% lower. In absolute money terms, this reduction in damages – the gross benefit of global methane action – equates to a little over $2 trillion per year in 2050 (in 2020 prices), or double the economic benefits of methane action under SSP2-4.5. The range of uncertainty across the high-low methane scenario variants is a 0.4-0.7 percentage point reduction in damages. The range of uncertainty (90% confidence interval) conditional on the central methane scenario is larger than this, running from 0.2 to 1.0 percentage points. This comes from climate and economic parametric uncertainties.

Figure S3: **Reduction in total climate damages due to methane action, relative to SSP3-7.0**. Top panel shows total climate damages expressed as a percentage loss in consumption relative to a no-climate-change counterfactual. Bottom panel shows the gross monetary value of avoided damages, i.e., benefits of methane action. The shaded area is the 90% confidence interval, based on parametric uncertainty in META sampled by 1000 Monte Carlo runs. Specification includes market damages and tipping points.

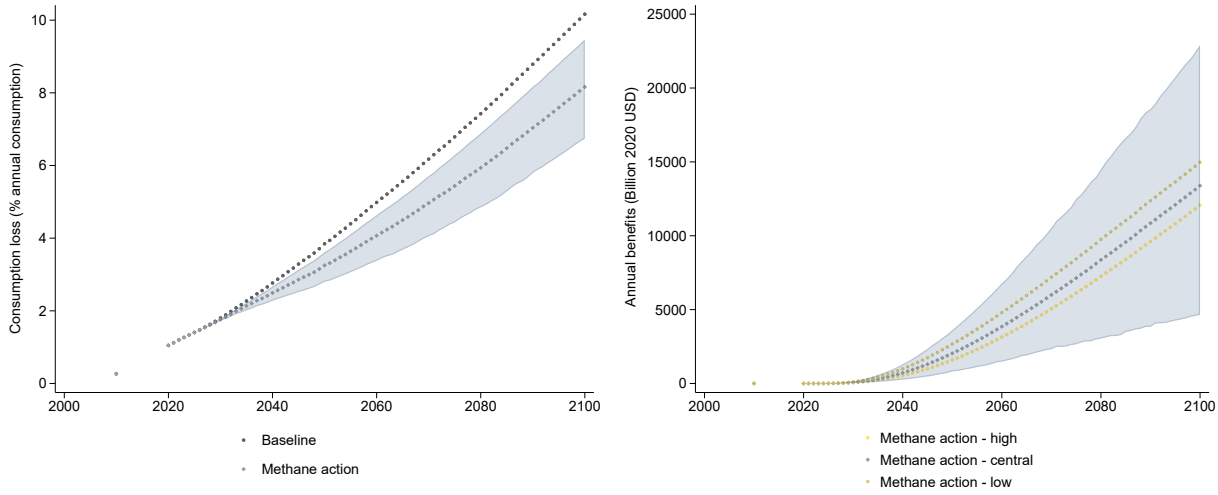

2.1.4 Distributional effects of methane action

Firstly, we test whether the distributional effects of methane action differ when we assume a different background scenario. To do so, Figure S4 disaggregates climate damages in 2050 avoided by the central methane action scenario relative to an SSP3-7.0 baseline scenario into World Bank country

income groups. Within each country income group, damages vary, and the four distributions are overlapping. Nonetheless, avoided damages tend to be greater in low- and lower-middle income countries relative to upper-middle and high-income countries. With the exception of low-income versus lower-middle income countries, group differences across countries are statistically significant at least at the 10% level for any pairwise comparison of World Bank income groups. This inequality result is similar to our main analysis with an SSP2-4.5 background scenario.

Figure S4: **Change in climate damages in 2050 by central methane action scenario, disaggregated by World Bank country income group**. Background scenario is SSP3-7.0. Violin plots combine a kernel density plot and a box plot. Box plot contains estimates for the median (white dot), interquartile range (black box) and +/- 1.5 times the interquartile range (range of thin dark gray line). Note negative values signify avoided climate change damages. Specification includes market damages and tipping points.

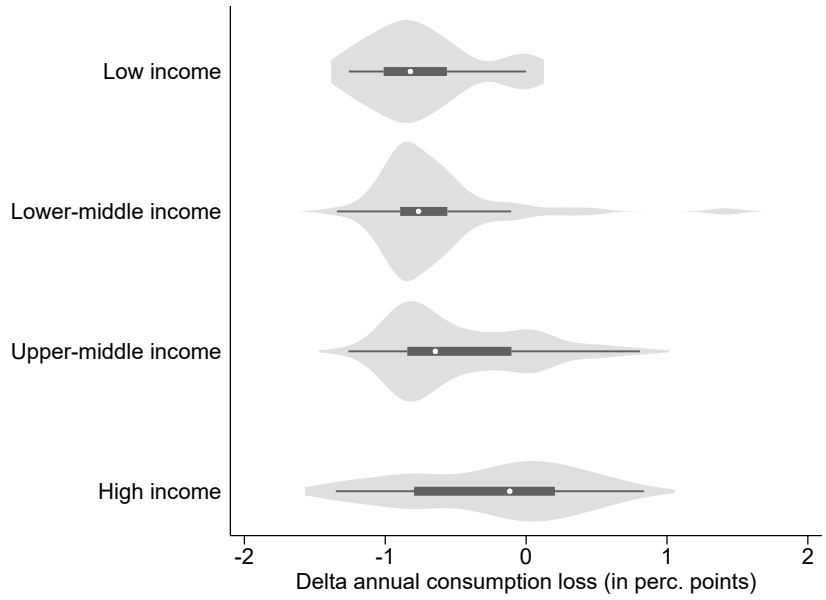

Next, we ask whether the distributional effects of methane action alone differ from the distributional effects of methane action combined with strong action on carbon dioxide. To do so, we make use of the 1.5°C scenario, which models a combination of ambitious mitigation of both gases. Figure S5 disaggregates climate damages in 2050, avoided by moving to the 1.5°C scenario from the SSP2-4.5 baseline scenario, into World Bank country income groups. As can be seen, the relative inequality effect of methane and carbon dioxide action combined is nearly identical to methane action alone. In other words, both types of climate policy are equally pro-poor. In absolute terms, methane and carbon dioxide action combined deliver about four times the climate benefits of methane action alone, however.

Figure S5: **Change in climate damages in 2050 by comprehensive climate action, disaggregated by World Bank country income group**. Comparison is for SSP2-4.5 vs. the 1.5°C scenario. Violin plots combine a kernel density plot and a box plot. Box plot contains estimates for the median (white dot), interquartile range (black box) and +/- 1.5 times the interquartile range (range of thin dark gray line). Note negative values signify avoided climate change damages. Specification includes market damages and tipping points.

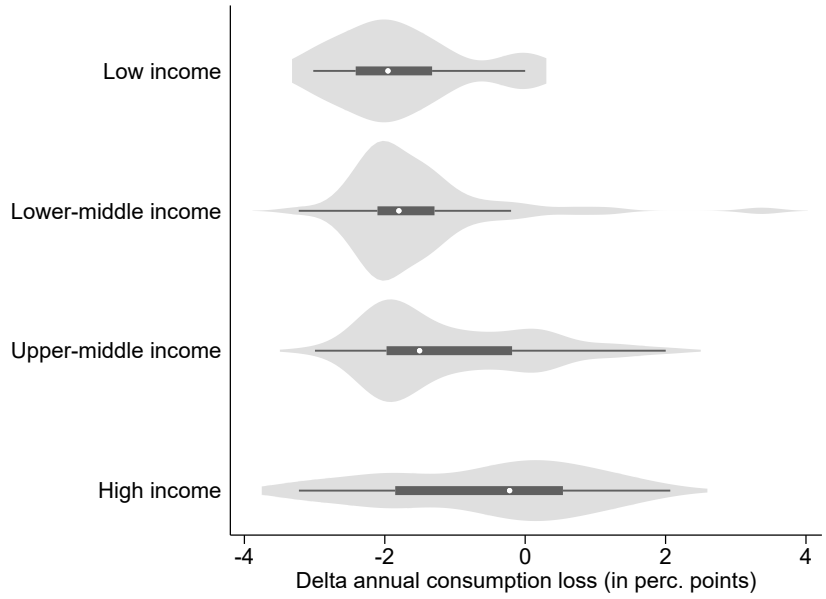

Lastly, Figure S6 shows the distributional effects of methane action including both market and non-market damages. The background scenario is SSP2-4.5. The effect of adding non-market damages to the analysis is broadly speaking to shift all the distributions to the left (higher avoided damages). The ordering of avoided damages across country-income groups is preserved, but because avoided non-market damages are relatively higher in high-income countries, the differences between groups are no longer statistically significant. This result derives from the positive income elasticity of willingness to pay in META's non-market damages function.

Figure S6: **Change in climate damages (market and non-market) in 2050 by central methane action scenario, disaggregated by World Bank country income group**. Background scenario is SSP2-4.5. Violin plots combine a kernel density plot and a box plot. Box plot contains estimates for the median (white dot), interquartile range (black box) and +/- 1.5 times the interquartile range (range of thin dark gray line). Note negative values signify avoided climate change damages. Specification includes market and non-market damages, and tipping points.

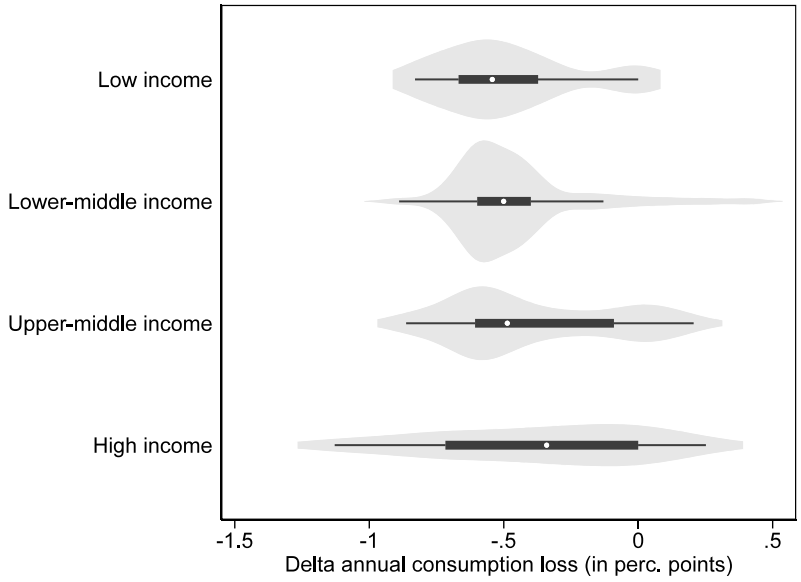

2.1.5 Effect of methane action on climate risk and tipping points relative to an SSP3-7.0 background scenario

Figure S7 reports the effect of methane action on climate risk. Figure S7 shows probability distributions for global climate damages in 2050, with and without methane action, and with and without tipping points. The baseline emissions/socio-economic scenario for these plots is SSP3-7.0. Methane action reduces climate risks, shifting the probability density function of damages in 2050 to the left (down). Mean damages fall from 3.8 to 3.3% as mentioned above, and the standard deviation of damages decreases from 1.6 to 1.5. Methane action reduces VaR at the 95% confidence level from 7.0 to 6.1%, and at the 99% confidence level from 8.4% to 7.6%. CVaR at the 95% confidence level is reduced from 8.1% to 7.0%, and at the 99% confidence level from 9.6% to 8.5%. Thus, methane action reduces climate risk in general, including tail risk. Without tipping points, the effects of methane action are very similar but if anything they are slightly larger in relative terms, indicating that methane action is slightly more effective in reducing damages from other channels. These results mirror those in our main analysis.

Figure S8 plots the effect of the central methane action scenario on tipping point intensity,

Figure S7: **Probability density functions for climate damages in 2050 with methane action (red) and without (grey), relative to an SSP3-7.0 baseline**. Left panel includes tipping points, right panel omits tipping points. Specification includes market damages. The height of each bar corresponds to the frequency of observations in the corresponding bin. Table reports associated distribution statistics (% of consumption lost in 2050 due to climate change).

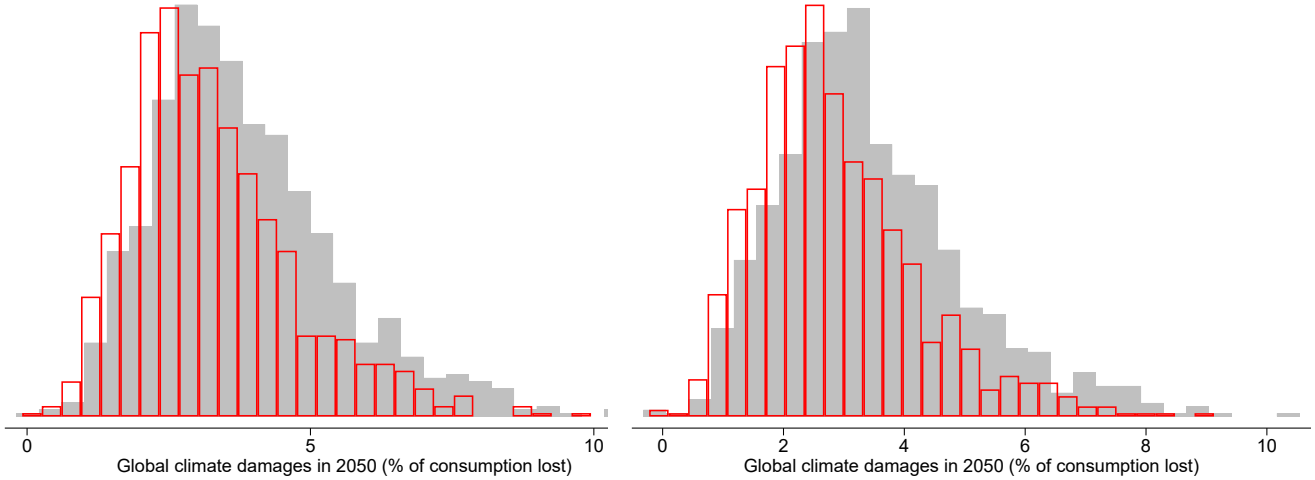

	Mean	Std. dev.	VaR 95%	VaR 99%	CVaR 95%	CVaR 99%
Tipping points						
Baseline	3.8	1.6	7.0	8.4	8.1	9.6
Methane action	3.3	1.5	6.1	7.6	7.0	8.5
No tipping points						
Baseline	3.4	1.5	6.3	8.0	7.5	8.8
Methane action	2.9	1.4	5.5	6.9	6.5	7.7

relative to an SSP3-7.0 baseline. Larger reductions in tipping point intensity are estimated for all six tipping points, compared with an SSP2-4.5 background scenario. Higher background emissions later in the century on SSP3-7.0 can be seen in most of the temporal profiles of tipping, where tipping intensity is highest in 2100 (except AMOC).

Figure S8: **Bar charts depicting the percentage change in tipping point intensity due to methane action. Background emissions scenario is SSP3-7.0. Tipping point indicators are described in the methods section.**

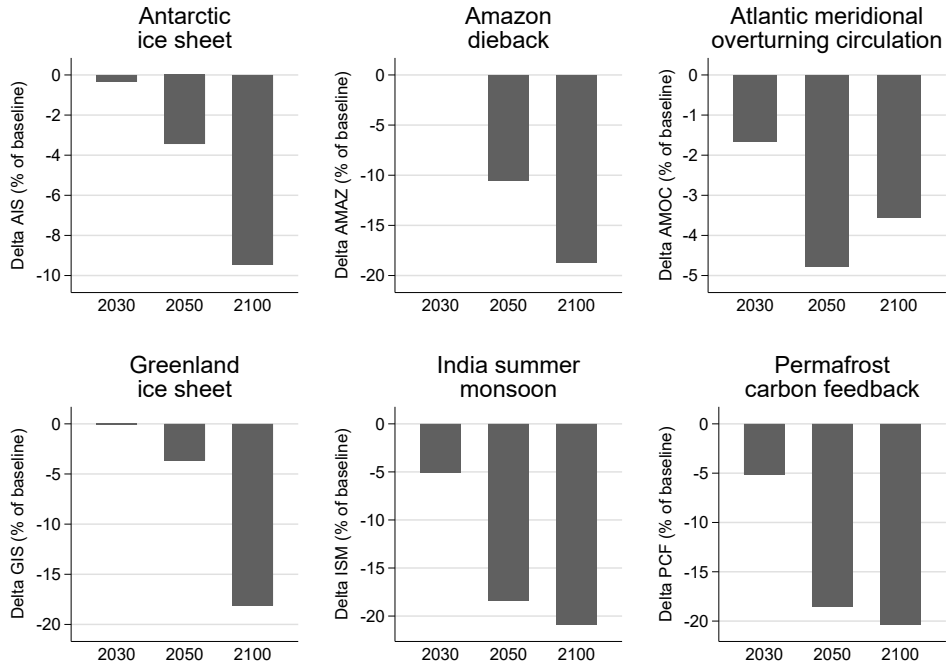

2.2 Additional analysis of SC-GHGs

2.2.1 Global SC-CH_4 and SC-CO_2 estimates over time

Table S1 reports global SC-CH_4 and SC-CO_2 estimates for different years in which a marginal emissions pulse is introduced. We report estimates both with and without tipping points. For an emission in 2020, the mean SC-CH_4 including tipping points is \$7,381.5/tCH_4, rising to \$9988.0 for an emission in 2030, \$13823,5 for an emission in 2050 and \$27043.6 for an emission in 2100. The corresponding mean SC-CO_2 is \$274.3/tCO_2 in 2020, rising to \$340.7 in 2030, \$434.7 in 2050 and \$646.8 in 2100. The SC-CH_4 grows at a compound real annual rate of 1.6% between 2020 and 2100, while the SC-CO_2 grows at a compound real annual rate of 1% over the same period. Tipping points add 17% to the SC-CH_4 in 2020 and 13% in 2100. They add 12% to the SC-CO_2 in 2020 and 6% in 2100. These are lower than comparable estimates of the contribution of tipping points in [40] due to the exclusion of the ocean methane hydrates tipping point compared to the previous paper. However, it remains important to emphasise that the set of tipping points synthesised in META is not comprehensive, being constrained by what has previously been modelled in the literature, and

some tipping modules included in META omit impact channels that are likely to be important. See [40] for further discussion.

Table S1: **Global SC-CH_4 and SC-CO_2 estimates for pulse years from 2020 to 2010**. Specification includes non-market damages, damage persistence $\phi = 0.25$, PRTP = 0.5% and EMUC = 1.05. Estimates are based on a trimmed sample of 1000 Monte Carlo runs. Values reported are in 2020 USD per ton of CH_4 and CO_2, respectively. Ratio depicts SC-CH_4/SC-CO_2 for comparison with Global Warming Potential.

	With tipping points			Without tipping points		
Pulse year	SC-CO2	SC-CH4	Ratio	SC-CO2	SC-CH4	Ratio
2020	308.5	7381.5	23.9	274.3	6306.5	23.0
2030	382.9	9988.0	26.1	340.7	8656.6	25.4
2040	444.8	12310.1	27.7	395.8	10669.8	27.0
2050	484.5	13823.5	28.5	434.7	12126.1	27.9
2080	611.9	21229.6	34.7	562.9	18497.2	32.9
2100	688.1	27043.6	39.3	646.8	23872.3	36.9

2.2.2 Sensitivity of global SC-CH4 and SC-CO2 estimates

Table S2 reports results of testing the sensitivity of the 2020 SC-CH_4 and SC-CO_2 to different assumptions regarding the persistence of damages to output, exclusion of non-market damages, and alternative values for the elasticity of the marginal utility of consumption and the pure rate of time preference, which together imply a higher discount rate.

Table S2: **Global SC-CH_4 and SC-CO_2 estimates for our preferred specification versus estimates with lower damage persistence, excluding non-market damages, and with alternative welfare parameters amounting to a lower discount rate**. Preferred specification includes non-market damages, damage persistence $\phi = 0.25$, PRTP = 0.5% and EMUC = 1.05. Estimates are based on a trimmed sample of 1000 Monte Carlo runs. Values reported are in 2020 USD per ton of CH_4 and CO_2, respectively.

	SC-CH4 in 2020			
	Preferred spec	Low persistence ($\varphi = 0.5$)	Non-market damages off	EMUC=1.5 and PRTP=0.01
Mean	7381.5	4511.6	6119.5	5756.3
Std dev	3076.9	2059.2	2451.4	2181.6

	SC-CO2 in 2020			
	Preferred spec	Low persistence ($\varphi = 0.5$)	Non-market damages off	EMUC=1.5 and PRTP=0.01
Mean	308.5	212.4	212.6	147.2
Std dev	121.9	91.8	81.8	54.2

Lowering the persistence of damages by increasing the parameter ϕ from our preferred, calibrated value of 0.25 to 0.5 as in [40] lowers both SC-GHG estimates by around one third. This is consistent

with other studies in the literature that have shown a large sensitivity of projected climate impacts to the persistence of temperature damages [70, 71, 68].

Deactivation of META's non-market damages module reduces the SC-CH_4 by around one sixth and the SC-CO_2 by around one third. This effect is somewhat less than the importance of non-market damage channels in DSCIM and GIVE – based on a 2030 emissions pulse, non-market damages account for 50-75% of the SC-CO_2 in these two models [34].

A higher discount rate lowers both social cost estimates. Given the relatively greater importance of near-term warming from a methane pulse compared to a carbon dioxide pulse, raising the discount rate reduces the SC-CH_4 by less than the SC-CO_2.

We test the consistency of our SC-CH_4 estimates across Monte Carlo samples and robustness to sample size. Computational constraints limit the sample size in our main analyses to 1,000. Here we take ten separate samples of size 1,000, estimating the SC-CH_4 for each sample, and then we pool all ten samples plus the original sample to create a large sample of size 11,000.

Figure S9 reproduces the top panel of Figure 6 in the main text. As can be seen, the distribution of our global SC-CH4 estimate for a 2020 pulse remains similar for different Monte Carlo seeds. The original sample is depicted as the solid black line, while the ten alternative samples are shown in light gray. The dashed black line shows the distribution of the global SC-CH_4 pooled across all eleven Monte Carlo seeds. Figure S9 therefore shows that an increase in the Monte Carlo sample size by an order of magnitude does not change our estimate. Table S3 reports quantitative information about the mean, standard deviation as well as minimum and maximum for each random seed as well as for the pooled sample.

Figure S9: **Global SC-CH_4 estimate for a 2020 emissions pulse across different Monte Carlo seeds**. Specification includes non-market damages, damage persistence $\phi = 0.25$, PRTP = 0.5% and EMUC = 1.05. Values reported are in 2020 USD per ton of CH_4. Estimates are based on a trimmed sample of 1000 Monte Carlo runs for different random Monte Carlo seeds. Solid black line indicates original Monte Carlo seed, light gray lines indicate alternative random seeds, and dashed black line indicates the distribution pooling across all Monte Carlo seeds, thus representing a Monte Carlo sample of size 11,000.

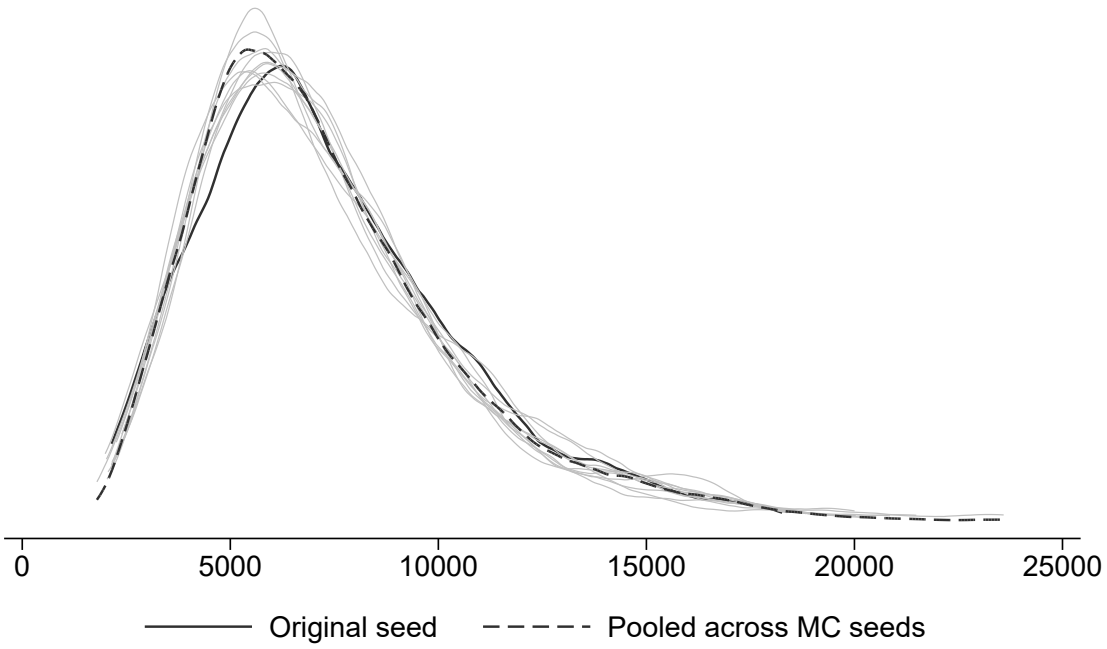

Table S3: **Robustness of global SC-CH_4 estimate for a 2020 emissions pulse to different Monte Carlo seeds**. Specification includes non-market damages, damage persistence $\phi = 0.25$, PRTP = 0.5% and EMUC = 1.05. Values reported are in 2020 USD per ton of CH_4. Estimates are based on a trimmed sample of 1000 Monte Carlo runs for different random Monte Carlo seeds. The pooled sample represents the distribution pooling across all Monte Carlo seeds, thus representing a Monte Carlo sample of size 11,000.

Random seed	Mean	Std. dev.	Min.	Max
Original seed	7381.5	3076.9	2150.6	18263.0
Alternative seed 1	7239.8	3244.9	1994.4	20002.8
Alternative seed 2	7346.7	3161.3	2040.2	20186.2
Alternative seed 3	7254.9	3100.8	2024.9	20031.6
Alternative seed 4	7429.9	3455.4	2143.4	23585.5
Alternative seed 5	7451.4	3130.4	2157.7	18386.4
Alternative seed 6	7161.9	3053.8	2259.4	20853.7
Alternative seed 7	7181.3	2888.8	2172.6	18837.3
Alternative seed 8	7428.7	3235.7	2394.2	21486.8
Alternative seed 9	7240.4	3101.3	1795.2	19005.1
Alternative seed 10	7277.1	3036.7	2063.1	18829.7
Pooled sample	7308.5	3138.2	1795.2	23585.5

2.2.3 National SC-CH_4 estimates

Table S4 reports national SC-CH_4 estimates as plotted in Fig. 6 in the main text. Tipping points are included.

Table S4: National SC-CH_4 estimates. Specification includes tipping points, non-market damages, damage persistence $\phi = 0.25$, PRTP = 0.5% and EMUC = 1.05. Estimates are based on a trimmed sample of 1000 Monte Carlo runs. Values reported are in 2020 USD per ton of CH_4.

ISO3	**Name**	**SC-CH4**
AFG	Afghanistan	0.7
AGO	Angola	17.7
ALB	Albania	1.1
ARE	United Arab Emirates	116.0
ARG	Argentina	46.4
ARM	Armenia	-0.4
ATG	Antigua and Barbuda	0.7

Continued on next page

Table S4 – continued from previous page

ISO3	Name	SC-CH4
AUS	Australia	97.3
AUT	Austria	1.5
AZE	Azerbaijan	3.3
BDI	Burundi	0.7
BEL	Belgium	17.1
BEN	Benin	2.6
BFA	Burkina Faso	4.0
BGD	Bangladesh	40.5
BGR	Bulgaria	1.0
BHR	Bahrain	20.0
BHS	Bahamas	2.7
BIH	Bosnia and Herzegovina	-0.1
BLR	Belarus	-3.3
BLZ	Belize	0.4
BMU	Bermuda	0.5
BOL	Bolivia	1.9
BRA	Brazil	331.5
BRB	Barbados	0.8
BRN	Brunei	2.6
BTN	Bhutan	0.1
BWA	Botswana	3.1
CAF	Central African Republic	0.5
CAN	Canada	-3.8
CHE	Switzerland	2.0
CHL	Chile	11.7
CHN	China	535.5
CIV	Côte d'Ivoire	8.4
CMR	Cameroon	15.5

Continued on next page

Table S4 – continued from previous page

ISO3	Name	SC-CH4
COD	Democratic Republic of the Congo	5.5
COG	Republic of Congo	3.5
COL	Colombia	42.8
COM	Comoros	0.3
CPV	Cape Verde	0.8
CRI	Costa Rica	5.1
CYP	Cyprus	3.7
CZE	Czech Republic	-0.6
DEU	Germany	64.7
DJI	Djibouti	0.5
DMA	Dominica	0.3
DNK	Denmark	13.6
DOM	Dominican Republic	10.9
DZA	Algeria	37.4
ECU	Ecuador	10.0
EGY	Egypt	153.8
ERI	Eritrea	0.9
ESP	Spain	94.1
EST	Estonia	-0.8
ETH	Ethiopia	6.7
FIN	Finland	-5.9
FJI	Fiji	1.1
FRA	France	83.3
FSM	Micronesia	1.0
GAB	Gabon	3.3
GBR	United Kingdom	112.2
GEO	Georgia	0.3
GHA	Ghana	12.4

Continued on next page

Table S4 – continued from previous page

ISO3	Name	SC-CH4
GIN	Guinea	3.3
GMB	Gambia	0.9
GNB	Guinea-Bissau	0.5
GNQ	Equatorial Guinea	5.1
GRC	Greece	25.9
GRD	Grenada	0.3
GTM	Guatemala	8.3
GUY	Guyana	0.8
HKG	Hong Kong	52.9
HND	Honduras	3.2
HRV	Croatia	2.0
HTI	Haiti	1.6
HUN	Hungary	2.7
IDN	Indonesia	265.6
IND	India	547.9
IRL	Ireland	8.9
IRN	Iran	135.6
IRQ	Iraq	66.1
ISL	Iceland	-0.2
ISR	Israel	17.5
ITA	Italy	114.4
JAM	Jamaica	4.6
JOR	Jordan	8.8
JPN	Japan	403.6
KAZ	Kazakhstan	-5.4
KEN	Kenya	11.6
KGZ	Kyrgyzstan	-0.6
KHM	Cambodia	4.9

Continued on next page

Table S4 – continued from previous page

ISO3	Name	SC-CH4
KNA	Saint Kitts and Nevis	0.1
KOR	South Korea	96.9
KWT	Kuwait	37.2
LAO	Laos	3.3
LBN	Lebanon	14.6
LBR	Liberia	0.9
LBY	Libya	12.0
LKA	Sri Lanka	22.6
LSO	Lesotho	0.1
LTU	Lithuania	-1.0
LUX	Luxembourg	0.7
LVA	Latvia	-0.6
MAR	Morocco	28.2
MDA	Moldova	-0.1
MDG	Madagascar	3.1
MEX	Mexico	150.6
MKD	Macedonia	0.1
MLI	Mali	5.9
MMR	Myanmar	21.9
MNE	Montenegro	0.2
MNG	Mongolia	-2.6
MOZ	Mozambique	4.7
MRT	Mauritania	2.4
MUS	Mauritius	3.0
MWI	Malawi	1.9
MYS	Malaysia	92.3
NAM	Namibia	2.8
NER	Niger	2.6

Continued on next page

Table S4 – continued from previous page

ISO3	Name	SC-CH4
NGA	Nigeria	121.2
NIC	Nicaragua	2.5
NLD	Netherlands	173.0
NOR	Norway	-0.6
NPL	Nepal	3.3
NZL	New Zealand	14.3
OMN	Oman	30.5
PAK	Pakistan	100.5
PAN	Panama	5.8
PER	Peru	15.3
PHL	Philippines	61.9
PLW	Palau	0.1
PNG	Papua New Guinea	1.9
POL	Poland	-3.5
PRI	Puerto Rico	17.2
PRT	Portugal	17.8
PRY	Paraguay	5.5
QAT	Qatar	32.4
ROU	Romania	2.2
RUS	Russia	-105.7
RWA	Rwanda	1.2
SAU	Saudi Arabia	219.9
SDN	Sudan	25.9
SEN	Senegal	9.8
SLB	Solomon Islands	0.2
SLE	Sierra Leone	2.7
SLV	El Salvador	4.8
SMR	San Marino	0.1

Continued on next page

Table S4 – continued from previous page

ISO3	Name	SC-CH4
SRB	Serbia	1.2
STP	São Tomé and Príncipe	0.1
SUR	Suriname	0.8
SVK	Slovakia	-0.2
SVN	Slovenia	0.6
SWE	Sweden	-0.6
SWZ	Swaziland	1.0
TCD	Chad	3.6
TGO	Togo	1.3
THA	Thailand	144.8
TJK	Tajikistan	0.0
TKM	Turkmenistan	2.3
TLS	Timor-Leste	0.8
TON	Tonga	0.3
TTO	Trinidad and Tobago	5.3
TUN	Tunisia	31.9
TUR	Turkey	38.0
TUV	Tuvalu	0.0
TZA	Tanzania	12.8
UGA	Uganda	5.4
UKR	Ukraine	0.1
URY	Uruguay	4.6
USA	United States	1111.5
UZB	Uzbekistan	3.2
VEN	Venezuela	54.0
VNM	Vietnam	62.7
VUT	Vanuatu	0.1
WSM	Samoa	0.2

Continued on next page

Table S4 – continued from previous page

ISO3	Name	SC-CH4
YEM	Yemen	14.3
ZAF	South Africa	71.0
ZMB	Zambia	4.8
ZWE	Zimbabwe	3.7

2.3 Global Sensitivity Analysis

Here we give an overview of our application of Global Sensitivity Analysis (GSA) to assess the drivers of variation in the social cost of CO_2 (SC-CO_2) and the social cost of methane (SC-CH_4). GSA is used across various fields, including environmental economics, climate science, and risk assessment, to evaluate how uncertainty in model inputs propagates through to model outputs [72, 73]. Sensitivity analysis can help identify key drivers of uncertainty and prioritize areas for further research or data collection, ultimately aiming to improve the robustness of policy recommendations.

We implement GSA using the GlobalSensitivity.jl package in Julia, employing multiple methods to ensure the robustness of our findings. These methods include the Efficient Algorithm for Sensitivity Indices (EASI) [74], the Delta moment-independent method [75], and regression techniques using both Pearson and Spearman correlation coefficients [76]. All of these methods rely upon Monte Carlo simulations, which we produce under the same configuration as the default in the main paper.

We perform 1000 Monte Carlo (MC) simulations for the SC-CO_2 and SC-CH_4. For each MC simulation, we extract a total of 17 parameters describing the Antarctic Ice Sheet (AIS) tipping point, 2 parameters for Amazon dieback, 2 for Atlantic Meridional Overturning Circulation (AMOC) slowdown, 2 for dissociation of ocean methane hydrates (OMH) when applicable, 2 for the Surface Albedo Feedback (SAF), 1 for Indian Summer Monsoon (ISM) weakening, 20 for tipping point interactions, 2 representing climate sensitivity, and 1 for Sea Level Rise (SLR) damages. Additionally, we include 2 parameters for temperature damages, although this uncertainty is not included in the standard results.

Certain parameters are not directly read from the model but are derived through specified calculations:

- The AIS model is represented by regional β and δ coefficients, and by the R functions summed according to $\sum_t R(t - 2010)$, which is a sufficient statistic under a linear SLR ramp.

- For ISM, an exogenous estimate of $\bar{P}$ is calculated using the same calculations as the normal $\bar{P}$, but holding the probability of a wet day constant at the baseline probability and the precipitation of a wet day constant at its baseline value.

- For OMH and AMOC, an exogenous "year of triggering" is generated by applying the uniform probability values to the constant probability of triggering from 2010, and a second "year of triggering" parameter is generated by using a probability 10% of this 2010 probability.

- Since the probability of Amazon Dieback starts at 0, we instead specify a probability of triggering of 0.5%, but otherwise use the same procedure as for OMH and AMOC.

- Climate sensitivity is represented by the first and second difference of GMST in 2010 (prior to the endogenous effects of tipping points) – so, $T_{2010} - T_{2009}$ and $(T_{2010} - T_{2009}) - (T_{2009} - T_{2008})$.

- The SLR damage coefficient parameter is $\sum_i L(i, 2010)\theta(i)$, across countries i with population $L(i)$, which is a sufficient statistic for SLR damages under the assumption of a log utility function.

We use the GlobalSensitivity.jl package in Julia, which supports the following methods for GSA when MC draws are already available:

- Efficient Algorithm for Sensitivity Indices (EASI);

- Delta moment-independent method;

- Regression methods using Pearson correlation or Spearman coefficient.

Each method provides a relative importance measure for the parameters considered.

Given that multiple parameters map on to individual sources of uncertainty (e.g., 17 AIS parameters), we combine the importance measures using the sum of squared relative importance measures, ($\sqrt{\sum_k r_k^2}$, for importance measure r_k), which is more conservative in its assumptions about the independence of these factors than a straight sum.

Finally, we normalize the resulting importance measures to sum to 1 for each method.

The results are shown in figure S10.

Figure S10: **Global Sensitivity Analysis on the SCC and SCCH4 in 2020, divided by tipping point and climatic or damage parameters.**

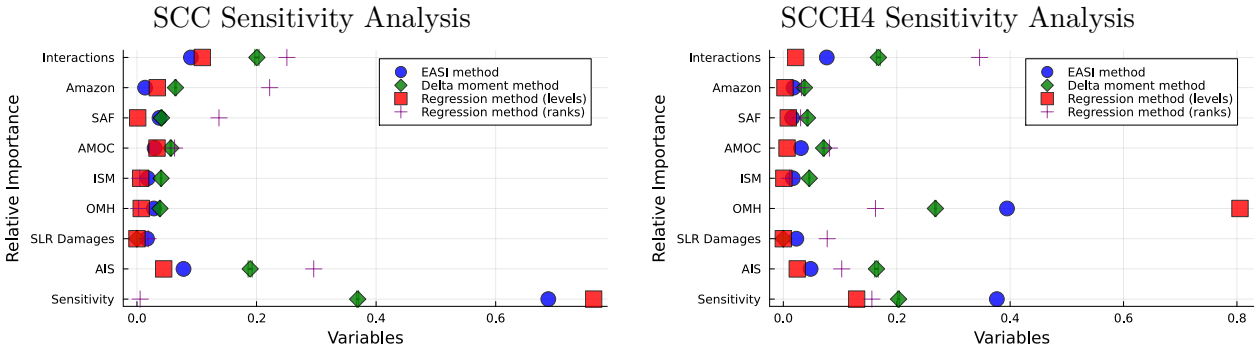

3 META model description

This section provides a complete description of the META (Model for Economic Tipping point Analysis) model, which is publicly available at `https://github.com/openmodels/META`. It largely reproduces the description provided in [40], but includes the various updates since META-2021. We have tagged the version of META used in this paper as META-2025 at `https://github.com/openmodels/META/releases/tag/META-2025`.

Figures S11 and S12 provide an overview of the model structure. Figure S11 provides a schematic diagram of the climate module. The inputs to the climate module are greenhouse gas (GHG) emissions from exogenous scenarios; the output is the change in global mean surface temperature (GMST). Three tipping points provide positive feedbacks from the increase in GMST to GHG emissions (the permafrost carbon feedback, dissociation of ocean methane hydrates, and Amazon rainforest dieback), while one provides a positive feedback from the increase in GMST to radiative forcing (Arctic sea-ice loss/surface albedo feedback).

Figure S12 provides a schematic diagram of the damages/economic module. The input to the damages/economic module is the change in GMST from the climate module. The output is discounted utility/social welfare. Slowdown of the Atlantic Meridional Overturning Circulation modulates the relationship between global and national mean temperature change. Disintegration of the Greenland and Antarctic Ice Sheets increases sea level rise. Variability of the Indian summer monsoon directly impacts GDP in India due to droughts and floods.

Figure S11: Schematic diagram of the climate module. Blue boxes indicate variables; yellow boxes indicate tipping point modules; orange boxes indicate other modules.

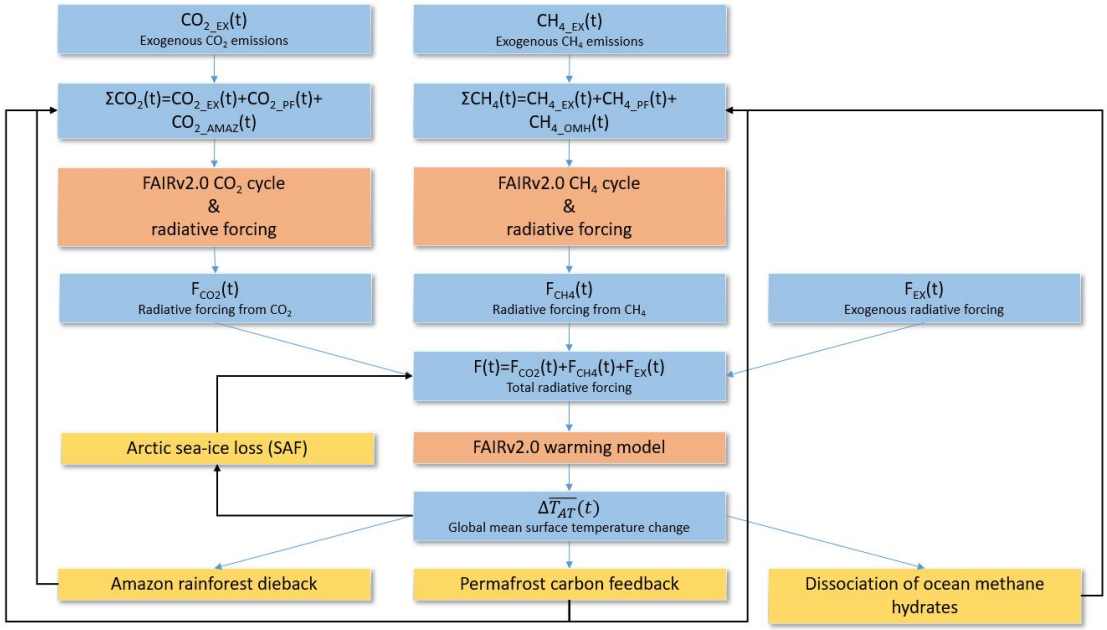

Figure S12: Schematic diagram of the damages/economic module. Blue boxes indicate variables; yellow boxes indicate tipping point modules; orange boxes indicate other modules.

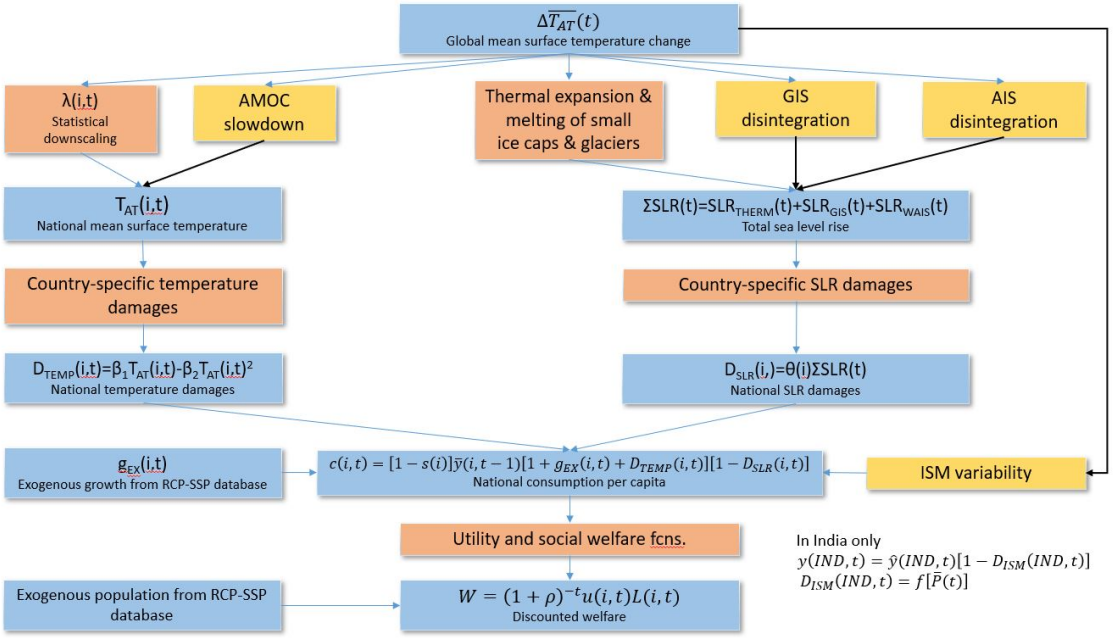

3.1 Tipping point modules

3.1.1 Permafrost carbon feedback

Our model of the permafrost carbon feedback (PCF) is taken from [77]. This is a tractable model that mimics in reduced form the physical-science literature quantifying permafrost carbon release by simulating two stages: (i) permafrost thaw as a function of rising temperatures and (ii) decomposition of thawed permafrost, leading to the release of CO_2 or CH_4. Kessler built the model for incorporation in DICE and, although we don't use DICE, the level of abstraction from the underlying physical processes is well suited to our approach. Despite the level of abstraction, however, the model retains enough structure to be directly calibrated on estimates reported in the underlying literature.

In the first stage, near-surface permafrost thaw is a linear function of warming relative to time zero:

$$\mathrm{PF}_{\mathrm{extent}}(t) = 1 - \beta_{\mathrm{PF}} \left[\Delta\overline{T_{\mathrm{AT}}}(t) - \Delta\overline{T_{\mathrm{AT}}}(0) \right], \tag{5}$$

where $\mathrm{PF}_{\mathrm{extent}}(t) \equiv \mathrm{PF}_{\mathrm{area}}(t)/\mathrm{PF}_{\mathrm{area}}(0)$, i.e., $\mathrm{PF}_{\mathrm{extent}}(t)$ is the area of permafrost remaining at time t relative to time zero, $\Delta\overline{T_{\mathrm{AT}}}$ is the global mean surface air temperature relative to pre-industrial, and β_{PF} is a coefficient representing the sensitivity of permafrost thaw to temperature, which Kessler calibrated by regressing estimates of thaw on temperature from the literature. $t = 0$ in our model is the year 2010.

The amount of carbon in freshly thawed permafrost at time t, C_{thawedPF}, is then the product of the total stock of carbon locked in the near-surface northern circumpolar permafrost region, C_{PF}, and the area of permafrost freshly thawed:

$$C_{\mathrm{thawedPF}}(t) = -C_{\mathrm{PF}} \left[\mathrm{PF}_{\mathrm{extent}}(t) - \mathrm{PF}_{\mathrm{extent}}(t-1) \right]. \tag{6}$$

Once thawed, the principal way in which carbon is released to the atmosphere is microbial decomposition and this happens slowly. Some of the carbon is released as CO_2 and some as CH_4. Kessler's model divides the stock of thawed carbon into a passive reservoir that releases no carbon and an active reservoir that decomposes exponentially and releases CO_2 and CH_4 in fixed proportion. Therefore, cumulative CO_2 emissions to the atmosphere from thawed permafrost, $\mathrm{CCum}_{\mathrm{PF}}$, are given by

$$\mathrm{CCum}_{\mathrm{PF}}(t) = \sum_{s=0}^{t} C_{\mathrm{thawedPF}}(s) \left(1 - \mathrm{propPassive}\right) \left(1 - e^{(-t-s)/\tau}\right), \tag{7}$$

Table S5: PCF model parameter values

	Kessler main spec.	Lower/upper bounds	Fit of [78]	Fit of [79]
β	0.172	0/1	0.066	0.085
C_{PF} (GtC)	1035	885/1185	1160	1066
propPassive	0.40	0.29/0.51	0.37	0.41
τ (years)	70	0/200	31	66

where propPassive is the proportion of thawed permafrost in the passive reservoir and τ is the e-folding time of permafrost decomposition in the active reservoir, which is multiple decades (see below). The fluxes of CO_2 and CH_4 are respectively given by

$$\mathrm{CO_{2\_PF}}(t) = (1 - \mathrm{propCH_4}) \left[\mathrm{CCum_{PF}}(t) - \mathrm{CCum_{PF}}(t-1)\right], \quad (8)$$

$$\mathrm{CH_{4\_PF}}(t) = (\mathrm{propCH_4}) \left[\mathrm{CCum_{PF}}(t) - \mathrm{CCum_{PF}}(t-1)\right], \quad (9)$$

where $\mathrm{propCH_4}$ is the share of CH_4 emissions in total carbon emissions.

We can directly reproduce the permafrost carbon emissions estimated by [77] just by imputing her reported parameter values for β_{PF}, C_{PF}, propPassive, τ and $\mathrm{propCH_4}$ into Equations (5)-(9). In addition, we use this model to fit the results of the two other papers contributed to the IAM literature on the PCF, namely [78] and [79]. [78] coupled the PAGE09 IAM to the SiBCASA model of the PCF. [79] developed a new version of the PAGE IAM called PAGE-ICE, which includes a representation of the PCF calibrated both on SiBCASA and another PCF model called JULES. We first obtain estimates of permafrost CO_2 emissions from each paper as a function of temperature, and then minimise the sum of squared residuals between these papers' estimates and estimates from Kessler's model, using four of the free parameters in Kessler's model, i.e. β_{PF}, C_{PF}, propPassive, and τ, each parameter restricted to lie within physically plausible bounds. Table S5 reports the various parameter values. Figure S13 shows the fit to cumulative CO_2 emissions from [78] and [79]. CH_4 emissions for these two papers are obtained simply by using the fitted parameters in combination with the fixed value of $\mathrm{propCH_4}$ from [77].

Figure S13: Fit of cumulative permafrost CO_2 emissions from [78], top panel, and [79], bottom panel

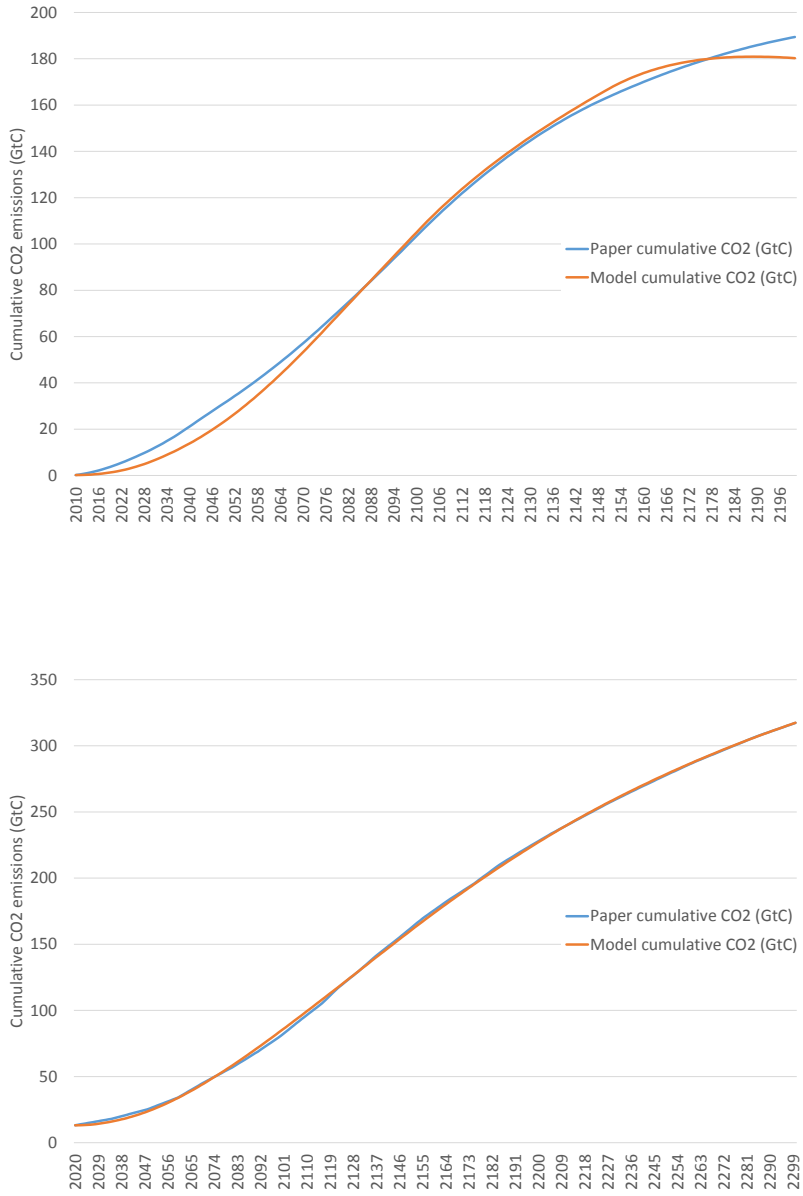

3.1.2 Ocean methane hydrates

There have been two studies of the economic cost of destabilization of ocean methane clathrates/hydrates. The first is [80], who implemented what-if scenarios in PAGE09, releasing a pulse of CH_4 emissions

of fixed size and duration into the model at a given point in time. These scenarios were based on the work of [81] on hydrates locked within subsea permafrost on the East Siberian Arctic shelf. [80] implemented various scenarios. Most of their scenarios involved injecting 50GtCH_4 in total over periods of 10 to 30 years, starting at different times from 2015 to 2035.[1] The other study is [82]. They implemented three what-if scenarios, in which pulses of CH_4 emissions from the reservoir of CH_4 distributed globally on continental shelves and slopes were released in the FUND IAM. These emissions pulses all commence in 2050 and comprise permanent flows of 0.2GtCH_4 per year, $1.784\text{GtCH}_4/\text{yr}$ and $7.8\text{GtCH}_4/\text{yr}$ respectively.

In order to incorporate these studies in our analysis, their what-if scenarios need to be assigned probabilities. To do this, we use the framework of survival analysis, treating each emissions pulse as a hazard event and assigning it a hazard rate, i.e. the conditional probability that the event will occur in a particular year, given the temperature in that year and that the event has not occurred previously. This is both convenient, and conforms with the way some of the other studies we synthesise treat tipping points, e.g., on Amazon rainforest dieback [83]. Once triggered, each CH_4 emissions pulse of given size lasts its pre-specified amount of time. In general, we can write the flow of CH_4 emissions from dissociation of ocean methane hydrates at time t, $\text{CH}_{4\_\text{OMH}}(t)$, as

$$\text{CH}_{4\_\text{OMH}}(t) = \left(\frac{\overline{\text{CH}_{4\_\text{OMH}}}}{\Delta_{\text{OMH}}}\right) I_{\text{OMH}}(t) \quad \Longleftrightarrow \quad \sum_{s=0}^{t-1} \text{CH}_{4\_\text{OMH}}(s) < \overline{\text{CH}_{4\_\text{OMH}}}, \tag{10}$$

$$\text{CH}_{4\_\text{OMH}}(t) = 0 \quad \Longleftarrow \quad \sum_{s=0}^{t-1} \text{CH}_{4\_\text{OMH}}(s) = \overline{\text{CH}_{4\_\text{OMH}}}, \tag{11}$$

where $\overline{\text{CH}_{4\_\text{OMH}}}$ is the pre-specified total amount of methane released, e.g., 50Gt in the case of the main specification of [80], and Δ_{OMH} is the duration of the release, e.g., 10 years. Applying this formalism to [82], $\overline{\text{CH}_{4\_\text{OMH}}}/\Delta_{\text{OMH}} \in \{0.2, 1.784, 7.8\}$ and total CH_4 released from ocean CH_4 hydrates is bounded only by the product of $\overline{\text{CH}_{4\_\text{OMH}}}/\Delta_{\text{OMH}}$ and the model horizon, i.e. the inequality constraint in Equations (10) and (11) does not bind. $I_{\text{OMH}}(t)$ is an indicator function taking a value of zero before the hazard event is triggered and one thereafter. In general, its transition function is

$$I_{\text{OMH}}(t) = f\left[I_{\text{OMH}}(t-1), \Delta\overline{T_{\text{AT}}}(t), \varepsilon(t)\right], \tag{12}$$

where $\varepsilon(t)$ is an i.i.d. random shock. That is, in each period the value of I_{OMH} depends on its own value in the previous period, the current atmospheric temperature, and the random shock.

[1] They also injected a smaller pulse of 25GtCH_4 between 2015 and 2025 in one scenario.

Specifically, the probability transition matrix for $I_{\text{OMH}}(t)$ is

$$\begin{bmatrix} 1 - p_{\text{OMH}}(t) & p_{\text{OMH}}(t) \\ 0 & 1 \end{bmatrix}, \tag{13}$$

where $p_{\text{OMH}}(t)$ is the probability that the CH_4 emissions pulse is triggered in year t. This is given by

$$p_{\text{OMH}}(t) = 1 - \exp\left[-b_{\text{OMH}}\Delta\overline{T_{\text{AT}}}(t)\right], \tag{14}$$

where b_{OMH} is the hazard rate.

In order to calibrate the hazard rate, we use the study of [84], which presents a global model of CH_4 hydrates on continental shelves and slopes and the release of CH_4 as temperatures rise. Their study shows the sensitive dependence of ocean CH_4 release on a critical bubble volume fraction threshold. That is, when ocean CH_4 hydrates melt, it is uncertain whether the CH_4 escapes the ocean sediment into the ocean.[2] Colder temperatures closer to the sea floor and chemical reactions (anaerobic oxidation by bacteria and archaea) both effectively trap the CH_4 from escaping. The more CH_4 is in bubbles, however, the more likely it is to escape. In the model of [84], the bubble volume upon melting of the hydrates must exceed the critical bubble volume fraction in order for the CH_4 to be released. Calibrating the hazard rate on [84] means that we re-interpret [80] in the context of the global reservoir of CH_4 hydrates on continental shelves and slopes, rather than the reservoir of CH_4 locked in subsea permafrost in the Arctic region. This is justified, since other research suggests a large release of CH_4 from the Arctic subsea permafrost within the next two centuries is extremely unlikely [85].[3]

According to [84], cumulative CH_4 released in very long-run equilibrium upon 1°C warming varies hugely from about 10GtCH_4 to 541GtCH_4 for critical bubble fractions of 10% and 1% respectively.[4] Upon 3°C warming the range increases to about 32-1084Gt. Moreover, [84] report that there is next to no empirical evidence on the critical bubble fraction. In the absence of such evidence, we try three alternative specifications of the probability distribution of equilibrium cumulative CH_4 release as a function of the critical bubble fraction (Table S6). The uniform distribution is an application of the principle of insufficient reason. The triangular and especially the beta dis-

[2]There is further uncertainty about whether the CH_4 that reaches the ocean bottom eventually escapes into the atmosphere (it depends on aerobic oxidation of CH_4 by bacteria in the water column), however this uncertainty is thought to be smaller.

[3]Indeed, the scenarios in [80] were criticised at the time of publication for being unrealistic in the context of Arctic subsea processes; see *Nature* volume 300, p529.

[4]Based on digitising Figure 7 in their paper.

tribution are more conservative in the sense of assigning more probability mass to higher critical bubble fractions and in turn lower equilibrium CH_4 releases.

Irrespective of the critical bubble fraction, CH_4 released from melting ocean hydrates is thought to take a very long time to reach the atmosphere, much longer than permafrost carbon. Therefore, in order to convert the equilibrium CH_4 release into a transient release, we conservatively assume a release rate of just 0.2%, implying an e-folding time of 500 years and approximately 3,000 years for equilibrium to be reached [also see 84].

The procedure for calibrating the hazard rate b_{OMH} has been modifed as part of the META model update for this paper. For a given GMST scenario, the approach just described to represent the modelling results of [84] gives us the probability of a cumulative CH_4 release of given volume in a given year. For example, on the mid-range RCP4.5 scenario of the Intergovernmental Panel on Climate Change (IPCC), fed into our climate module excluding tipping points, the middle scenario from [80] of a cumulative release of $50GtCH_4$ over 20 years from 2015 to 2035 has a probability of 24.4%, assuming a beta distribution over critical bubble fractions. The corresponding hazard rate b_{OMH} is then the value that, given GMST of 1.07°C above pre-industrial in the initial release year of 2015 (also on RCP4.5), triggers the $50GtCH_4$ release with 24.4% probability. In this example, $b_{\text{OMH}} = 0.059$. We follow the same procedure to assign hazard rates using the uniform and triangular distributions, and apply it to different durations of emissions pulse investigated by [80], as well as the scenarios in [82]. Table S6 reports all the estimated hazard rates. We prefer the beta distributions except in sensitivity analysis, as they are more conservative.

Table S6: Calibration of OMH hazard rate, b_{OMH}. Triangular distribution assumes modal critical bubble fraction of 10%, supports of 1% and zero CH_4 release. Beta distribution assigns cumulative probabilities of 0.67, 0.9, 0.95, 0.99 and 1 to critical bubble fractions of 10%, 7.5%, 5%, 2.5% and 1% respectively.

		uniform	triangular	beta
[80] 50GtCH$_4$ by 2035	p_{OMH}	95.3%	90.2%	24.4%
	b_{OMH}	0.648	0.491	0.059
[80] 50GtCH$_4$ by 2025	p_{OMH}	86.4%	8.9%	12.0%
	b_{OMH}	0.422	0.020	0.027
[80] 50GtCH$_4$ by 2045	p_{OMH}	97.7%	97.8%	33.0%
	b_{OMH}	0.801	0.811	0.084
[82] 0.2GtCH$_4$/yr 2050-2200	p_{OMH}	100%	100%	67.1%
	b_{OMH}	0.133	0.205	0.019
[82] 1.784GtCH$_4$/yr 2050-2200	p_{OMH}	99.7%	100%	52.4%
	b_{OMH}	0.096	0.131	0.013
[82] 7.8GtCH$_4$/yr 2050-2200	p_{OMH}	98.5%	99.2%	39.1%
	b_{OMH}	0.071	0.081	0.008

3.1.3 Amazon rainforest dieback

Dieback of the Amazon rainforest was included in the study of [83] as a carbon-cycle feedback. This is the study we incorporate in our analysis. Naturally a wide range of other economically important consequences of Amazon rainforest dieback are thereby excluded, including those on biodiversity, ecosystems, and precipitation patterns. These have yet to be incorporated in any economic modelling study, to the best of our knowledge.

As mentioned above, [83] model tipping points through survival analysis. In the case of Amazon rainforest dieback, 50GtC is released over 50 years upon triggering the hazard event. Using parallel formalism to ocean methane hydrates, CO_2 emissions from Amazon rainforest dieback at time t, $\text{CO}_{2\_\text{AMAZ}}(t)$, are given by

$$\text{CO}_{2\_\text{AMAZ}}(t) = \left(\frac{\overline{\text{CO}_{2\_\text{AMAZ}}}}{\Delta_{\text{AMAZ}}}\right) I_{\text{AMAZ}}(t) \quad \Longleftrightarrow \quad \sum_{s=0}^{t-1} \text{CO}_{2\_\text{AMAZ}}(s) < \overline{\text{CO}_{2\_\text{AMAZ}}}, \tag{15}$$

$$\text{CO}_{2\_\text{AMAZ}}(t) = 0 \quad \Longleftarrow \quad \sum_{s=0}^{t-1} \text{CO}_{2\_\text{AMAZ}}(s) = \overline{\text{CO}_{2\_\text{AMAZ}}}, \tag{16}$$

where $\overline{\text{CO}_{2\_\text{AMAZ}}}$ = 50GtC and Δ_{AMAZ} = 50 years. The probability of the indicator function

$I_{\text{AMAZ}}(t)$ transitioning from zero to one is

$$p_{\text{AMAZ}}(t) = 1 - \exp\left[-b_{\text{AMAZ}}\Delta\overline{T_{\text{AT}}}(t) - 1\right], \tag{17}$$

where the hazard rate $b_{\text{AMAZ}} = 0.00163$ in [83] is taken from the expert elicitation study of [69].

3.1.4 Greenland Ice Sheet

Our model of disintegration of the Greenland Ice Sheet (GIS) is based on [86], which follows an approach conceptually similar to Kessler's [77] PCF model by building a simple, reduced-form process model of GIS disintegration for incorporation in DICE.[5] The GIS model is calibrated on results from the underlying literature modelling ice-sheet dynamics. At the heart of the GIS model is the very long-run equilibrium relationship between atmospheric temperature and the volume of the GIS. Assuming this is reversible, [86] specified

$$\overline{\Delta T^{*}_{\text{GIS}}}(t) = \Delta\overline{T_{\text{GIS\_MAX}}}\left[1 - V_{\text{GIS}}(t)\right], \tag{18}$$

where $\Delta\overline{T^{*}_{\text{GIS}}}(t)$ is defined as the atmospheric temperature increase relative to initial temperature that is associated with a particular degree of melting of the GIS in equilibrium and $V_{\text{GIS}}(t) \in [0, 1]$ is the volume of the GIS expressed as a fraction of the initial volume.[6] In Nordhaus' main specification, Eq. (18) was calibrated on paleoclimatic data from [87], which gives $\Delta\overline{T_{\text{GIS\_MAX}}} = 3.4$ and implies that the GIS is fully melted in equilibrium when the global mean surface temperature is 3.4°C above pre-industrial. If [88] is used for calibration instead, $\Delta\overline{T_{\text{GIS\_MAX}}} = 1.8$.[7] An alternative, cubic specification of the equilibrium temperature-volume relationship allows for hysteretic behaviour. Fitted on [87], this is given by

$$\Delta\overline{T^{*}_{\text{GIS}}}(t) = \Delta\overline{T_{\text{GIS\_MAX}}} - 20.51V_{\text{GIS}}(t) + 51.9\left[V_{\text{GIS}}(t)\right]^2 - 34.79\left[V_{\text{GIS}}(t)\right]^3. \tag{19}$$

Nordhaus [86] showed that the change in specification makes little difference on the optimal emissions path, which involves relatively limited warming, but can make a difference on high-emissions scenarios.

[5] The resulting model is called DICE-GIS and builds on DICE-2016R2.
[6] [86] also reports runs in which $T^{*}_{\text{GIS}}(t) = T_{\text{GIS\_MAX}}\left[1 - V_{\text{GIS}}(t)\right]^{0.5}$ and finds the results are very similar.
[7] Noting that the melt rate coefficient β_{GIS} below also needs to be recalibrated to -0.0000088 to fit [88].

The difference equation for $V_{\text{GIS}}(t)$, i.e. the GIS melt rate, can be written as

$$\begin{aligned} V_{\text{GIS}}(t) - V_{\text{GIS}}(t-1) &= \beta_{GIS}\text{sgn}\left[\Delta\overline{T_{\text{AT}}}(t-1) - \Delta\overline{T^*_{\text{GIS}}}(t-1)\right] \times \\ &\quad \times \left[\Delta\overline{T_{\text{AT}}}(t-1) - \Delta\overline{T^*_{\text{GIS}}}(t-1)\right]^2 V_{\text{GIS}}(t-1)^{0.2}, \end{aligned} \tag{20}$$

where $\beta_{GIS} = -0.0000106$ based on regression analysis of estimates from [88].[8] The basic idea embodied in Eq. (20) is that melting of the GIS depends on the difference between the actual atmospheric temperature and the equilibrium GIS temperature, as well as the volume of the GIS at the time.

Sea level rises linearly in response to GIS melt,

$$SLR_{\text{GIS}}(t) = 7\left[1 - V_{\text{GIS}}(t)\right], \tag{21}$$

where SLR_{GIS} is defined relative to the year 2000. This implies that complete disintegration of the GIS would increase global mean sea level by 7 metres.

3.1.5 Antarctic Ice Sheet

In the latest version of META, melting of the Antarctic Ice Sheet (AIS) is based on a module developed by [41]. This takes a process-based approach. The contribution of the AIS to SLR is divided into the surface mass balance (SMB) contribution and the dynamic contribution. SMB is the balance of surface mass accumulation (precipitation) and ablation (melting) on the ice sheet. Dynamic contributions come from the physical transportation of grounded ice into the ocean through glacier flow. Once afloat, this ice contributes to SLR through the displacement of water. Dynamic contributions are much more important than SMB on the AIS [89].

SMB is modelled using a simple, adjusted linear relationship between SMB and global mean temperature change. The unadjusted annual mass change ΔSMB is given by

$$\Delta\text{SMB} = \gamma\,(t - t_0)^{-0.1}\,\Delta A(t), \tag{22}$$

where t_0 is 2010 and $\gamma = 7.95$mm/yr [90]. $\Delta A(t)$ is the change in continental-scale accumulation

[8] This corresponds with Nordhaus' [86] reported value per five years divided by 5 to bring it into line with our annual time step, then divided by 100 given that we define $V_{\text{GIS}}(t)$ as a fraction.

from 2010, which is given by

$$\Delta A(t) = \varphi\omega \left[\Delta\overline{T_{\mathrm{AT}}}(t) - \Delta\overline{T_{\mathrm{AT}}}(0)\right], \tag{23}$$

where φ is a temperature scaling coefficient of 1.2 that converts $\Delta\overline{T_{\mathrm{AT}}}(t)$ into continental-scale temperature change based on the modelling of [89], and ω is the change in continental accumulation per degree of Antarctic warming, estimated by [90] at approximately 5 +/- 1% per degree warming. We calibrate a normal distribution with a mean of 5% and a standard deviation of 0.4 percentage points.

Equations (22) and (23) permit estimation of the snowfall-induced mass gain for any scenario of global mean temperature change, without needing to rely on runs of a complex ice sheet model. However, [90] only analysed the relationship for continental-scale warming of up to 5°C above pre-industrial and temperatures could increase to the extent that SMB in Antarctica turns negative. [89] report that the SMB of the ice sheet will turn negative at approx. 7°C warming. To account for this, we model an evolving adjustment factor based on a generalized logistic function:

$$\mathrm{Adjustment}(t) = \frac{K - \Delta\mathrm{SMB}(t)}{\left(C + Qe^{-B(t)}\right)^{1/V}}, \tag{24}$$

where K, C, Q and V are constants, and $B(t) = \left[\Delta\overline{T_{\mathrm{AT}}}(t) - 6.75\right]$. K is calibrated so that the SMB contribution approaches a maximum of 8mm/yr at very high temperatures. This value follows the prognosis from [89] that, above c. 7°C warming, the AIS is committed to losing 70% of its mass via the surface elevation feedback. Seventy percent of AIS mass is equivalent to c. 40m of SLR and taking a rapid deglaciation of approximately 5,000 years yields a maximum of 8mm/yr SLR.

Combining (22) and (23) with the adjustment factor and cumulating over time yields the adjusted total mass change:

$$\widehat{\mathrm{SMB}}(t) = \sum_{s=0}^{t} \left[\Delta\mathrm{SMB}(s) + \frac{K - \Delta\mathrm{SMB}(s)}{\left(C + Qe^{-B(s)}\right)^{1/V}}\right]. \tag{25}$$

Dynamic contributions to SLR from the AIS are modelled using the reduced-form model of [59], which is designed to emulate basal ice shelf melting and the resulting contribution of the AIS to SLR in 16 state-of-the-art ice sheet models. The five major ice basins on the continent are modelled separately: East Antarctica, the Ross Sea, the Amundsen Sea, the Weddell Sea, and

the Antarctic Peninsula. This is because the dynamic discharge of one basin minimally affects the dynamic discharge of another. The first step is to translate $\Delta\overline{T_{\mathrm{AT}}}$ into subsurface oceanic warming at the mean depth of the ice shelf base in each of the five basins:

$$\Delta T_0(r,t) = \beta(r)\Delta\overline{T_{\mathrm{AT}}}\,(t-\delta(r))\,. \tag{26}$$

[59] derived the scaling coefficients $\beta(r)$ and time-delays $\delta(r)$ from 19 CMIP5 models. Each region of Antarctica thus has 19 possible pairs of scaling coefficients and time delays, drawn at random with equal probability. If $t = 2050$ and $\delta(r) = 30$ years, for example, then the input to Equation (26) is $\Delta\overline{T_{\mathrm{AT}}}$ in 2020.

The second step is to map subsurface ocean warming into enhanced basal ice shelf melting:

$$\Delta M(r,t) = \lambda\Delta T_0(r,t), \tag{27}$$

where the basal melt sensitivity parameter λ is randomly chosen from a uniform distribution with lower and upper bounds of $7\mathrm{ma}^{-1}\mathrm{K}^{-1}$ and $16\mathrm{ma}^{-1}\mathrm{K}^{-1}$ respectively. This interval corresponds to values from experimental observations.

The third step translates the enhanced basal ice shelf melting into ice loss/SLR. This utilises reduced-form response functions, which [59] estimated on the behaviour of the 16 ice sheet models. Each ice sheet model was initially subjected to a control run from 1900 to 2100. In this control run, the models were forced with historically observed basal ice shelf melting until 2010 and constant forcing thereafter. After the control run, each ice sheet model was then subjected to an artificial external forcing experiment involving an additional stepwise increase of 8m/yr of basal ice shelf melting. The difference in the dynamic contribution to SLR between the experiment and the control run forms the basis of the response function for the particular model and region. The approach assumes that increasing the magnitude of the forcing by a specific factor will increase the magnitude of the response of the ice sheet by the same factor. However, the temporal evolution of the response is not a linear function of time. Response functions can capture the irregular oscillations of ice sheet dynamics in response to external forcing. One must also assume that over the forcing period the five regions of Antarctica respond independently. [59] showed this is a good assumption. [59] also subjected the 16 ice sheet models to forcing experiments of 4m/yr and 16m/yr of additional basal melting and compared these responses to the main 8m/yr experiment. Generally, there was good agreement between the responses to the step increases of different size. SLR from dynamic

processes S is given by

$$S(r,t) = \sum_{r=1}^{5} \sum_{s=0}^{t} \Delta M(r,s) R(r,s), \tag{28}$$

where R is the value of the response function at time s, drawn at random from the set of 16 models. The total Antarctic SLR contribution is the sum of (25) and (28).

[59] derived response functions for the period 1900 to 2100. The period to 2100 is long enough for many of our purposes in this paper, but not for estimating the social cost of CO_2, as a large portion of the current social cost of CO_2 stems from damages after 2100. Therefore, we developed a method of extrapolating the response functions to 2200 using time-series analysis techniques. This makes tractable the extrapolation problem in the absence of being able to run the ice sheet models themselves. We treat the dynamic contribution to SLR estimated by each ice sheet model over the period 1900 to 2100 as a time series. This is first detrended to achieve stationarity and then the properties of the series are estimated using a moving average function of the first or second order, or an ARMA function of the first or second order, with the model being chosen based on best fit under the Akaike Information Criterion.

3.1.6 Arctic sea-ice loss/surface albedo feedback

Changes in global ice and snow cover also affect the surface albedo feedback (SAF), increasing net radiative forcing. While these effects are implicitly captured in the equilibrium climate sensitivity (ECS) parameter in simple climate models, i.e., the steady-state increase in temperature in response to a doubling of the atmospheric CO_2 concentration, doing so assumes that the marginal forcing from an increase in temperature is constant across temperatures. However, as the area of ice and snow diminishes, the marginal response for further increases in temperature decreases. This SAF dynamic has been modelled by [79] using PAGE-ICE and we replicate their model here.

[79] use a quadratic fit of the SAF observed across the CMIP5 models, shown in the top panel of Figure S14. This falling SAF curve describes the weakening feedback loop between changes in temperature and changes in albedo. For low levels of warming, the SAF is greater than the constant value represented in the ECS; as sea-ice and land snow diminish, the feedback effect drops. When sea ice and land snow are absent, the SAF effect is zero. The total radiative forcing due to albedo, however, always increases with temperature, and reaches its maximum when sea ice and land snow are absent.

Total SAF forcing is the integral of the SAF feedback effect across the change in temperature,

Figure S14: Variation in surface albedo feedback (SAF) effects as a function of GMST. **Top:** SAF as a function of temperature, in terms of marginal increases in forcing per degree Kelvin. **Middle:** adjusted value of the ECS when SAF forcing is removed. **Bottom:** cumulative forcing from the SAF, as a function of temperature, in Wm^{-2}.

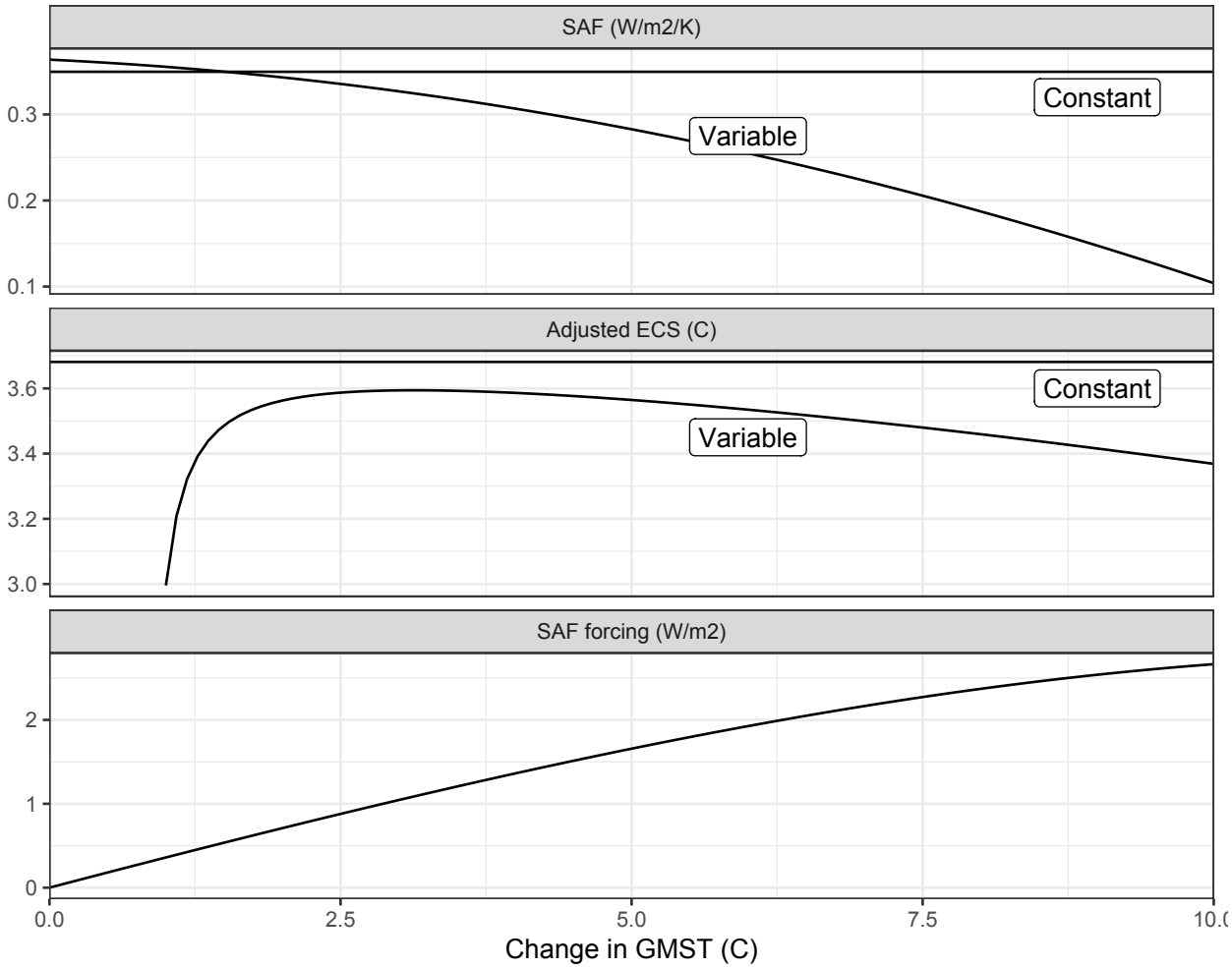

reaching 2.67 Wm^{-2} at warming of 10°C. The ECS follows a non-linear curve calculated as a function of the ECS in the last period, and accounting for the different level of feedback compared to a constant level. As a consequence, adding the SAF to the base climate model can result in lower warming eventually.

The calculations for the SAF correction are shown below. The principle of the SAF model is to correct temperatures calculated under the process used in PAGE-ICE, so we first reproduce this temperature calculation. Global PAGE-ICE atmospheric temperature is calculated as

$$\begin{aligned}\Delta\overline{T_{ATM-PAGE1}}(t) = &\Delta\overline{T_{ATM-PAGE1}}(t-1)\\ &+\left(A(t-1)-\mathrm{FRT}B(t-1)-\Delta\overline{T_{ATM-PAGE1}}(t-1)\right)\left(1-e^{-1/\mathrm{FRT}}\right)\\ &+B(t-1)\end{aligned}$$

where

$$A(t-1)=\frac{\mathrm{ECS}}{F_{sl}\ln 2}F(t-1)$$
$$B(t-1)=\frac{\mathrm{ECS}}{F_{sl}\ln 2}(F(t-1)-F(t-2))$$

$F(t)$ is the anthropogenic forcing in our model

F_{sl} is the forcing slope, 5.5 W/m2

FRT is the warming half-life, from a triangular distribution from 10 to 55 with mode of 20

The surface albedo feedback is then calculated using a quadratic approximation, where SAF decreases more rapidly as temperature increases. The equations are described as an integral over this quadratic:

$$\mathrm{SAF}(t)=\frac{C(\Delta\overline{T_{ATM-PAGE1}}(t))-\mathrm{FSAF}_0}{\Delta\overline{T_{ATM-PAGE1}}(t)-\Delta\overline{T_{ATM-PAGE1}}(2010)}$$

where

$$C(\Delta T) = \beta_2 \Delta T^3/3 + \beta_1 \Delta T^2/2 + \beta_0 \Delta T + \gamma \Delta T \delta$$

β_2 is the T^2 coefficient for the SAF quadratic ($\mathrm{W/m^2/K^3}$)

β_1 is the T^1 coefficient for the SAF quadratic ($\mathrm{W/m^2/K^2}$)

β_0 is the T^0 coefficient for the SAF quadratic ($\mathrm{W/m^2/K}$)

γ is the standard deviation of the SAF quadratic ($\mathrm{W/m^2/K}$)

δ is the nonlinearity of SAF, drawn from a symmetric triangular distribution from -1 to 1

FSAF_0 is the base year SAF forcing ($\mathrm{W/m^2}$)

The adjustment to the SAF forcing is given by a two-segment correction

$$\begin{aligned}\Delta\mathrm{FSAF}(t) = &- \mathrm{SAF}(t)\Delta\overline{T_{ATM-PAGE2}}(t-1) \\ &+ \begin{cases} C(\Delta\overline{T_{ATM-PAGE2}}(t-1)) & \text{if } \Delta\overline{T_{ATM-PAGE2}}(t-1) < 10 \\ D(\Delta\overline{T_{ATM-PAGE2}}(t-1)) & \text{if } \Delta\overline{T_{ATM-PAGE2}}(t-1) \geq 10 \end{cases}\end{aligned}$$

where

$$D(\Delta T) = \psi + \alpha(\Delta T - 10) + \sigma(\Delta T - 10)\delta$$

$\Delta\overline{T_{ATM-PAGE2}}(t)$ is defined below.

ψ is the integration constant for SAF forcing at the segment switch point

α is the linear SAF segment mean

σ is the linear SAF segment standard deviation

Also using $SAF(t)$, the adjusted ECS and FRT values are calculated as

$$\mathrm{ECS}' = \mathrm{ECS}\left(1 - \frac{\mathrm{ECS}\left(\mathrm{SAF}(t) - \overline{SAF}\right)}{F_{sl}\ln 2}\right)^{-1}$$

$$\mathrm{FRT}' = \mathrm{FRT}\left(1 - \frac{\mathrm{ECS}\left(\mathrm{SAF}(t) - \overline{SAF}\right)}{F_{sl}\ln 2}\right)^{-1}$$

where $\overline{SAF}$ is the constant approximation to the SAF (0.34959 W/m^2/C).

Then $\Delta\overline{T_{ATM-PAGE2}}(t)$, the adjusted temperature time-series, is calculated identically to $\Delta\overline{T_{ATM-PAGE1}}(t)$, but using ECS′, FRT′, and with the additional forcing ΔFSAF(t). The temperature adjustment produced by the SAF model, $\Delta\overline{T_{ATM-PAGE2}}(t) - \Delta\overline{T_{ATM-PAGE1}}(t)$, is then added to the main temperature in the model.

3.1.7 Slowdown of the Atlantic Meridional Overturning Circulation

Weakening of the Atlantic Meridional Overturning Circulation (AMOC) or thermohaline circulation,[9] whether partial or full, has inspired a number of numerical modelling studies in climate economics [91, 92, 93, 82, 94, 95, 96, 97, 98]. The majority of these take a stylised approach. Of those aiming for realism, we choose to incorporate the results of [91] in our model, because of their unique focus on the effects of AMOC slowdown at the national level. This is arguably central to the economic evaluation of AMOC slowdown, because its physical effects would vary significantly across the world, from a reduction in regional temperature of several degrees, all else being equal, to an increase in regional temperature of a few tenths of a degree [see 91, fig. 1]. The basic logic is that the ocean circulation redistributes heat, rather than creating or destroying it, and countries vary in their exposure to this heat redistribution, as well as the effects of global warming more broadly, depending on their physical location. AMOC slowdown is expected to have physical effects other than temperature change, for instance effects on precipitation and regional sea levels [99], but these have yet to be incorporated in economic studies.

[91] implement four what-if scenarios known in the context of AMOC slowdown as 'hosing experiments'. In these experiments, a large exogenous pulse of freshwater is added to the representation of the North Atlantic in General Circulation Models – hence the term hosing – and the consequences for the AMOC are simulated. Note this is additional to any gradual slowdown of AMOC captured by the climate models of CMIP6, which our calibrated pattern scaling of global into national temperatures already captures (see below). The four scenarios result in an AMOC slowdown of 7%, 24%, 27% and 67% respectively. This slowdown is assumed to be reached in the year 2085, after being phased in linearly from a 2050 starting point. As is by now familiar, we convert these what-if scenarios into hazard events and assign them probabilities. The national temperature delta arising

[9] We use these two terms interchangeably.

from AMOC slowdown is hence given by

$$\begin{aligned}
\Delta T_{\text{AT_AMOC}}(i,t) &= \Delta T_{\text{AT_AMOC}}(i,t-1) + \left(\frac{\overline{\Delta T_{\text{AT_AMOC}}(i)}}{\Delta_{\text{AMOC}}}\right) I_{\text{AMOC}}(t) \\
&\iff \sum_{s=0}^{t-1} \Delta T_{\text{AT_AMOC}}(i,s) < \overline{\Delta T_{\text{AT_AMOC}}(i)}, \qquad (29) \\
\Delta T_{\text{AT_AMOC}}(i,t) &= \overline{\Delta T_{\text{AT_AMOC}}(i)} \\
&\iff \sum_{s=0}^{t-1} \Delta T_{\text{AT_AMOC}}(i,s) = \overline{\Delta T_{\text{AT_AMOC}}(i)}, \qquad (30)
\end{aligned}$$

where $\overline{\Delta T_{\text{AT\_AMOC}}(i)}$ is the permanent difference in national annual average temperature as a result of AMOC slowdown in country i. The data points corresponding to $\overline{\Delta T_{\text{AT\_AMOC}}(i)}$ were kindly provided by Anthoff and colleagues for all countries they covered. Δ_{AMOC} is the time taken for AMOC slowdown to phase in, i.e. 35 years. $I_{\text{AMOC}}(t)$ is the indicator function, whose transition probability from zero to one is

$$p_{\text{AMOC}}(t) = \begin{cases} 1 - \exp\left[-b_{\text{AMOC}}\Delta\overline{T_{\text{AT}}}(t)\right] & \text{if } t = 1 \\ (1 - \exp\left[-b_{\text{AMOC}}\Delta\overline{T_{\text{AT}}}(t)\right]) - (1 - \exp\left[-b_{\text{AMOC}}\Delta\overline{T_{\text{AT}}}(t-1)\right]) & \text{if } t > 1 \end{cases} \qquad (31)$$

conditional on $I_{\text{AMOC}}(t-1) = 0$.

To calibrate the hazard rate for each of the four scenarios in [91], we compile likelihoods as a function of global mean temperature increase for distinct AMOC shutdown events ranging from a weakening of 11% to a full shutdown. We obtain these from the IPCC *Fifth Assessment Report* [100], its *Special Report on Global Warming of 1.5°C* [101], and [102]. Given the limited measurements of AMOC intensity, these numbers reflect a combination of model-based estimates and expert judgement. We proceed in two steps: (i) we take the convex combination of the AMOC shutdown events from the literature that most closely resembles the what-if scenario at hand. To obtain a hazard rate b_{AMOC}, we then (ii) calibrate Equation (31) by minimizing the sum of squared differences to the likelihoods obtained in step (i). We estimate $b_{\text{AMOC}} = 1.6$ for a 7% slowdown, 0.611 for a 24% slowdown, 0.54 for 27% and 0.135 for 67%.

3.1.8 Weakening of the Indian Summer Monsoon

The first integrated assessment of the Indian Summer Monsoon (ISM) and its response to climate change has recently been carried out by [103]. This is based on coupling a version of Nordhaus' regionally disaggregated RICE IAM [104] to a model of the ISM [105]. The ISM is driven by greater heating of the land surface relative to the ocean in summer, which creates a pressure gradient that drives moist ocean air over the Indian subcontinent, where it rises and condenses. However, ISM rainfall displays important year-to-year variation and the ISM has the potential to abruptly change regime from wet to dry and *vice versa*. Schewe and Levermann's model generates these dynamics by incorporating reduced-form representations of two competing feedback processes. The first is the so-called moisture advection feedback, a positive feedback whereby monsoon rains release latent heat, which strengthens the monsoon circulation and brings more rainfall in turn. The second is the dry-subsidence effect, a negative feedback whereby high pressure reduces rainfall, the decreased rainfall leads to less latent heat being released, which in turn sustains the dry phase. High pressure also deflects winds away from the monsoon region. In [103]'s model , rainfall depends on both climate change, through multiple channels, and regional emissions of sulphur dioxide, which reflect incoming solar radiation, reduce heating over the Indian subcontinent and weaken the ISM.

The key output of the ISM model that feeds into damages to India (see below) is average rainfall over the Indian subcontinent over the summer monsoon season:

$$\overline{P}(t) = \frac{1}{136}\sum_{d=1}^{136} P(d,t), \tag{32}$$

where $P(d,t)$ is rainfall on day d of year t and there are 136 days in each monsoon season.[10] Each day is either wet or dry, depending on

$$P(d,t) \quad = \quad \begin{cases} P_{\text{wet}}(t), & Pr(d,t) < p(d,t), \\ P_{\text{dry}} & Pr(d,t) \geq p(d,t), \end{cases} \tag{33}$$

where $Pr(d,t) = U(0,1)$, capturing random variation in day-to-day weather. There is no rainfall on a dry day, whereas rainfall on a wet day is an increasing function of atmospheric temperature,

[10] For computational reasons, we use a four-day time step, so $P(d,t)$ changes at most once every four days and there are 136 days in the season, compared with 135 in [103].

since a warmer atmosphere can hold more water:

$$P_{\text{wet}}(t) = p'' \left[\Delta\overline{T_{\text{AT}}}(t) - \Delta\overline{T_{\text{AT}}}(0)\right] + P_{\text{wet}}(0). \tag{34}$$

The initial value of P_{wet} is 9mm per day and it increases by 0.42mm/day/°C of global warming.

The probability of a wet day during the first δ days of the season – the onset – is

$$p_{\text{init}}(t) \quad = \quad \begin{cases} p_{\text{init},1}(t), & A_{\text{pl}}(t) < A_{\text{pl,crit}}(t), \\ 1 - p_{\text{m}}, & A_{\text{pl}}(t) \geq A_{\text{pl,crit}}(t), \end{cases} \tag{35}$$

where $p_{\text{m}} = 0.82$ is the maximum probability of a wet day.[11] The formulation in Eq. (35) makes rainfall during the onset of the season a function of albedo $A_{\text{pl}}(t)$, in particular its relation to a critical albedo value $A_{\text{pl,crit}}(t)$. If the actual albedo exceeds the critical value, the probability of a wet day is at its minimum. The critical albedo value is increasing in the atmospheric concentration of CO_2,

$$A_{\text{pl,crit}}(t) = \alpha_{\text{pl},1} \ln \left[\sum_{i=0}^{3} S_i(t) + \underline{S}\right] + \alpha_{\text{pl},2}. \tag{36}$$

$\sum_{i=0}^{3} S_i(t) + \underline{S}$ gives the atmospheric CO_2 concentration and its derivation is explained in the following section. The actual albedo is given by

$$A_{\text{pl}}(t) = A_{\text{pl}}(0) + 2T_{\text{pl}}^2(1 - A_{\text{s}})^2 \beta_{\text{pl}} \alpha_{\text{pl},3} B_{\text{SO4}}(t), \tag{37}$$

where T_{pl} is the fraction of light transmitted by the aerosol layer, A_{s} is the present value of the surface albedo, β_{pl} and $\alpha_{\text{pl},3}$ are coefficients representing the backscatter fraction and mass scattering efficiency respectively and $B_{\text{SO4}}(t)$ is the regional sulphate burden over the Indian peninsula. This last quantity depends on SO_2 emissions in the region:

$$B_{\text{SO4}}(t) = \text{SO}_2(t) H_{\text{SO2}} V/\Omega. \tag{38}$$

Emissions of SO_2 are exogenous and sourced from the Representative Concentration Pathway (RCP) database [106]. The emissions scenarios we use are discussed in greater detail below. The RCP database only disaggregates SO_2 emissions to the level of the Asian continent/region, so we down-

[11] By bounding the probability of a wet day during the onset of the monsoon season, the system does not become irrevocably locked into either a wet or dry state.

scale to the Indian level by assuming a constant ratio of Indian/Asian emissions, estimated based on 2010 data [107]. The parameter H_{SO2} is the fractional sulphate yield, V is the atmospheric lifetime of sulphate and Ω is the land area. Thus the dependence of rainfall on albedo in the model ultimately captures the local cooling effect of SO_2 emissions in the region, which weakens the ISM.

Assuming the actual planetary albedo does not exceed the critical value, the probability of a wet day during the first δ days of the season is

$$p_{\text{init},1}(t) = p' \left[m_{\text{NINO3.4}}(t) - m_0 \right] + p_0, \tag{39}$$

where $m_{\text{NINO3.4}}$ is the strength of the Walker circulation, i.e., the Pacific Ocean atmospheric circulation, in May. The subscript NINO indicates that the strength of this circulation depends on whether there is an El Niño or not. El Niño suppresses the ISM. The parameters p', m_0 and p_0 are used to calibrate the response of $p_{\text{init},1}(t)$ to $m_{\text{NINO3.4}}$. The strength of the Walker circulation in May is in turn given by

$$m_{\text{NINO3.4}}(t) = m' \left[\Delta\overline{T_{\text{AT}}}(t) - \Delta\overline{T_{\text{AT}}}(0) \right] + m_{\text{NINO3.4}}(0). \tag{40}$$

The probability of a wet day after the first δ days of the season is

$$p(d,t) = \frac{1/\delta \sum_{i=d-\delta}^{d-1} P(i,t) - P_{\text{dry}}}{P_{\text{wet}}(t) - P_{\text{dry}}}, \tag{41}$$

where $\delta = 16$ days.[12] The probability of a wet day depends positively on how wet the previous δ days were, a representation of the moisture advection and dry-subsidence feedbacks.

3.1.9 Tipping point interactions

Tipping points can interact with each other in multiple ways [83, 69]. Some of these interactions are hardwired into the structure of our model. For example, the PCF increases GMST, which affects all seven remaining tipping points in our study, because all of them depend on temperature. However, the structure of our model can only capture a limited subset of all the possible interactions between tipping points. To increase the number of interactions, we use the expert elicitation study of [69], which attempted to quantify how the triggering of one tipping point can cause the hazard rates of other tipping points to change, with a focus on mechanisms other than temperature.

[12] With a four-day time step, we set the memory period $\delta = 16$ days, rather than 17 days as in [103].

We apply a hierarchical Bayesian analysis to obtain best estimates of the hazard rate changes provided by the experts in [69]. The hazard rate changes – the interactions – are represented by a range for expert i from lower bound u_i to upper bound n_i. Each change/interaction is a multiplier on the base hazard rate, so a value of 1 means no change. We posit a true, expert-specific hazard rate change, θ_i, and further assume that these true values are drawn from a normal distribution with unknown mean and variance. This allows the expert opinions to be partially pooled to inform the hyperparameters of the normal distribution:

$$\theta_i \sim \mathcal{N}(\mu, \tau)$$
$$\theta_i \sim \mathcal{U}(u_i, n_i)$$

We treat cases where experts were uncertain about the lower bound of the hazard rate change as having a lower bound of 0, and cases where they were uncertain about the upper bound as an upper bound of 10. Figure S15 presents the results.

Figure S15: The posterior distribution of μ, the mean of the hyperdistribution, for each interaction. The error bars in each plot show the 95% credible interval on μ for the given interaction. The light grey lines show each expert's upper and lower bounds (dots are used if the upper bound equals the lower bound). Abbreviations are as follows: Atlantic Meridional Overturning Circulation (AMOC), melt of the Greenland Ice Sheet (GIS), disintegration of the West Antarctic Ice Sheet (WAIS), and dieback of the Amazon rainforest (AMAZ).

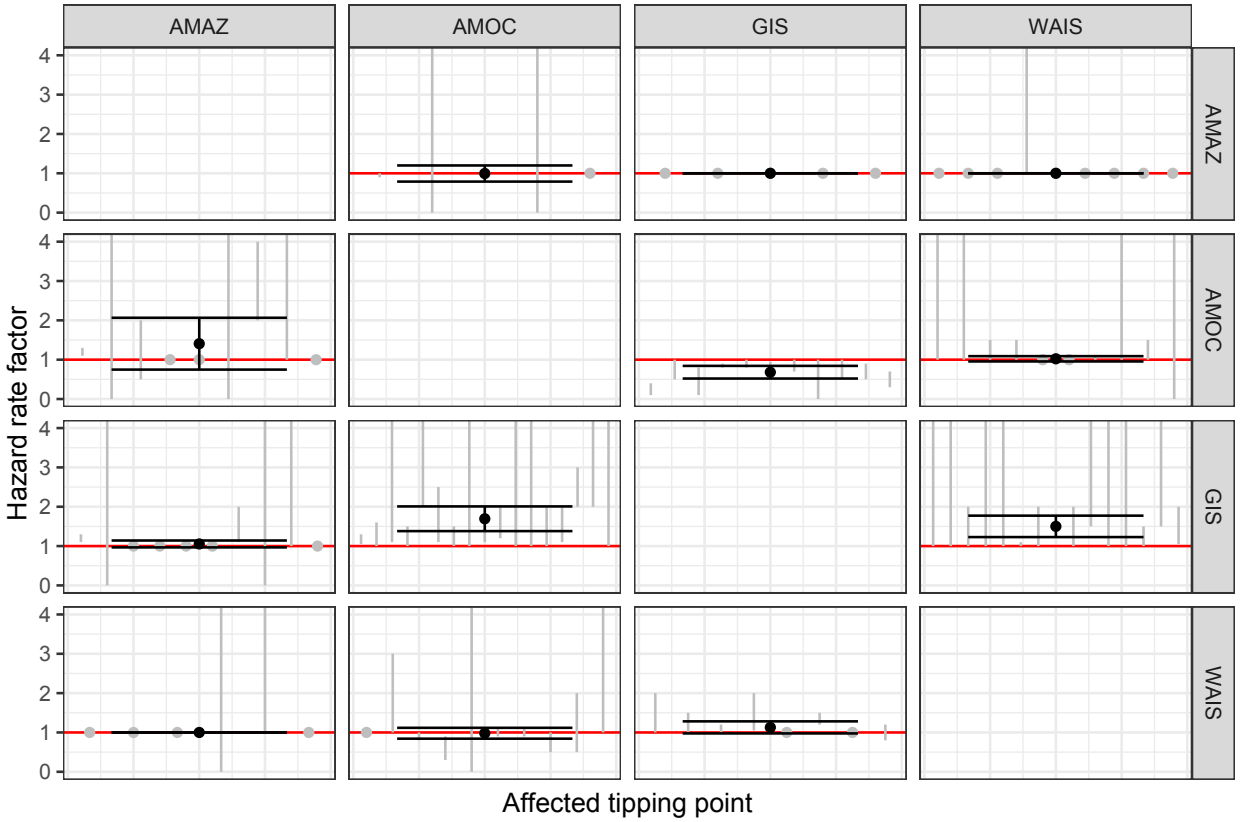

The set of tipping point interactions included in our study is the union of the set of interactions hardwired in our model and the set of interactions quantified by [69]. To aid understanding of how many interactions are thereby included, as well as the direction of each interaction, Table S7 provides a matrix.

Table S7: Interactions between tipping points included in this study. Each cell indicates the qualitative effect of the row tipping point on the column tipping point. Where the row tipping point can increase or decrease the intensity/likelihood of the column tipping point, depending on time or state, we write +/-. Parentheses indicate the interaction is calibrated on the expert elicitation study by [69]. The absence of parenthesis indicates the interaction is hardwired in the model structure. Zeros indicate an interaction that is included, but that has a statistical zero effect according to [69]. No int. means the interaction is not included at all. n.b. ISM affects other tipping points via ENSO, implicit in the expert estimates of the relevant hazard rate changes. AIS interactions are calibrated on the ice sheet responses of the four Western regions of Antarctica only, to match with the notion of WAIS in [69].

	PCF	OMH	SAF	AMAZ	GIS	AIS	AMOC	ISM
PCF		+	+	+	+	+	+	+/-
OMH	+		+	+	+	+	+	+/-
SAF	+/-	+/-		+/-	+/-	+/-	+/-	+/-
AMAZ	+	+	+		+ (0)	+ (0)	+ (+/-)	+/- (+/-)
GIS	no int.	no int.	no int.	(+/-)		(+)	(+)	(0)
AIS	no int.	no int.	no int.	(0)	(+/-)		(+/-)	(0)
AMOC	no int.	no int.	no int.	(+/-)	(-)	(+/-)		(0)
ISM	no int.	no int.	no int.	(+)	(0)	(0)	(+/-)	

3.2 Climate module

3.2.1 Emissions

The principal inputs to the climate model are global emissions of CO_2 and CH_4. Other anthropogenic and natural sources of radiative forcing, both positive and negative, are aggregated into an exogenous residual radiative forcing series.[13] Anthropogenic emissions come from the scenarios described in the scenario section above. The second source of emissions is the carbon-cycle feedbacks described in the previous section, i.e., permafrost melting, dissociation of ocean methane hydrates, and Amazon rainforest dieback.

[13]This is the sum of forcing from: (i) N_2O; (ii) flourinated gases controlled under the Kyoto Protocol; (iii) ozone-depleting substances controlled under the Montreal Protocol; (iv) total direct aerosol forcing; (v) the cloud albedo effect; (vi) stratospheric and tropospheric ozone forcing; (vii) stratospheric water vapour from methane oxidisation; (viii) land-use albedo; (ix) black carbon on snow.

3.2.2 CO_2 and CH_4 cycles

CO_2 and CH_4 emissions are mapped into atmospheric concentrations using the FaIR simple climate model, version 2.0.0 [42], specifically the Julia-Mimi implementation of the model available at https://github.com/FrankErrickson/MimiFAIRv2.jl.git. This updates the CO_2 and CH_4 cycles from META-2021, which were based on FaIRv1.0 [108] for CO_2 and our own representation of the CH_4 cycle.

In FaIR, each gas cycle is represented by the following system of equations (sticking with discrete time notation and following closely the Julia-Mimi implementation):

$$C(t) = \underline{C} + \frac{1}{2}\left[\sum_{i=1}^{n} R_i(t-1) + \sum_{i=1}^{n} R_i(t)\right], \tag{42}$$

$$R_i(t) = E(t)\frac{a_i}{\delta_i(t)}\left[1 - e^{-\delta_i(t)}\right] + R_i(t-1)e^{-\delta_i(t)}, \tag{43}$$

$$\delta_i(t) = \frac{1}{\alpha(t)\tau_i}, \tag{44}$$

$$\alpha(t) = g_0 \exp\left(\frac{r_0 + r_u G_u(t-1) + r_T \Delta\overline{T_{AT}}(t-1) + r_a G_a(t-1)}{g_1}\right), \tag{45}$$

where

$$G_a(t) = \sum_{i=1}^{n} R_i(t), \tag{46}$$

$$G_u(t) = \sum_{s=t_0}^{t} E(s) - G_a(t), \tag{47}$$

and

$$g_1 = \sum_{i=1}^{n} a_i \tau_i \left[1 - (1 + 100/\tau_i)\, e^{-100/\tau_i}\right], \tag{48}$$

$$g_0 = \exp\left(-\frac{\sum_{i=1}^{n} a_i \tau_i \left[1 - e^{-100/\tau_i}\right]}{g_1}\right). \tag{49}$$

$C(t)$ is the atmospheric stock/concentration of a given GHG, which is the sum of the pre-industrial stock $\underline{C}$ and the stock above pre-industrial. This stock above pre-industrial comprises $i = n$ boxes/reservoirs R_i (four for CO_2 and one for CH_4). Emissions E of the GHG in question are apportioned to box i according to its uptake fraction a_i and are removed at rate δ_i, which itself is a function of the decay timescale of the box τ_i and a state-dependent adjustment α, which

links the removal rate of the GHG from the atmosphere to current cumulative uptake G_u, warming $\Delta\overline{T_{AT}}$, and the stock above pre-industrial G_a. This state-dependent adjustment is a signature of the FaIR model and is capable of simulating positive and negative feedbacks in the gas cycle. r_0 is the strength of pre-industrial uptake from the atmosphere. The constants g_0 and g_1 are used for calibration of the state-dependent adjustment.

3.2.3 Radiative forcing and temperature

We also use FaIRv2.0.0 to convert atmospheric concentrations into effective radiative forcing and temperature change. This is also an update on META-2021, which used FaIRv1.0 [108] for CO_2 and [109] for CH_4. In general, the FaIR forcing equation includes logarithmic, square-root and linear terms:

$$F(t) = \sum_{x}^{\text{forcing agents}} \left\{ f_1^x \ln\left[\frac{C^x(t)}{\underline{C^x}}\right] + f_2^x \left[C^x(t) - \underline{C^x}\right] + f_3^x \left[\sqrt{C^x(t)} - \sqrt{\underline{C^x}}\right] \right\} + F_{\text{ext}}. \tag{50}$$

In META, the number of forcing agents $x = 2$, namely CO_2 and CH_4; F_{ext} is the sum of forcings from all other agents. For CO_2, the forcing relationship comprises the logarithmic and square-root terms only; for CH_4, just the square-root term [42].

From forcing, the increase in GMST is governed by a model comprising three heat boxes, which is one more than FaIRv1:

$$\Delta\overline{T_{AT}}(t) = \frac{1}{2}\left[\sum_{j=1}^{3} \Delta\overline{T_j}(t) + \sum_{j=1}^{3} \Delta\overline{T_j}(t-1)\right], \tag{51}$$

$$\Delta\overline{T_j}(t) = \Delta\overline{T_j}(t-1)e^{-1/d_j} + F(t)q_j\left(1 - e^{-1/d_j}\right), \tag{52}$$

where $\Delta\overline{T_j}$ is the temperature change for box j, e^{-1/d_j} is the thermal response decay factor, where d_j represents the thermal response timescale, and q_j is a radiative forcing coefficient.

3.3 Damages/economic module

3.3.1 Sea level rise

Sea level rise comprises a contribution from thermal expansion and melt from glaciers and small ice caps, $SLR_{\text{THERM}}(t)$, as well as a contribution from disintegration of the GIS and AIS:

$$\sum SLR(t) = SLR_{\text{THERM}}(t) + SLR_{\text{GIS}}(t) + SLR_{\text{AIS}}(t). \tag{53}$$

Sea level rise is defined relative to the year 2000 and $\sum SLR(0) = 0.04$m [110]. To model the contribution from thermal expansion and melt from glaciers and small ice caps, we follow [111] in specifying SLR as a linear function of warming:

$$SLR_{\text{THERM}}(t) = (r_{\text{TE}} + r_{\text{GSIC}})\,\Delta\overline{T_{\text{AT}}}(t) + SLR_{\text{THERM}}(t-1), \tag{54}$$

where $r_{\text{TE}} = 0.00078$ and $r_{\text{GSIC}} = 0.00081$ parameterise the rates of SLR from thermal expansion and melt from glaciers and small ice caps respectively. Sea level rise from thermal expansion is parameterised such that 1°C warming results in a very long-term equilibrium increase of 0.5m (i.e., over the course of approximately 1000 years).

3.3.2 National temperature

We convert the increase in GMST relative to pre-industrial into the increase in national mean surface temperature using statistical downscaling. This procedure has been updated from META-2021 and now uses data from CMIP6. We subsequently add the effect of AMOC slowdown.

For country i, the change in mean surface temperature relative to pre-industrial is estimated using the following relationship:

$$\Delta T_{\text{AT}}(i,t) = \alpha(i) + \beta(i)\Delta\overline{T_{\text{AT}}}(t) + \Delta T_{\text{AT\_AMOC}}(i,t). \tag{55}$$

The coefficients α and β are estimated by regressing national mean surface temperature change from the CMIP6 dataset on corresponding GMST change. National mean surface temperature is constructed from the gridded CMIP6 output using population weights. We pool all available CMIP6 models and, for each model, we pool temperature changes from the historical runs with future projections on RCP2.6, RCP4.5, RCP7.0 and RCP8.5. We also tested quadratic and cubic specifications of the national-global temperature change relationship, but the linear model was preferred based on the AIC and BIC; the relationship appears to be highly linear for all countries.

3.3.3 Damages and national income per capita

Income growth depends on exogenous drivers, as well as damages from changing temperatures and SLR (and from the summer monsoon in India, only). Post-damage income per capita in country i,

$y(i,t)$, grows according to

$$y(i,t) = \overline{y}(i,t-1)\left[1 + g_{\mathrm{EX}}(i,t) + D_{\mathrm{TEMP}}(i,t)\right]\left[1 - D_{\mathrm{SLR}}(i,t)\right], \tag{56}$$

where $g_{\mathrm{EX}}(i,t)$ is an exogenous, country- and time-specific growth rate that is taken from the SSP database [112].[14] The SSP scenarios are only defined until 2100. To extend these scenarios until 2300, we follow a procedure described in Section 3.4.1.

$D_{\mathrm{TEMP}}(i,t)$ are temperature damages, which are given by

$$D_{\mathrm{TEMP}}(i,t) = \beta_1\left[T_{\mathrm{AT}}(i,t) - T_{\mathrm{AT}}(i,0)\right] + \beta_2\left[T_{\mathrm{AT}}(i,t) - T_{\mathrm{AT}}(i,0)\right]^2, \tag{57}$$

where the coefficients β_1 and β_2 are taken from the econometric analysis of [53].

$D_{\mathrm{SLR}}(i,t)$ are SLR damages, which are given by

$$D_{\mathrm{SLR}}(i,t) = \theta(i)\sum SLR(t), \tag{58}$$

where $\theta(i)$ parameterises the cost to country i per unit SLR. We obtain SLR damages from Diaz's CIAM model [66]. We run CIAM to obtain estimates of national coastal damage/adaptation costs as a function of SLR in two scenarios, (i) no adaptation and (ii) optimal adaptation. We treat each country's adaptation decisions as uncertain and obtain a symmetrical triangular distribution for each $\theta(i)$ with a minimum corresponding to costs in (i) and a maximum corresponding to costs in (ii). We use costs/SLR in 2050 for the calibration, a simple approach facilitated by the fact that the relationship between the two is approximately linear over the 21st century [66].

In India, there is an additional damage multiplier $D_{\mathrm{ISM}}(IND,t)$, so that national income per capita is given by

$$\begin{aligned} y(IND,t) &= \overline{y}(IND,t-1)\left[1 + g_{\mathrm{EX}}(IND,t) + D_{\mathrm{TEMP}}(IND,t)\right] \times \\ &\quad \times \left[1 - D_{\mathrm{SLR}}(IND,t)\right]\left[1 - D_{\mathrm{ISM}}(IND,t)\right]. \end{aligned} \tag{59}$$

[14] https://tntcat.iiasa.ac.at/SspDb

Following [103], the ISM damage multiplier is given by

$$D_{\text{ISM}}(t) \quad = \quad \begin{cases} D_{\text{drought}}, & \overline{P}(t) \leq \overline{P}_{\text{drought}}, \\ 0, & \overline{P}_{\text{drought}} < \overline{P}(t) < \overline{P}_{\text{flood}}, \\ D_{\text{flood}}, & \overline{P}(t) \geq \overline{P}_{\text{flood}}. \end{cases} \tag{60}$$

This structure implies that only extremely wet monsoon seasons and extremely dry monsoon seasons affect income in India, with the measure of precipitation being average rainfall for the monsoon season $\overline{P}(t)$. The drought threshold $\overline{P}_{\text{drought}} = 2.8667\text{mm/day}$, while the equivalent flood threshold $\overline{P}_{\text{flood}} = 7.6667\text{mm/day}$. Drought-related damages $D_{\text{drought}} = 3.5\%$ of GDP, while flood-related damages $D_{\text{flood}} = 0.85\%$. All these parameter values are taken from [103].

The level of income per capita in the previous year, on which damages in the current year work, is given by

$$\overline{y}(i, t-1) = \varphi y_{\text{EX}}(i, t-1) + (1-\varphi)\, y(i, t-1), \tag{61}$$

where $y_{\text{EX}}(i, t-1)$ is counterfactual income per capita, also taken from the SSP database, $y(i, t-1)$ is the *actual* post-damage income per capita experienced, and φ parameterises the weight given to each. This specification enables us to explore two different interpretations of the empirical evidence on temperature damages, as well as convex combinations of them. The first interpretation is that temperatures impact the level of income in each year, in effect driving a wedge between what output is feasible given implicit factors of production and productivity, and what output is actually achieved. This has been the traditional approach in climate economics, e.g., in Nordhaus' DICE model. The production possibilities frontier is assumed to evolve exogenously. Such 'levels' damages correspond with $\varphi = 1$. The second interpretation is that temperatures impact the growth rate of income by directly impacting the accumulation of factors of production and/or by impacting productivity growth [113]. Such 'growth' damages correspond with $\varphi = 0$. The persistence of damages and the extent to which they impact growth/levels is an active area of debate in climate economics [70, 71, 68]. We calibrate φ on the long-run projections of [68], which suggest that warming on the RCP8.5 scenario would reduce global GDP by 11.5% by 2100. Given estimates of temperature, SLR and ISM damages, this implies $\varphi = 0.25$.

3.3.4 Utility and welfare

Post-damage national income per capita is first converted into consumption per capita using a country-specific but time-invariant savings rate,

$$c(i,t) = [1 - s(i)]\, y(i,t), \tag{62}$$

where the country savings rates $s(i)$ are calibrated on observed national savings rates averaged over the period 2005-2015, using World Bank data. Savings data are missing for many countries, in which case we impute the global average, also obtained from the World Bank. This specification assumes savings are exogenous and do not respond to changing income prospects. Fully endogenous savings are computationally infeasible in a model with this much complexity and detail. The limitations of assuming constant/exogenous savings have been discussed in the literature, e.g., [114]. Small to moderate climate damages do not appear to shift savings rates measurably.

Consumption is converted into utility using a standard, constant-elasticity-of-substitution representation,

$$u(i,t) = \frac{c(i,t)^{1-\eta}}{1-\eta}, \tag{63}$$

where η is the elasticity of marginal utility of consumption.

To compute overall welfare, we specify a discounted classical/total utilitarian social welfare functional. We begin by calculating welfare for each country i:

$$W(i) = \sum_{t=2020}^{T} (1+\rho)^{-t}\, u(i,t) L(i,t), \tag{64}$$

where ρ is the utility discount rate, a.k.a. the pure rate of time preference. Discounted, population-adjusted current period utility is then summed over the whole modelling horizon to obtain total welfare. Population data are exogenous and taken from the SSP scenarios.

Global welfare follows naturally as the sum of welfare across all countries i:

$$W = \sum_{i} W(i) \tag{65}$$

3.3.5 Non-market damages

The above damages from temperature, SLR and the ISM can be regarded as 'market' damages. Market damages are those climate damages affecting economic activity mediated by money. Market

damages do not include estimates of the welfare cost of climate change outside markets, for example loss of human life [115] or damages to ecosystems that can be priced at people's willingness to pay (WTP) to preserve those ecosystems' existence. 'Non-market' damages are more uncertain than their market counterparts, but in many IAMs they occupy a substantial share of total welfare damages from climate change [e.g. 116, 117].

We use the non-market damage module of the MERGE IAM [67], with an updated calibration derived from [54]. The MERGE model places particular emphasis on the representation of non-market damages, with a WTP measure that depends on both income and temperature. While the parameters of the MERGE non-market damage module are speculative, its use of an S-shaped elasticity of WTP with respect to income is theoretically coherent.

Like the MERGE model, the damage function meta-analysis by [54] assumes that damages grow quadratically with warming from a pre-industrial baseline. Under their preferred model, total damages as a percent of GDP (including market and non-market impacts) follow $0.595\Delta\overline{T_{AT}}(t)^2$. Considering only damage functions that exclude non-market damages, their key coefficient is reduced by 0.487.[15] We use this as evidence that non-market damages follow $0.487\Delta\overline{T_{AT}}(t)^2$. As in [54], we increase this coefficient by 25%, to 0.609, to account for potential omitted (non-catastrophic) damages. This gives a 90% increase in WTP relative to [67]. At 2.5°C warming, WTP is 3.8% of GDP, compared to 2.0% in the original MERGE calibration (see Figure S16).

This WTP applies at high incomes. MERGE provides a model to link WTP to income, which we maintain. At \$25k/capita, WTP to avoid 2.5°C warming is held at 1%. As income increases above that level, WTP asymptotically approaches the non-market damages from [54]. WTP to avoid warming as a function of income is shown in Figure S17.

We calculate this WTP measure at a national level. The non-market damage multiplier, or economic loss function, is

$$D_{\mathrm{NM}}(i,t) = \left[1 - \left(\left(\frac{\Delta\overline{T_{\mathrm{AT}}}(t)}{\Delta T_{\mathrm{cat}}}\right)^2 - \left(\frac{\Delta\overline{T_{\mathrm{AT}}}(0)}{\Delta T_{\mathrm{cat}}}\right)^2\right)\right]^{h(i,t)} . \tag{66}$$

where $\overline{T_{\mathrm{AT}}}(0)$ is the temperature in the baseline period, which is taken to be 2010.

This is a hockey-stick function embodying the assumption that non-market damages can increase rapidly as temperatures become more extreme. ΔT_{cat} is a catastrophic warming parameter set to

[15] This coefficient comes from table 2, column 3 of [54]. While their preferred model is column 4, that model has a market-only reduction of 0.622, larger than the total damage coefficient. Columns 3 and 4 estimate identical values for the total damage coefficient, so we use the more conservative value.

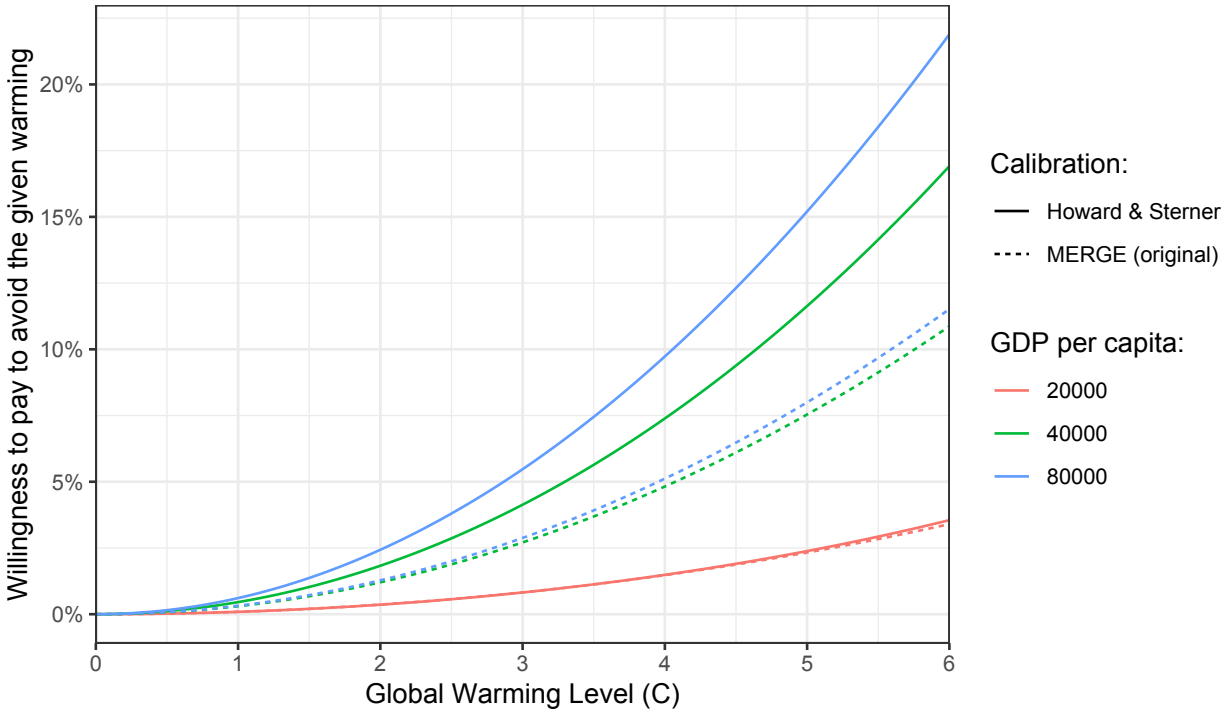

Figure S16: Willingness to pay to avoid levels of warming, split by levels of income. The original and updated calibrations are shown.

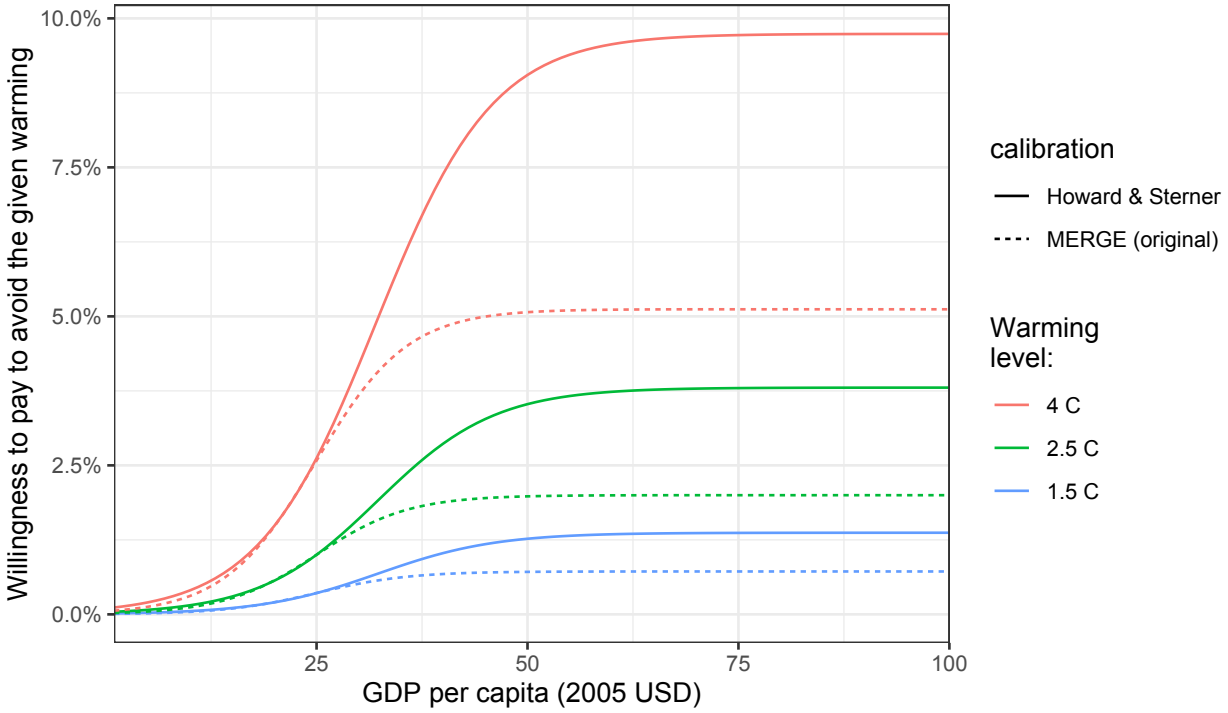

Figure S17: Willingness to pay to avoid 1.5, 2.5, and 4 °C, as a function of income, under the original and updated calibrations.

12.82°C, which people are assumed to be willing to avoid at any cost[16]. $h(i,t)$ is the hockey-stick parameter, which depends on country income per capita ($y(i,t)$):

$$h(i,t) = \min\left[\frac{\log\left[1 - \frac{D_{\text{ref}}}{1+100\exp\left[-WTP_{\text{ref}}y(i,t)\right]}\right]}{\log\left[1-\left(\Delta T_{\text{ref}}/\Delta T_{\text{cat}}\right)^2\right]}, 1\right], \tag{67}$$

where

$$WTP_{\text{ref}} = 0.143 \qquad \text{WTP 1\% of GDP to avoid reference warming at \$25k/capita}$$
$$D_{\text{ref}} = 0.038 \qquad \text{WTP loss at reference warming}$$
$$\Delta T_{\text{ref}} = 2.5\,\text{C} \qquad \text{WTP reference warming}$$

The non-market damage multiplier is applied to country-level utility:

$$u(i,t) = u\left(D_{\text{NM}}(i,t)c(i,t)\right)$$

for utility function $u(\cdot)$ as specified above.

3.3.6 Marginal and total damages

The marginal damage cost/social cost of carbon or methane along a particular scenario of emissions, income and population is the difference in welfare caused by a marginal emission of the gas, normalised by the marginal welfare value of a unit of consumption in the base year:

$$\text{SCC}(t) = \frac{\partial W/\partial E(t)}{\partial W/\partial c(t)}. \tag{68}$$

To calculate the numerator, we run the model twice with identical assumptions, the second time with an additional pulse of emissions. Let ϑ_m represent a vector of parameter values from the model, representing in abstract form the many parameters described above. These are in most cases random draws from a distribution, including individual tipping event realisations. Then we calculate

$$\left[\frac{\partial W}{\partial E(t)}\right]_m = \frac{W[E(t)+\Delta_E(t),\vartheta_m] - W[E(t),\vartheta_m]}{\Delta_E(t)}, \tag{69}$$

where Δ_E is the emissions pulse. We focus on an emissions pulse in 2020.

[16]The catastrophic warming temperature is derived from the assumption that economic losses rise quadratically according to the [54] calibration.

The denominator of (68), $\partial W/\partial c(t)$, depends on the consumption level of the normalising agent. We define this as the global average individual, i.e., global mean consumption per capita:

$$\bar{c}(t,\theta_m) = \frac{\sum_i c(i,t,\vartheta_m)L(i,t)}{\sum_i L(i,t)}. \tag{70}$$

Note that this is also uncertain and depends on the vector of random parameters. Differentiating the utility function, we then have

$$\left[\frac{\partial W}{\partial c(t)}\right]_m = \bar{c}(i,t,\theta_m)^{-\eta}. \tag{71}$$

We focus on a base year of 2020. We then calculate the negative of the ratio of Equations (69) and (71) for each draw of random parameters m and take expectations over all draws. The numeraire in the model is year 2010 US dollars, corresponding to the year in which GDP is initialised. We inflate our reported SCC values to year 2020 US dollars using a factor of 1.2, based on data from [118].[17]

3.4 Supporting analysis

3.4.1 Extending the SSP scenarios beyond 2100

To estimate post-2100 income and population along the SSP scenarios, we fit a model to the available pre-2100 SSP scenario data and use the fitted model to extrapolate. The same model is applied to both income and population and is defined in terms of growth rates. The model postulates that changes in pre-2100 income and population growth rates are explained by a rate of convergence and a rate of decay.

The model is as follows:

$$\text{Growth}(i,t) = (1-\beta-\delta)\text{Growth}(i,t-1) + \delta\text{MeanGrowth}(t-1), \tag{72}$$

where δ is the rate of convergence, β is the decay rate and

$$\text{MeanGrowth}(t-1) = \sum_i \frac{\text{Population}(i,2015)}{\sum_j \text{Population}(j,2015)}\text{Growth}(i,t-1). \tag{73}$$

Below, we write this as $\text{Growth}(\cdot,t-1)\cdot w$, where w is the vector of global population shares for

[17] The inflation factor is 1.2 whether one uses the Consumer Price Index or the GDP deflator.

each country.

SSP data are not available in every year, so fitting Eq. (72) requires a model with dynamics. We use a two-step approach, fitting the model using Stan, a computational Bayes system. The first step uses the available data directly, fitting

$$\text{Growth}(i,s) \sim \mathcal{N}\left([1-\Delta t(\beta+\delta)]\text{Growth}(i,s-1) + \Delta t\delta\text{MeanGrowth}(s-1), \sigma_i\right), \tag{74}$$

where s is a time step, Δt is the number of years between time steps, and country i has uncertainty σ_i. We apply a prior that both β and δ are between 0 and 0.5.

Next, we fit the full model, using the results of the simplified model to improve the Bayesian model convergence. In this case, for a given Markov chain Monte Carlo draw of β and δ, we calculate the entire time series:

$$\widehat{\text{Growth}}(i,t) \sim \mathcal{N}\left((1-\beta-\delta)\widehat{\text{Growth}}(i,t-1) + \delta\left[\widehat{\text{Growth}}(\cdot,t-1)\cdot w.\right], \sigma_i\right) \tag{75}$$

starting with $\widehat{\text{Growth}}(i,2015)$ as reported in the SSP dataset.

The probability evaluation is over both the performance of the fit and the priors:

$$\begin{aligned}
\text{Growth}(i,s) &\sim \mathcal{N}\left(\widehat{\text{Growth}}(i,t(s)), \sigma_i\right) \\
\beta &\sim \mathcal{N}\left(\mu_\beta, \sigma_\beta\right) \\
\delta &\sim \mathcal{N}\left(\mu_\delta, \sigma_\delta\right) \\
\log\sigma_i &\sim \mathcal{N}\left(\mu_{\sigma,i}, \sigma_{\sigma,i}\right)
\end{aligned}$$

where μ is the mean estimate of the corresponding parameter and σ is the standard deviation across its uncertainty. The prior for σ_i is defined as a log-normal, centered on the mean of the estimates of $\log\sigma_i$. The estimates for each SSP are shown in Table S8.

Table S8: Estimated convergence and decay rates for extrapolation of growth of GDP per capita and population in the SSP socio-economic scenarios beyond 2100

SSP	Variable	δ	β
1	GDP per capita	0.006205028	0.005930520
1	Population	0.008967453	0.005215835
2	GDP per capita	0.004190444	0.007228942
2	Population	0.001276993	0.011064426
3	GDP per capita	0.006273030	0.009597363
3	Population	0.001064697	0.007688331
4	GDP per capita	0.006895296	0.009651277
4	Population	0.001867587	0.003461600
5	GDP per capita	0.007766807	0.003843256
5	Population	0.003470952	0.004305310